UNIVERSITAT POLITÈCNICA DE CATALUNYA BARCELONATECH

Development and characterization of mineral-filled (calcium carbonate or talc) polypropylene porous membranes obtained by extrusion

Kian Habibi

Development and characterization of mineral-filled (calcium carbonate or talc) polypropylene porous membranes obtained by extrusion

The dissertation submitted to the Department of

Materials Science and Metallurgy

Universitat Politècnica de Catalunya

BarcelonaTech

By

Kian Habibi

In partial fulfillment of the requirements for the degree of

Doctor of Philosophy

In

Materials Science and Metallurgy Engineering

Supervised by

Dr. David Arencón Osuna

November 2018

DEDICATION

This dissertation is dedicated to my beloved parents, brothers, and grandparents who have been encouraging me during this stage of my life

ACKNOWLEDGMENTS

Both the academic and personal education that I have received here at Polytechnic University of Catalonia (Barcelona Tech) has made me grow in a way that will benefit me and hopefully those I come in contact with for the rest of my life. This would not have been possible without the people, academic researches, and environment that is present here at Polytechnic University of Catalonia (Barcelona Tech). Thus, I must thank those who have provided me with this opportunity. First of all, I would like to express my sincere appreciation and thanks to my advisor Dr. David Arencón Osuna for his patience, guidance, and understanding with many of my shortcomings. I can recall the first time I talked to him during our meeting here in the spring of 2015. I immediately knew afterward that Polytechnic University of Catalonia (Barcelona Tech) was the place I wanted to come so that I could work with him. During what feels like a short stay in Barcelona, he has taken the time to make me feel welcome. Whether this was through, working, or spending time with him during the weekends, I truly have enjoyed every minute with him, although he may not say the same.

Thanks, are also due to the other instructors that I have had here at Polytechnic University of Catalonia (Barcelona Tech) as well as at Centre Català del Plàstic (CCP). I would like to thank the Centre Català del Plàstic (CCP) and the people there that have helped me. I

thank you all for putting up with and helping me in times of crisis. Thanks, Hooman!

Many thanks, more than can be said in a sentence or two are given to those who have worked in this lab. I would like to thank professors Maria Lluisa Maspoch, Antonio Martinez Benasat and Marcelo Antunes for their guidance/advice/and helpful discussions regarding many topics. I would also like to thank the lab staff Anna Carreras and Susana Ortiz for their instruction, kindness/understanding and their help with everything!

I especially value the time and effort professor Jordi Bou has taken to teach me the techniques of FT-IR and his friendship. I would also like to thanks Josep Palou and Isaac Lopez-insa for their time regarding the SEM images and pore calculation respectively.

I am beholden to the two people in my life that I love, my mom and dad (Farah Ahmadi and Parviz Habibi) for their continued support in times of feast or hard times; they have always been there for me to provide guidance, wisdom, and most importantly love to finish this stage of my life and they are a crucial part of my life. Also, my lovely brothers Kiavash and Mohammed Amin (a.k.a. Sir), are thanked for being by my side and my motivation. It certainly would be much less fun and a lot lonelier without you all! I also hope that with me moving back to the “Gach Saran”, we would be able to spend much more time with each other because I miss you. My grandfather, Grandmother

Nourallah (Babaji) and Farangis as well, I will forever be thankful to you!

Lastly but not least, I thank God for my creator, savior, and guide who has carried me when I needed help, provided sustenance when I needed food, clothed me when I was cold and cared for me when I was sick. I can simply never do enough to thank him!

ABSTRACT

One of the techniques to make porous membranes from polymers is based on the stretching a polymer film containing a row-nucleated lamellar structure. This special crystalline structure may be achieved using a processing technology called MEAUS, which is based in the extrusion of a polymer film under fast cooling, its annealing and at last a uniaxial strain along the machine direction is applied.

While many signs of progress have been made in material polymers such as polypropylene, filled polypropylene compounds have scarcely received attention for in order to produce this kind of membranes. In this sense, two of the main fillers employed in the industrial market used in polypropylene are calcium carbonate and talc. This thesis deals with the possibility of producing polypropylene/based membranes, using these two types of fillers. Commercial grades of calcium carbonate and talc were selected for this purpose.

The first step of the experimental tasks has been the production of stable precursor films at scale laboratory, using an extrusion-calender system. These films had a nominal thickness of 25 μm, and the extrusion processing was stable. Annealing was performed mainly at 140°C but in some cases the annealing temperature was varied. Finally, the uniaxial strain was carried out on the annealed precursor films, giving this last step of the methodology a porous structure.

Rheological studies did not show any significant differences that could affect the first stage of the MEAUS process. The orientation of non-annealed and annealed precursor films showed the high dependence of this feature on the annealing treatment, filler content, and filler type. Also, thermal studies carried out through DSC revealed differences in aspects related to the melting endotherm of the non-annealed precursors, annealed precursors, and membranes.

The surface pore morphology was analyzed through electron microscopy. It was observed that the pore density, porous area and finally the permeability of the produced membranes was highly dependent on the crystalline orientation factor, as well as on the filler content and the filler type.

The thermal stability of the membranes, studied through TGA, was not affected by the different porous morphology, and only depended on the chemical composition. Finally, the mechanical characterization carried out through tensile tests, revealed significant changes due to the annealing treatment, and also, due to the polymer composition.

INDEX

LIST OF TABLES

LIST OF FIGURES

ABBREVIATIONS AND SYMBOLS

$A_{\parallel}$	Parallel absorbance measured at 0° polarized light
$A_{\perp}$	Perpendicular absorbance measured at 90° polarized light
BET	Specific surface area
D	Dichroic relationship
d_{50}	A cumulative 50 % point of diameter
DR	Draw ratio
DSC	Differential scanning calorimetry
E	Young's modulus
E'	Storage Modulus
E''	Loss modulus
F	Herman factor
F_{am}	Orientation factor of amorphous phase
F_{av}	Average orientation factor
F_c	Orientation factor of crystalline phase
FT-IR	Fourier transform infrared spectroscopy
G'	Shear storage modulus
GPC	Gel permeation chromatography
MD	Machine direction

MEAUS Melt extrusion annealing uniaxial strain

M_n Average number molecular weight

M_W Mass molecular weights

$Ø_{\%}$ Porosity percentage

PP Polypropylene

T_c Crystallization temperature

TD Transverse Direction

TGA Thermogravimetric Analysis

T_m Melting temperature

V_b Bulk volume

V_g Grain volume

V_p Pore volume

W_{dry} Weight of dry sample

W_{sat} Saturated weight

X_c Degree of crystallinity obtained by crystallization

X_m Degree of crystallinity obtained by melting

ΔH° Theoretical value of the enthalpy of fusion

ΔH_c Enthalpy of crystallization

ΔH_m Enthalpy of fusion

ε_b Deformation of break

ρ_{water} Density of water

σ_{max} Tensile stress

UNITS

°C	Celsius degree
°F	Fahrenheit degree
bar	Bar
Hz	Hertz
kN	Kilonewton
kV	Kilovolt
ml	milliliter
mm	Millimeter
mol	Mole
MPa	Megapascal
P	Pressure
μm	Micrometer

CHAPTER 1

INTRODUCTION

1.1 Membrane industrial framework

Membranes are increasingly employed for separation processes such as battery separation and medical applications to control the permeation rate of chemical components. In terms of battery separators applications, membranes are vastly employed to control the permeation rate of chemical components due to its excellent thermal resistance, superior electrical resistance, and chemical inertness. Also, in the battery framework, they play a significant role on the battery's safety and electrochemical property, including ion conductivity, charge and discharge capacity and cycle performance.

From energy and process reliability points of view, they progressively compete for conventional separation processes such as distillation [1-5]. In past years, membrane gas separation (GS) technology due to their distinct advantages over conventional techniques has become one of the fastest emerging technologies. In particular, membrane GS exhibits operational flexibility, low operating costs, easy scale-up, high product quality and compact design [6-14].

Many hot gas streams in all chemical industries must remain at high temperature during the GS process. Many of these streams cannot be subjected to membrane-based separation processes. In some applications, the process streams are cooled solely to accommodate a membrane GS process, after which is warmth back. This cooling

followed by re-heating causes the waste of a considerable amount of energy [13-19].

Capture and recover CO_2 from gas streams is one of the most important applications of membrane GS. Over the past century, the concentration of carbon dioxide (CO_2) in the atmosphere has been increasing significantly. For almost 40 % of CO_2 emissions, the industrial part is responsible, also for one-third of all the energy utilized globally. Capture and recovery of CO_2 have become a global issue by given the significant effect of greenhouse gas emission on climate change and global warming [9, 20-24].

There are several different types of membrane materials such inorganic materials (ceramics, metals, zeolites, carbons), polymeric materials (rubbery, glassy, and polymer blends) and porous hybrid materials (metal-organic framework (MOFs), zeolitic imidazolate frameworks (ZIFs)). Due to the high cost of inorganic membranes and porous hybrid materials, and their modularizing problem, numerous studies [6, 8, 14] have been focused on modifying polymers to create synthetic polymeric membranes which survive at elevated temperatures.

In the meantime, numerous polymers-based membrane materials have been evaluated in academic research [6, 10], and some of them exhibited encouraging performance. As one of the main advantages, the polymer membranes are most of the time quite economic and

simply manufactured into large-scale modules [6], if compared with the production of other kinds of membranes.

However, in real life, because the properties of the selectivity and permeability membrane aren't the only requirements for a successful application just a few polymers are used [6, 8, 10]. Some aspects that polymeric membranes have to be overcome, in terms of physical and chemical properties, their relative lack of tolerance to high temperatures [14, 11], an increase of some mechanical properties as stiffness and strength [1, 4, 11].

Most of the polymeric membranes are in form of thin films, being this fact another issue, as the processing technologies have to yield a constant thickness film, along with the desired membrane morphology that provides its final performance. Polymeric membranes are made through various techniques such as phase separation, track etching, leaching, thermal precipitation, and stretching [2, 11].

In phase inversion [1-6], the polymeric raw material is mixed with a solvent as well as a no solvent and during phase separation, a first phase rich in polymer forms the matrix and the second phase poor in polymer creates the pores. In track etching [1-4], the polymeric film is irradiated to create tracks followed by acid etching. Leaching is based on extrusion of the polymeric row material added with the solid particles followed by the extrusion of the solid, leading to pores

formation [1-4]. In thermal precipitation [1-4] cooling of a mixture of a polymer with a solvent is applied to enable phase separation followed by extrusion of the solvent. Stretching technique [11, 23, 24] is based on the stretching of a polymer film containing a dispersed phase whereupon stretching pores are created due to stress concentration at the interface of these sites or stretching specific crystalline morphology. In the particle stretching process, the polymeric material is mixed with solid particles, this mixture is extruded, and pores are formed during stretching in the interface between the polymer and solid particles.

Phase separation is the most employed technology to produce polymeric membranes. Nevertheless, environmental concerns have to be considered, such as solvent contamination and costly solvent recovery is two drawbacks for solution casting, although some improvements have been made in the recent decade [1-5]. The commercial production process has been commercialized by Asahi and Tonen (Japan), Entek (USA), SKC (South Korea), Jinhui and Senior (China), for the production of microporous high-density polyethylene membranes [15, 16].

Among the technologies to create an inexpensive and environmentally friendly membrane, there is one technique, which is applicable to semi-crystalline polymers, which is based on the stretching of a thin film with a row nucleated lamellar structure. In this case, pores are created as a result of lamellae separation. This

stretching technique is commonly known as MEAUS (melt extrusion – annealing – uniaxial strain), based on three consecutive stages to obtain porous membranes.

Firstly, it involves the production of a precursor film, possessing a row-nucleated lamellar structure, through shear and elongation-induced crystallization of the polymer. Secondly, the precursor film is annealed to remove imperfections in the crystalline phase and to increase lamellae thickness. Finally, the annealed precursor films are uniaxially stretched along the extrusion direction, to create and enlarge pores, giving, as a result, a porous material.

In MEAUS process, the extrusion and production of the precursor films is a delicate process since the samples should be produced under high draw ratio and cooling rates. Obtaining a very uniform film is a major concern since any non-uniformity and thickness variations cause irregularities in the stress distribution. This method is relatively less expensive and there is no solvent contamination. Some drawbacks of the technology and industrial market of this products are the difficulty to have a homogenous distribution of the pore morphology created, and the narrow range of polymers that are able to create the initial row-lamellar structure, being the most employed in the industry polypropylene [11, 28].

This methodology has been commercially used for the production of polypropylene and high-density polyethylene microporous

membranes, by companies such as Celgard (USA), Ube (Japan) and Senior (China) [17].

The first related patent was proposed in 1969 [7]. Although this kind of methods has been used to fabricate microporous membrane for more than 20 years for companies, mainly Celgard (USA), the reports about the detailed material – processing –structure-property relationship in the web of science were near zero before 2000. Even now, the related articles in the web of science are less than a hundred.

The main research group that has expanded the knowledge of microporous membranes produced with MEAUS process, above all concerning to polypropylene systems, has been the one led by prof. Ajji of Montreal [28], and in a minor extent the research group of Caihong [11]. Prof. Arencón had a staying with the research group of prof. Ajji and has initiated a research line in the field of membranes in our research group [29, 30].

Nevertheless, in some applications, the properties of polypropylene microporous membranes obtained by MEAUS does not fulfill the industrial requirement. Sometimes, it may be necessary the increase of the stiffness of the membrane, and or increase the thermal performance of based polypropylene blends. One classical method to overcome these issues is based on the addition of mineral fillers. Mineral fillers most employed in the polymer industry are calcium carbonate, talc, and glass, being employed in several industrial fields.

In this sense, in the 90's Nakamura and Nago [31, 32]. worked in the production of microporous membranes of PP/calcium carbonate by extrusion. The porous were created just by debonding of calcium carbonate from polypropylene matrix and/or removing calcium carbonate by solution methods. Recently, some works have tried to produce microporous membranes of a filled polymeric system, with MEAUS process. Nevertheless, these fillers are not the most produced in polymer compounding industry, as raw materials for extrusion and injection moulding processes.

Using magnesium sulfate whiskers as a filler showed that the strength along the Machine Direction (MD) decreased by increasing in magnesium sulfate whiskers content. Whereas the strength increased along Transverse Direction (TD) when the amount of magnesium sulfate whiskers is low. Caihong *et al* [33], based on their investigation, illustrated that an increase in the mechanical properties of the Transverse Direction (TD) for polypropylene microporous membranes occurs by adding a small content of magnesium sulfate whiskers.

Cai *et al* [34], by adding silicon dioxide into polypropylene microporous membrane designated an improvement of mechanical properties, an increase in the modulus and a structure. Tensile strength at break and yield strength will increase by using silicon dioxide. Tabatabaei and Saffar [35, 36], to optimize annealing and stretching conditions, they used fast cooling as it is used in MEAUS

process, membrane performance and changes in the crystalline structure were investigated in details by developing the polypropylene microporous hydrophilic membranes.

The aim of the present thesis is to develop microporous membranes obtained by MEAUS processes, by using more conventional industrial fillers employed in polypropylene blends, such as calcium carbonate and talc. Commercial grades of calcium carbonate and talc will be used. Concerning talc, differences in particle size, morphology and aspect ratio will be analyzed.

Up to now, no works are found in the literature concerning the use of calcium carbonate or talc in microporous membranes obtained by MEAUS processes (involving high draw ratios and very fast cooling). Potential enhancement of mechanical performance in terms of stiffness and thermal stability is expected. Also, changes in the crystallization mechanisms of polypropylene due to the presence of filler are affected. These changes can affect the row lamellar structure generated during the production of the precursor film, and then affect the final pore morphology created.

1.2 Aims of the work

The main aim of the work is the development of microporous membranes of PP/calcium carbonate and PP/talc, by MEAUS processing technology. From this main aim, several specific aims are derived:

a) Production at laboratory scale of stable and uniform thickness precursor films of polypropylene compounds by MEAUS, with different filler contents (1, 5, 10 wt. %).

b) Analyzing the influence of the type of extruder employed on the membranes produced (single or twin-screw extruder).

c) Evaluate the evolution of the crystalline phase orientation due to annealing of the precursor films.

d) Evaluate the influence of annealing temperature on the crystalline phase orientation.

e) Analyze through differential scanning calorimetry, the nucleation efficiency of the different fillers employed.

f) Analyze through differential scanning calorimetry, changes of the melting of crystalline phase on precursor films – annealed precursor films – membranes.

g) Analyze the thermal resistance of the membranes through Thermogravimetric Analysis (TGA).

h) Analyze the surface pore morphology of the membranes.

i) Analyze the permeability performance of the membranes.

j) Analyze the tensile properties of the non-annealed and annealed precursor films.

1.3 Personal motivation of doctoral

The doctorand has worked for Iranian industries and knows that calcium carbonate membranes are used in a vast area. In case of filtering the outflow gases from flares in refineries or oil productions, the calcium carbonate microporous membrane is deploying for separating of harmful gases from using one.

Separation of well stream gas from free liquids is the first and most critical stage of field-processing operations. The composition of the fluid mixture and pressure determine what type and size of the separator are required. Calcium carbonate microporous membranes can also deploy in well-head separators, where they are implanted on the top of the inner perforated plates (scrubber) for helping separation of water, gas and possible solid particles like sands from oil.

In the drilling industry for having the pure drilling mud to inject into the annulus, it needs to have a separation system for returning mud from the bottom of well, in which the returning mud is mixed with solid particles and possible fluids inside the well. Moreover, by using calcium carbonate microporous membranes as separators we might able to separate solid parts and more importantly other liquid phases that mixed with the mud inside the well.

The largest application, currently under development, is the production of CO_2 from flue gases from gas-fired cogeneration plants and re-use in greenhouses. Membrane gas absorption based on the

novel absorption liquids and porous polyolefin membranes is an efficient technique for the removal of sulfur dioxide from various burning flare gases. A feasibility implement has demonstrated that the sulfur dioxide can be captured economically from flue gas on a large scale.

On outgassed talc, the adsorption of water which seems to occur through the growth of hydrogen-bonded clusters anchored on the Hydroxyl groups controlled by the presence of highly hydrophilic sites isolated on a hydrophobic surface. Hydroxyl, groups of the octahedral layer mainly control the surface behavior of talc, which points directly toward the basal surfaces, because of the perfect trioctahedral nature of the mineral. In the natural state, organic and inorganic species are adsorbed on the talc surface and screen these highly energetic sites.

Talc then behaves like a special material as very strong interaction occurs between the Hydroxyl groups and polarizable molecules. It can then be considered as microscopically very hydrophilic. On such a surface, water adsorbs through the growth of hydrogen-bonded clusters over the Hydroxyl sites, so it should be expected a water absorption in such kind of water-oil separator systems.

CHAPTER 2

LITERATURE REVIEW

2.1 Definition of membranes

A membrane is a semi-permeable barrier to separate components of a solution or particles dissolved in a fluid due to their chemical or physical properties when a driving force is applied. Figure 2.1 shows schematically the working procedure of a membrane. Also, when material as a flux restrictor, this can be considered industrially as a membrane. This process, in contrast with simple filtration, is a continuous process where there is a progressive variation of the concentration, without any change of state of the separation material nor any solid accumulation of material on the separation material.

In nature, there are membranes that fulfill the definition mentioned previously, and they are called biological membranes. The biological membranes carry out a key role, for example in the exchange of cells with the surrounding environment. These biological membranes have currently a limited industrial application [1]. For several purposes, synthetic membranes were developed and successfully applied in selective separations from mid-'50s [1-6].

It is necessary for a membrane to act as a separation material, that the membrane is sensitive to one or several molecular or physic-chemical properties. To provide this role, the membranes have to have certain chemical properties or some special structure. Also, it is necessary a driving force, that is, a difference of the physic-chemical magnitudes between the phases that is manifested as a gradient

through the membrane, being able to create a flux of components. Some examples of driving forces are gradients of pressure, concentration, temperature or an electrical voltage.

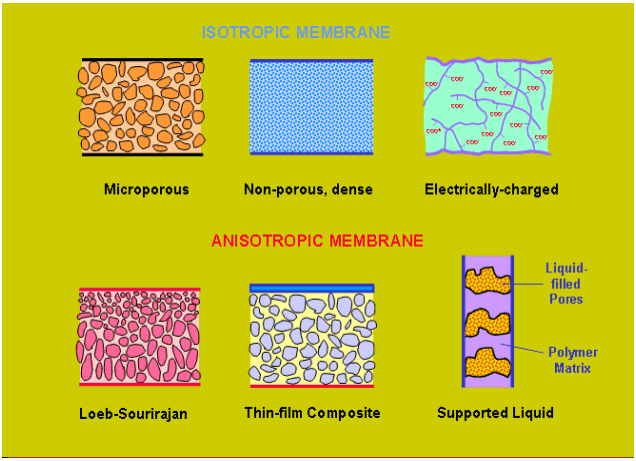

Figure 2.1 Schematic illustration of various polymeric membranes [1].

2.2 Symmetrical and asymmetrical (membranes)

The type of structure of the membrane has a decisive influence on its separation ability and/or as a flux restrictor. One of the main structural criterions to categorize membranes is bases in its symmetric or asymmetrical structure [1-6].

2.2.1 Symmetrical membranes

Symmetric membranes refer to the membranes with uniform structure (uniform pore size or nonporous) throughout the entire membrane thickness [37]. Symmetric membranes are used today mainly in dialysis, electrodialysis, and to some extent also in microfiltration [38]. The thickness of symmetric membranes is usually between 30 and 500 μm. The total resistance of the mass transfer relies on the total thickness of the membranes. Hence, a decrease in membrane thickness results in an increased permeation rate. They contain uniform structures and can be subdivided in porous membranes, Membranes with symmetric pores are more uniform, while asymmetric pores have variable pore diameters. In addition, porous membranes are mostly used for microfiltration and ultrafiltration, as separation is based on particle size, while non-porous membranes are used more for nanofiltration and reverse osmosis processes.

Porous membranes have physical pores. The pore size and the pore shape are the most important factor that determines its performance as separators/flux restrictor. Their mechanism is based on the fact that they allow the transit of substances molecular sizes lower than the pore size of the membrane, and reject the substances with too large size. Generally, only components, which differ considerably in their particle size can be separated by this type of membranes (Figure 2.2).

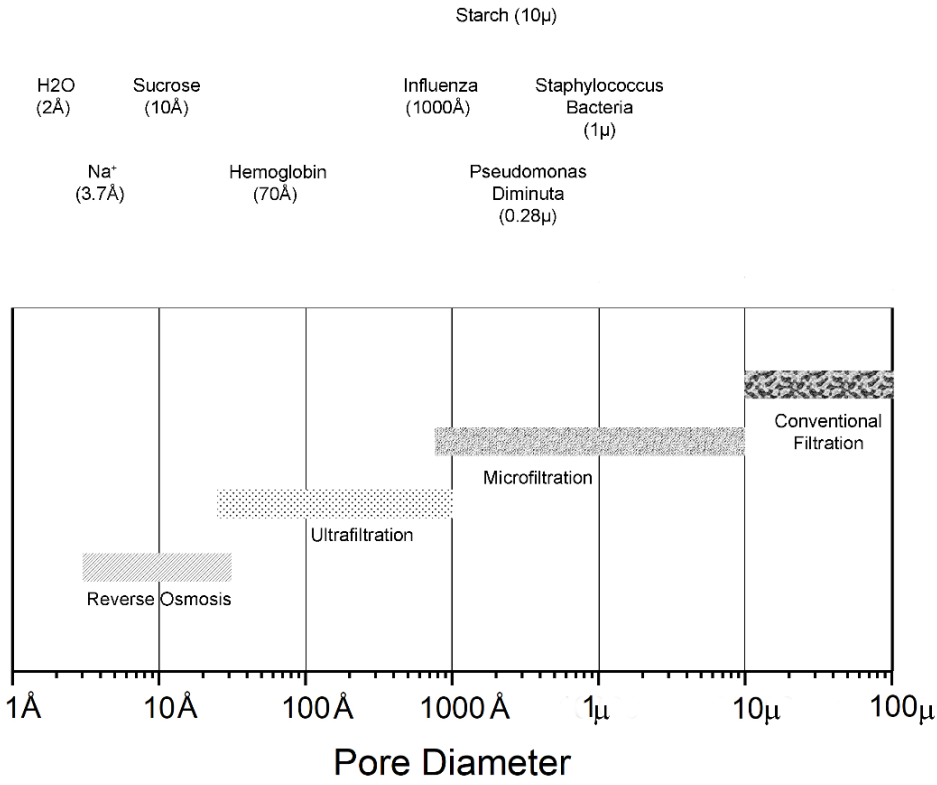

Figure 2.2 Particle size of separated components by a membrane [39].

Non-porous membranes do not contain macroscopic pores. Usually, they are a solid film, through which permeates a component by diffusion under the driving force of a pressure, concentration, electrical potential gradient (or a combination of two or three). The main mechanism is adsorption and diffusion of components through the membrane, which is a function of diffusivity and solubility of the permeate. With this technique material with similar size can be separated due to a difference in their diffusion rate through the membrane (which depends on their solubility in the membrane).

In electrically charged membranes separation is obtained by extrusion of the particles with the same charge. Electrically charged membranes can be dense or microporous, but are most commonly very finely microporous, with the pore walls carrying fixed positively or negatively charged ions. A membrane with fixed positively charged ions is referred to as an anion-exchange membrane because it binds anions in the surrounding fluid. Similarly, a membrane containing fixed negatively charged ions is called a cation-exchange membrane. Separation with charged membranes is achieved mainly by exclusion of ions of the same charge as the fixed ions of the membrane structure, and to a much lesser extent by the pore size. The separation is affected by the charge and concentration of the ions in solution. For example, monovalent ions are excluded less effectively than divalent ions and, in solutions of high ionic strength, selectivity

decreases. Electrically charged membranes are used for processing electrolyte solutions in electrodialysis [1-4].

2.2.2 Asymmetrical membranes

When a higher permeate flux is required, asymmetrical membranes are commonly employed. This kind of membranes has a skin-core structure. The skin is also called active layer and it is normally thinner than the core. The skin is the place where the separation usually takes place. With the aim of having a global increased strength of the membrane, the skin is formed/supported onto a substrate (core). The core is usually a porous membrane with higher thickness than the skin.

2.3 Main separation/flux restrictor processes that employ membranes

2.3.1 Microfiltration, ultrafiltration, nanofiltration, and inverse osmosis

These processes have in common pressure as a driving force. The pressure of the feeding substances is increased using a pump. Although the feeding pressure can be to some extent diminished at trespassing the membrane, it is at a higher pressure than one of permeate substances, creating a pressure gradient through the membrane. Another common characteristic of these processes is that both permeate and feeding substances are liquid. These four

processes are usually employed to concentrate or purify liquid aqueous solutions [1, 40].

In microfiltration and ultrafiltration, the separation mechanism is based on size, having an enormous influence on the separation performance the pore size and its distribution along the membrane. In both processes, an increase of the feeding speed leads to a build-up of the permeate flux. Microfiltration is able to separate small particles and ultrafiltration is able to separate macromolecules.

Concerning inverse osmosis (also known as hyperfiltration), the separation mechanism is based on adsorption-diffusion. The permeate components must have some affinity with the components of the membrane, to get adsorption/dissolved into its structure. That is the reason for the most important role that material selection has in order to produce membranes for inverse osmosis, rather than the ones used form microfiltration and ultrafiltration [40].

Nanofiltration is an intermediate process between inverse osmosis and microfiltration, as the separation mechanisms is a combination of size exclusion and adsorption/diffusion. In inverse osmosis and nanofiltration, it is not so important the feeding speed, having instead a key role in the osmotic pressure. The membranes for these two processes are commonly less permeable than the ones of micro and ultrafiltration. That causes that the pressure gradients employed are higher.

2.3.2 Dialysis

This process is carried out between two aqueous flows, but in this case, the driving force is a concentration gradient between these two phases. The separation takes place due to the different diffusion speeds of the two components through the membrane [1-4].

2.3.3 Pervaporation

The driving force is the chemical activity gradient that it is to have a very low partial pressure on the permeate substance (in the gas phase). In this process, the feeding is a liquid pushed at atmospheric pressure, that sometimes can be heated. In the permeate side of the membrane, the partial pressure must be low enough to the substances which have to permeate. This is achieved either the use of an inert gas carrier with a pressure close to the atmospheric pressure that drags the permeate substance or through creating a vacuum pressure [1-6].

2.3.4 Gas permeation

In this process, the driving force is a pressure gradient created between two gaseous phases located at both sides of the membrane. The separation is achieved due to either difference in the adsorption-diffusion mechanism than gases have on non-porous membranes, or different Knudsen flow behavior that is displayed by porous membranes [1,4, 6, 7].

2.3.5 Liquid membranes

Here, the driving force is a concentration gradient. This is a process where the membrane does not consist of a solid phase, but a liquid one. Two types of membranes are employed in this process: membranes where the liquid is immobilized within porous membranes, or emulsion liquid membranes [1, 2, 6, 7].

2.3.6 Electrodialysis

It is based on the ability of some membranes to get electrically charged, avoiding the movement on one direction of ions that have the same electrical charge that the electrical charge of the membrane. By this way, the membranes can be classified in anionic, cationic and bipolar. An electrical field between two electrodes create ions that are selectively separated based on the different electrical charge [1-4].

2.3.7 Distillation and thermo-osmosis

In distillation, the separation is possible due to vapor pressure gradients, acting as the driving force, the difference of temperature between the phases. The membrane is usually porous with a marked hydrophobic character. The vapor is condensed in the permeate that circulates in backflow. The membrane acts simply as a barrier, not influencing the selectivity. The thermo-osmosis process uses the same separation principle. In this process, it is set a volumetric flux from the hotter phase to the colder one [1-3].

2.3.8 Other processes

Per-extraction is a special extraction carried out with membranes that get in contact the feeding substance with an extracting dissolvent phase (membrane contactor). Piezodialisis uses pressure gradient as driving force and it is carried out between two liquid phases; it is different from inverse osmosis, as the ionic solutes permeate in the higher degree through the membrane due to an interaction between electrical charges [1-3].

2.4 Fabrication of polymeric membranes

Among various techniques to make membrane the four major production methods for polymeric membranes are phase separation, irradiation, sintering, and stretching.

2.4.1 Phase separation

A polymer with other component phases is separated by adding a non-solvent, cooling or solvent evaporation. The first phase is rich in a polymer that forms the matrix and the second is poor in a polymer that forms the pores. Except for the polymer, the other components will be removed later to stabilize the structure. The control of the precipitation conditions helps to control the membrane morphology.

The most common method is that known as Leob-Souirajan based on phase separation by immersion in a non-solvent (Cheryan, 1998)

[39]. Almost all the reverse osmosis, ultrafiltration and many gas separation membranes are produced in this way. The process is illustrated in Figure 2.3. A solution usually of 20 % dissolved polymer is cast onto a moving drum. As the drum goes into the water the polymer is precipitated and forms a dense layer on the top. The dense skin thickness varies from 0.1 to 1 μm, and this skin will act as a barrier for further water permeation from the depth.

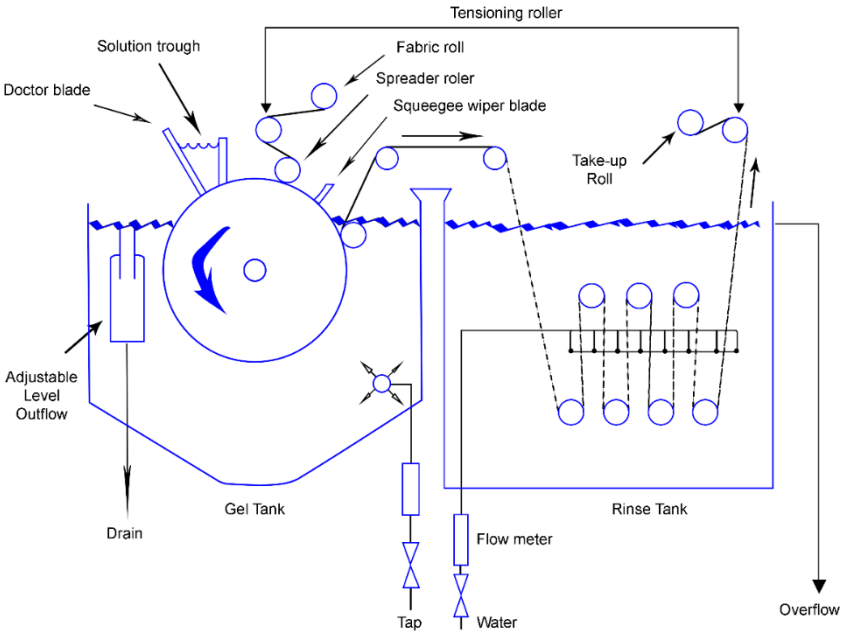

Figure 2.3 Loeb-Souirajan process [39].

This cause very slow precipitation for the under layers, which gives more time for the formation of large pores. The ideal case is to make the skin as thin as possible and defect free. The pores (if are formed) in the skin are very small in the range of nanometer. The thickness of the skin is usually around 50 to 100 nm and the total membrane thickness goes over 50 μm. A ternary diagram in Figure 2.4 shows the phase evolution during the membrane formation.

The precursor solution is at point A and it moves towards B as the precipitation begins. At point C a solid rich polymer is formed as a

solid dense layer is in equilibrium with another phase that is liquid poor in the polymer. The composition is fixed at D where the non-solvent is extracted totally. Kinetics of the process determines the time of the pathway of A-D. one example of this type of the membrane is DuPont polyamide membrane.

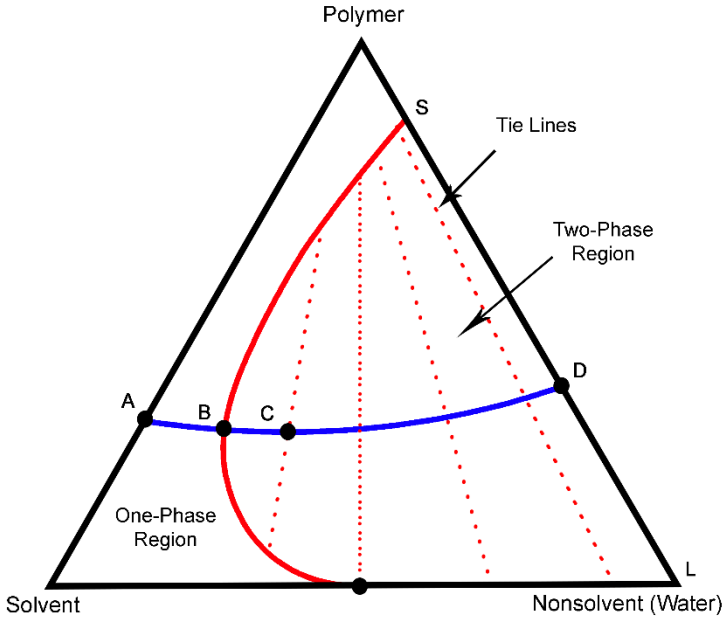

Figure 2.4 Phase diagram showing the composition pathway traveled by a casting solution during the preparation of a porous membrane A: Initial casting, B: Point of precipitation, C: Point of solidification [39].

2.4.2 Irradiation

The polymer film is exposed to a flow of charged particles generated from an irradiation source. Typical polymers employed in this technology are polycarbonate or polyethylene terephthalate [41], This will cause the chain scission and damaged tracks, which with further etching leads to cylindrical pores along the thickness. The time period of exposition and the etching time determine membrane performance such as pore diameter. For this membrane, the tortuosity is very close to 1 (Figure 2.5). Usually, the porosity of this kind of membrane is very low and therefore the flux is small. However, this membrane is used when a precise analytical separation is to be carried out. This kind of membrane was initially developed by *Nucleopore Corp* [39].

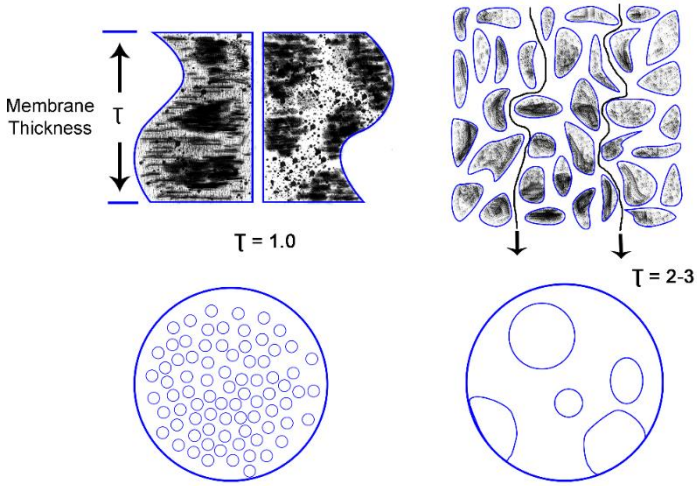

Figure 2.5 Phase diagram showing the composition pathway traveled by a casting solution during the preparation of a porous membrane A: Initial casting, B: Point of precipitation, C: Point of solidification [39].

2.4.3 Sintering

It is a process to obtain porous membranes that consist of the compression of powder (organic and/or inorganic), under a temperature a bit lower than the melting point. In this way, through solid state diffusion processes, it is achieved a partial melting that will agglomerate the powder particles. As a result, a compact porous structure is generated. Higher sintering temperatures need lower times of processing. The pore size ranges between 0.1-10.0 μm [42].

2.4.4 Stretching

Stretching of sheets of filled polymers

In this manufacturing process, a filled polymer blend is extruded in order to produce a sheet. This sheet is subsequently stretched, generating a porous structure, due to the weak interfacial adhesion polymer/filler. The porous structure is due to the debonding of mineral filler from the polymeric matrix, and a further crack propagation along that interface.

This kind of membranes generally contains big pores (in the range of 1 μm). The porosity and pore distributions depend mainly on the filler content, the interfacial adhesion filler/particle, the dispersion and distribution of filler within the polymer matrix and also the film thickness. Typical size filler employed ranges within 0.4-4.0 μm. Using a filler larger than that might limit the stretchability and create a non-uniform pore distribution and, in some cases, the breakdown might occur.

The amount of the inorganic filler to be added should be sufficient to attain the desired porosity, but it depends to some extent on the kind and particle size of the inorganic filler. Inorganic fillers such as calcium carbonate are preferably surface treated to be hydrophobic so that the filler can repel water to reduce agglomeration of the filler.

Different inorganic fillers can be used, as for instance calcium carbonate and barium sulfate. Nago *et al* [32]. developed porous membranes by biaxial stretching sheets of a mixed polypropylene with an inorganic filler ($CaCO_3$). By decreasing the mean particle size of the filler, the effective porosity increased and also the equivalent pore size decreased.

Stretching of polymeric immiscible blends

In this method, the membranes are obtained due to the interfacial debonding of immiscible polymer blends, which results in a porous membrane. An accurate dispersion of the minor component is the key factor to control de pore size [5, 6].

Stretching of polymeric precursors in a dissolvent

In this methodology, firstly used by Williams *et al* [6]**,** a polymeric film containing at least two components, is submerged in a solvent. The minor component of the polymer film is dissolved. Then, the film in solution is stretched uniaxially or biaxially and finally while the film is stretched, the solvent is evaporated, creating a porous membrane.

Stretching and transformation of b-crystalline structures

This process is based on the allotropic transformation that some semicrystalline polymers, as for example polypropylene [37]**,** display. The most common crystalline structure of PP is monoclinic (α),

whereas hexagonal (β) is less usual. For the generation of β-crystals, specific nucleating agents are used, along with control of cooling speed. β-crystals are metastable and under certain temperature and strain conditions convert to α-crystals. This change leads to a volumetric shrinkage of polymer that generates a porous morphology [5, 6-8].

Stretching of precursor films highly oriented

This procedure has three stages. Firstly, precursor films are obtained through extrusion with a high orientation of the crystalline phase, along with a crystalline structure called “row nucleated”. Secondly, precursor films are annealed to increase lamellar thickness and to eliminate crystal imperfections. Finally, a uniaxial strain is applied to the annealed precursor films to nucleate pores and allow them to be enlarged. This process is commonly known as MEAUS (melt extrusion – annealing – uniaxial strain) [6, 36].

2.5 Analysis of MEAUS technology

2.5.1 Flow-induced crystallization of precursor films background

When a semicrystalline polymer crystallizes under stable conditions, without any external perturbation, the melted polymer normally crystallizes in a spherulitic structure. A large number of works in the literature dealing with the crystalline structure of polymers accounts for the spherulitic growth from polymer melts [42, 43].

Nevertheless, in most industrial technologies that involve the melting of polymers, the melted polymers are under some kind of external stress during its crystallization. This external stress leads to the development of other crystalline morphologies, different from that of the spherulitic pattern [44].

When a semicrystalline polymer crystallizes under flowing and or stretching simultaneously, the resulting structure is often a row nucleated one. These conditions are the one than semicrystalline polymers are subjected in industrial processing technologies as for example extrusion-calendering. Analogous structure to the row nucleated is formed when polymer solutions are stirred or forced to flow. In both cases, the basic structure is probably the same, but when they are obtained from polymeric solutions, they usually are known as shish-kebab structures [45].

During the row-nucleated crystallization, initially, some macromolecules get aligned along the flow/stretching direction, to generate macromolecules with a crystalline structure quite extended (Figure 2.6a –b). In this case, the end-chains of the macromolecules are not perfectly aligned, but they are staggered through the shish (Figure 2.6c). These non-aligned areas are shish areas that will nucleate the lamellar crystallization. Lamellae grow in the perpendicular direction with respect to shish (Figure 2.6d), giving, as a result, a crystal stacking. The final result is a crystalline structure with amorphous areas.

The final row-nucleated structure has most of the macromolecules as lamellar structures that have grown in a large extent (Figure 2.6e). That makes difficult to quantify the percentage of macromolecules that are part of the central core. It is usually assumed that it is obtained a shish-kebab (solution) or row-nucleated when this lamellar stacking is observed (Figure 2.6f) [46-48].

It must be considered that depending on the applied stretching/strain on the polymer flow, torqued kebabs can be generated (low-stress level), whereas a high-stress level produces plain kebabs, in which the lamellae grow radially onto the shish without torsion.

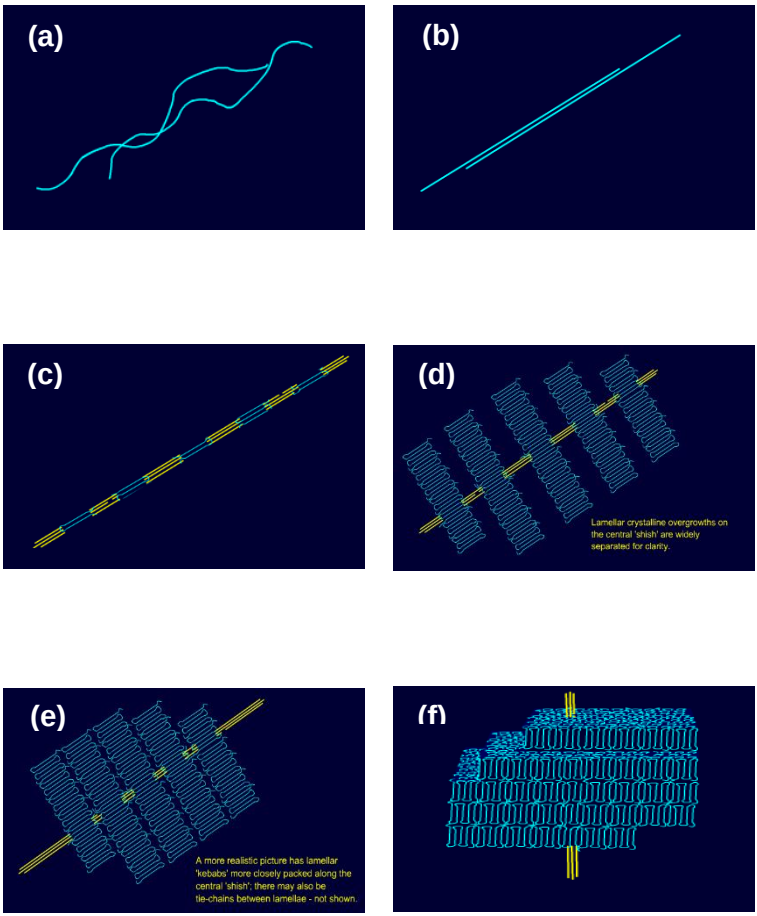

Figure 2.6 Generation of row-lamellar structure [46].

2.5.2 Production of precursor films with a row-lamellar structure

As stated previously, semi-crystalline polymers with a stacked lamellar morphology can be produced as a result of stress-induced crystallization. Johnson [45] introduced a set of criteria to help in the selection of semi-crystalline polymers capable of forming microporous membranes via crystal lamellae separation. The proposed criteria are fast crystallization kinetics, a highly planar lamellar morphology for the extruded film, the high orientation of the crystalline phase, proper film thickness, and the presence of an α relaxation.

Extrusion-Calendering processing can provide these conditions. In extrusion-calendering, a rectangular die is adapted to the extruder, and then a roll-calendering system is responsible to apply a high stretching that will provoke a high macromolecular alignment along the extrusion direction.

Influence of cooling speed

To avoid that macromolecular relaxation diminishes this degree of orientation, rapid cooling is necessary just the polymer melt comes out from the extrusion die**.** In this sense, the use of semicrystalline polymers with fast crystallization kinetics will help to the macromolecular alignment without relaxation after the rapid cooling. Also, a low film thickness, is beneficial, in terms of providing rapid cooling of the polymer melt.

Influence of stretching speed

The stretching speed applied (speed of calendering rolls) influences the shear flow and the elongational flow of the polymer. The shear flow is generally considered as a weaker flow so as to extend macromolecular chains, as only macromolecular with a certain length above a critical value are able to create stable row-nucleated structures, whereas the rest of macromolecules are not oriented [9, 45].

Higher stretching speed leads to a higher global macromolecular orientation. The higher amount of highly extended macromolecular crystals, the higher the number of nucleation sites, and thus, the higher the number of lamellae. It is defined as lamellar torsion and/or inclination and global crystalline orientation, as the distance between extended macromolecules [41]. If it is generated a structure with a reduced number of extended macromolecules, there is a big spacing between macromolecules, which leads to the generation of a spherulitic structure or similar.

On the contrary, a high number of oriented macromolecules with small room between them will lead to a partial or non-remarkable lamellae torsion, which will result in a stable macromolecular orientation. It has been proved [15] that a higher crystalline orientation due to higher stretching conditions helps to the further lamellae separation that creates pores. Sadeghi *et al* [43] state that an

orientation factor (obtained by polarized FT-IR) higher than 0.3 is necessary to obtain polypropylene membranes.

Influence of molecular weight

The movement of polymer macromolecules under strain fields is based on several factors, such as the entanglement density, the friction ratio between the macromolecules, its rigidity and the relaxation time, between others. In isothermal conditions, the molecular weight and the macromolecular architecture play an important role in the control of the elongation and stability of the obtained structures [43, 46].

Polymer macromolecules with high molecular weights and/or branching need more time for the relaxation, and thus, there is a higher probability that the applied orientation is maintained. Low molecular weight macromolecules get relaxed in short time after straining, and thus, have difficulties to create stable nucleation sites [28, 47] that would promote further lamellar crystallization.

Figure 2.7a shows schematically the crystallization model, using linear macromolecules, proposed by Kitade *et al* [48]. When the polymer melt is cooled, punctual nuclei sites appear (such as the local orientation of macromolecules or packing between polypropylene helix) (A-1). Once shearing is applied, the longer macromolecules start to orientate due to a higher relaxation time, and when the segments of this macromolecules get in touch with the primary nuclei

sites, it is created a physical interconnection that gives as a result pending macromolecule (A-2). These pending chains, subjected to a straining due to shearing, provoke the creation of new nucleation sites along the oriented macromolecules. That leads to the creation of precursor in a fibrillar, which act as a starting site for the perpendicular lamellar (A-3).

Figure 2.7b shows the Kitade *et al* model [48], for shear-induced crystallization of a highly branched polypropylene, with high molecular weight branches. The authors considered that an increase in the number of branches is potentially beneficial for the generation of a higher number of nuclei sites, due to an increase of macromolecular entanglement. This higher entanglement provokes longer relaxation times than those of linear macromolecules (B-1). The entanglements favor the macromolecular orientation (helped by the applied shearing), and gives place to the creation of a large number of crystallization sites, that along with the rest of oriented macromolecules promote a fast creation of fiber-like structures (B-2). Nevertheless, due to the high percentage of branching, it was observed the impossibility of perpendicular radial growth of secondary lamellae (B-3).

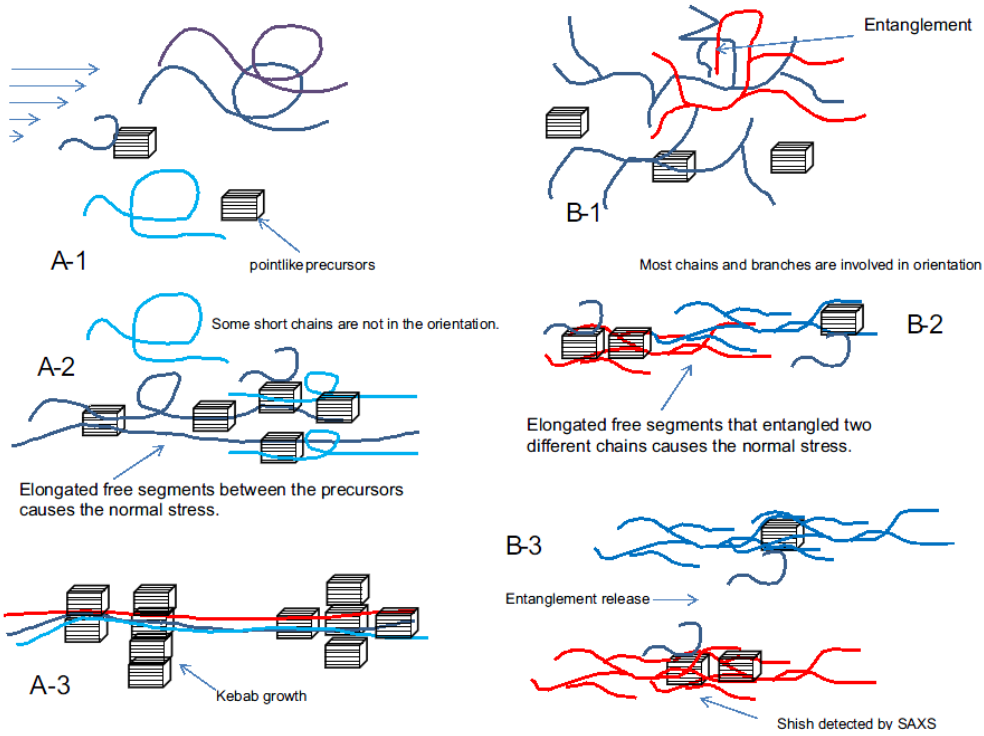

Figure 2.7 Effects of the introduction of macromolecules with long branches [48].

Somani *et al* [49] investigated the role that the high molecular macromolecules had on the development and generation of oriented structures of two isotactic polypropylenes, under shear flow. They concluded that the samples with a higher percentage of longer macromolecules exhibited a higher fraction of oriented crystalline phase, along with faster crystallization kinetics. Moreover, they found

that the time to create shish, initiated from the macromolecular segments already aligned, was shorter for the sample with higher molecular weight. Similar results have been reported by Zuo [50].

Sadeghi *et al* [43] found that the resin with a higher molecular weight tended to form a planar crystalline morphology. In another work, they reported that the addition of up to 10 wt. % of a high molecular weight component to a low molecular weight one enhanced the formation of the row-nucleated structure.

Usually, the low molecular part is unfavorable for the formation of an initial crystalline structure. However, it was found that for PP resin with certain high molecular weight chains, the existence of low molecular weight tail was also important to the deformation and stabilization of pore structure [24]. The existence of low molecular weight tail resulted in higher lamellae thickness in the precursor film and higher content of connecting in the cold-stretched film.

2.5.3 Annealing of precursor films

This stage has the aim to eliminate defects of the crystalline structure, increase the orientation of the crystalline phase and raise the thickness and uniformity of lamellae (Figure 2. 8). During annealing, the macromolecules of the amorphous phase usually alter its oriented configuration, so as to convert to a randomer configuration. The importance of annealing of the formation of a porous structure was firstly elucidated by Sprague *et al* and confirmed

by other researchers [53-55]. The three key factors involved during the annealing stage are the annealing temperature, the annealing time and if the annealing is carried out under any external stress.

The annealing gives the possibility that lamellae get reorganized along the extrusion flow direction (machine direction, MD), giving, as a result, an increase of the orientation along that direction. The reordering and increase in the lamellae orientation would also affect to the ending of macromolecules, that act as union bridges between lamellae. That could be an explanation for the increase in orientation in the amorphous phase [21-23].

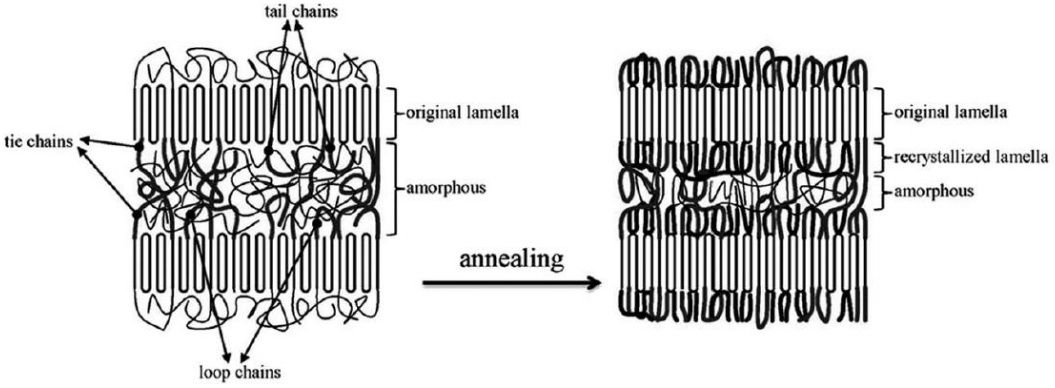

Figure 2.8 Effect of annealing in the crystalline phase [21].

2.5.4 Uniaxial strain

Once the precursor film has been annealed, the next step is to promote the lamellar separation that will create the porous morphology. This is carried out through a uniaxial strain of the precursor films along the extrusion direction. This process is usually done in two steps, with very different temperatures in each of these steps. Some authors also use the third step, consisting of a heat setting for a certain time, after the total uniaxial strain has been applied.

Cold strain

The first step of the uniaxial strain is commonly done at room temperature [41], also known as “cold strain stage”. The process to create a pore is mainly ruled by the stretching of two kinds of bridge macromolecules: the shorter macromolecules when reaching the maximum of the elastic region break, producing pores; the longer macromolecules, act as linking sites between crystalline lamellae and are responsible for the final elastic recovery [27]. It has been reported [26] that the use of high molecular weight polymers can lead to a higher elastic recovery during this cold strain, and thus in a lower number of pores created.

In the series work reported by Ajji group on unfilled polypropylene systems, the cold stretching ratio was set at 35-40 % [28, 35, 43]. Higher stretching ratio will induce the deformation of lamellae

structure. Sadeghi at el [43] attributed the pore initialization to the stretching and session of short tie chains. In fact, during cold stretching, the stretching and movement of the amorphous region are difficult due to the entanglement. In addition, the deterioration of the crystalline structure by stretching is unavoidable. Hence, it is necessary to clarify the origin of initial pores during cold stretching.

It is well accepted that cold stretching is carried out to initiate pores, but how to initiate pores is in fact unclear. The α crystal polypropylene shows specific mother-daughter crystalline structure. In the annealed film with a row-nucleated crystalline structure, main lamellae, melting and recrystallized regions, secondary crystallization from tie chains, daughter crystal and tie chains in the amorphous region coexist. Figure 2.9 gives the schematic or pore formation process. 10 % stretching lead to the pronounced increase of amorphous region thickness and the appearance of a few initial connecting bridges.

At this time, the daughter crystal content is decreased from 45 % to 29 % and the recrystallized part is decreased by 77.6 %. the stretching of daughter crystal and recrystallized part contributes to the formation of initial bridges. At stretching ratio of 30 %, uniform-distributed connecting bridges are observed. Here, except for the stretching of daughter crystal, the stretching of tie chains and secondary crystals within the amorphous region leads to the formation of more connecting bridges.

During cold stretching, the pores are formed progressively and the initial few pores are from the deterioration crystalline structure, not amorphous regions. At high stretching ratio to 100 %, the stretching of main lamellar occurs and lamellae deformation is inevitable. The stretching ratio of 30 %, situated at the transition point from the plastic plateau to the strain-hardening region in the stress-strain curves of annealed film, is appropriate for the initiation of pores.

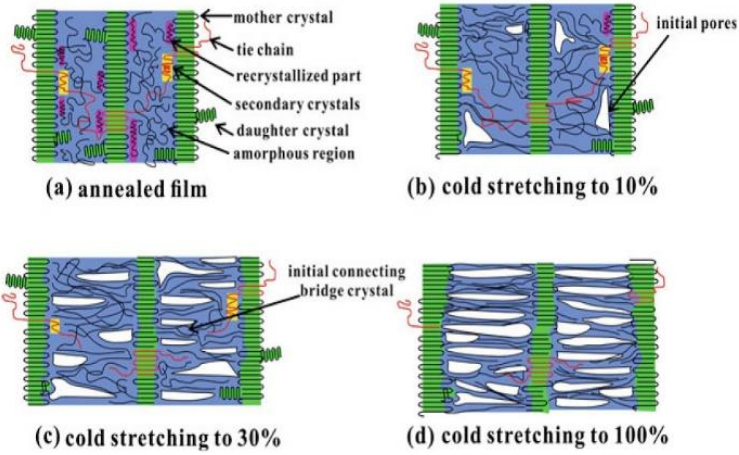

Figure 2.9 Schematic of initial pore formation during cold stretching [43].

Hot strain

The second step of this uniaxial strain is carried out at higher temperatures, in order to promote a pore size enlargement in a stable growth regime. Straining at higher temperatures provides higher ductility of lamellae [41, 43].

During the cold strain, the low macromolecular mobility hinders its sliding, and, as a result, there is a concentration of local stress on the macromolecular entanglements located at the amorphous zone (interlamellar), that promote the extraction of macromolecular segments from the crystalline areas. In the case of polypropylene, these strained macromolecules can transform in a mesomorphic phase (yellow color), which consists in oriented macromolecules, but without an accurate regularity to form stable crystals (green color).

Straining at higher temperatures, (normally 140 ºC reported for polypropylene [43]), promotes higher macromolecular mobility. This weakens the entanglement network of the amorphous zone. Finally, the applied stress disentangles these macromolecules, allowing to rearranging and folding, and creating new crystalline blocks.

Sadeghi *et al* [28] found that for a constant hot stretching level, the Gurley permeability (that measures the time that is needed for air to pass to a sample with standard geometry) decreased, which means that the permeability increased, as the temperature of the hot stretching was increased. Also, it was found that compared with cold and hot stretching under the same stretching rate and whole stretching ratio, the sample only by hot stretching showed lower Gurley value and better air permeability Figure 2.10 a) the membrane stretched 120 % T 105°C directly with Gurley Value 151 s/100 ml, b) the membrane stretched 15 % at room temperature and 105°C with Gurley Value 229 s/100 ml and c) the membrane stretched 15 % at

room temperature and 105 % at 145°C with Gurley Value 233 s/100 ml (Figure 2.10).

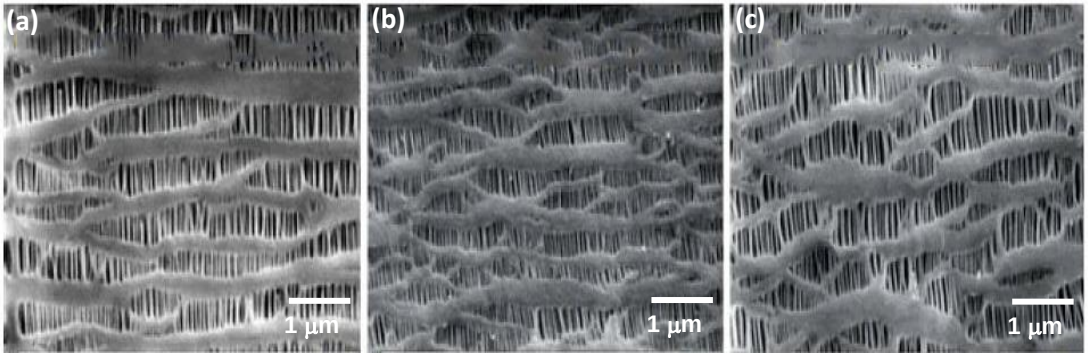

Figure 2.10 SEM surface morphology of hot stretched polypropylene membranes [28].

Compared with that by only cold stretching, the unrestrained tie chains due to the chain disentanglement at high temperature could be stretched and crystallized into bridges. At the same time, some unstable chains could also be pulled out from the initial lamellae and converted to the fiber connecting bridges. All these can contribute to the increase in bridge number after hot stretching but which one is more prominent in the formation of stable connecting bridges is still unclear.

During the direct hot stretching, the crystalline part is stronger than that of amorphous entanglement network. Hence, during the stretching under a higher temperature, the tie chains between the lamellae are stretched and converted to connecting bridges. Less

deterioration to lamellae structure occurs, resulting in better lamellae structure arrangement after stretching-induced lamellae separation.

Sadeghi *et al* [28] related the strain hardening observed in strain-stress curves of annealed precursor films (Figure 2.11), with the creation and crystallization of interlamellar interconnection bridges, where continuing the stretching some pores can be created and finally, the higher lamellar separation ends with the collapse of the sample.

Recent works have tried to develop porous structures using only a hot strain stage, omitting the cold strain stage [41]. Moreover, it has been studied the influence of the influence of the heat setting time previous to the release of the uniaxial stress [27, 28].

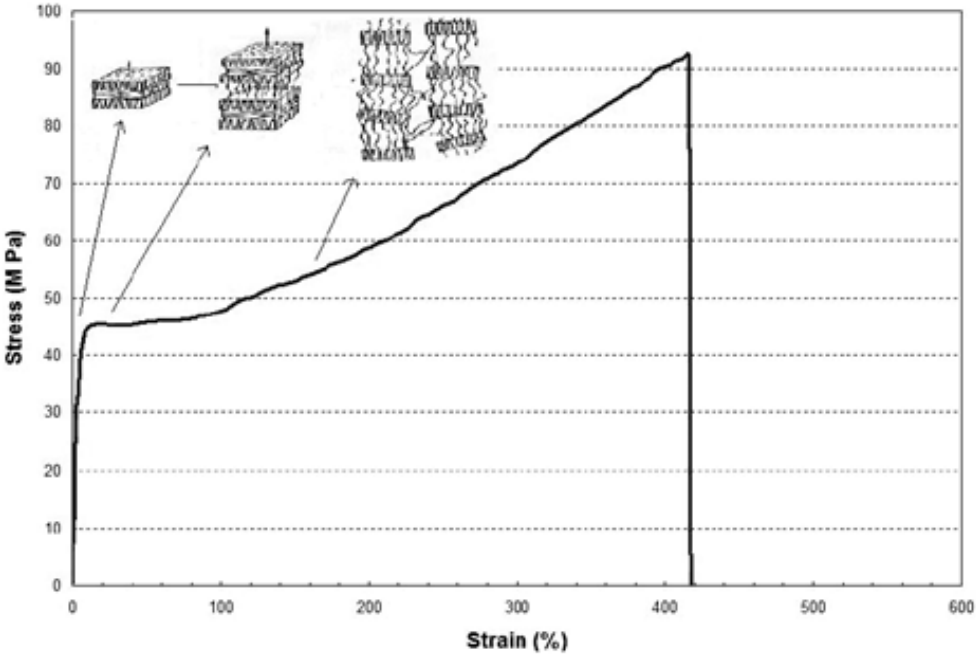

Figure 2.11 Evolution of the row-nucleated structure during uniaxial stretching [28].

Heat setting

Normally, the heat setting increases the crystallinity, leading to increased tensile strength and modulus. Also, the film after heat setting shows better dimensional stability because crystallization occurs. For the preparation of microporous membrane based on melt-stretching mechanism, the heat setting is necessary since the above-annealed film shows higher elastic recovery, the value of which is up to 96 % [28]. Since this, the annealed film is often called hard

elastomer. Without heat setting, the stretched pore structure could not be kept after the stretching stress is relieved. Figure 2.12 shows the SEM micrograph and property of stretched membrane heat set at different temperatures. With the increase in heat setting temperature from 115 to 145°C, the Gurley value is decreased from 245 to 190.

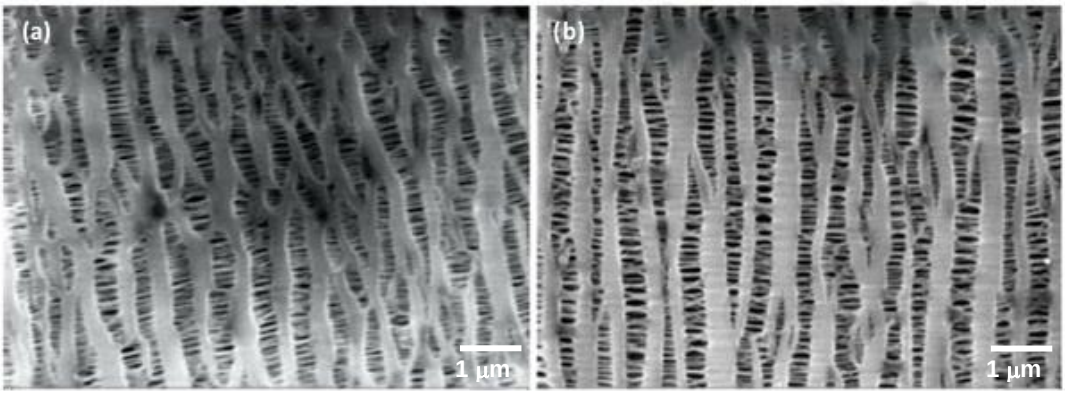

Figure 2.12 SEM surface morphology of stretched membrane heat set at different temperatures 135°C (a) with porosity 44.6 % and shrinkage percent 4.5 %. 145°C (b) with porosity 46.8 % and shrinkage percent 0.3 % [28].

CHAPTER 3

EXPERIMENTAL PROCEDURE

3.1 Materials

3.1.1 Polypropylene

A commercial extrusion grade with tradename PP020 kindly supplied by *Repsol* has been selected. The melt flow rate (230 ºC, 2.16 kg) was 1.0 dg/min. Average number and mass molecular weights were M_n =118466 g·mol^{-1} and M_W=658666 g·mol^{-1} respectively, showing a monomodal mass molecular weight distribution (Figure 3.1). This commercial grade has been proved [28] to provide an adequate viscosity for extrusion processing and its melt strength is high enough to support the high draw ratio imposed during the production of precursor films.

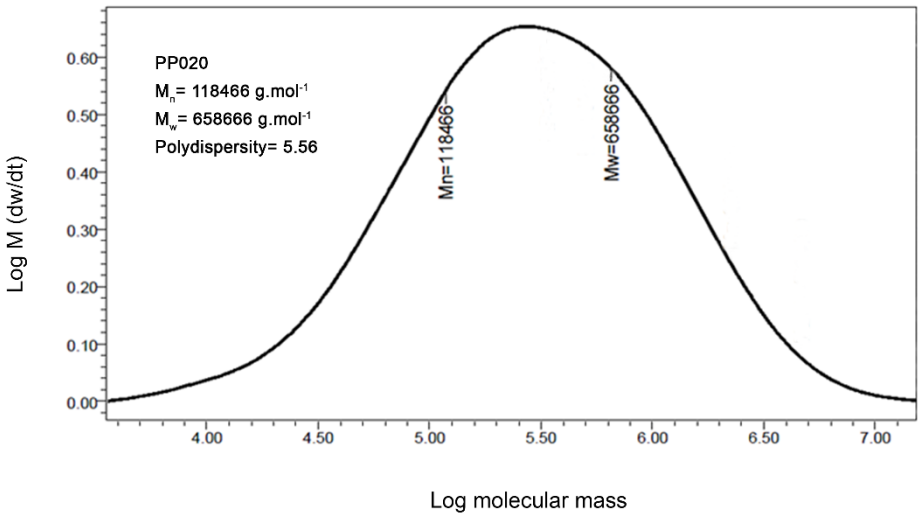

Figure 3.1 Molecular weight distribution of PP020 [28].

3.1.2 Mineral Fillers

An ultrafine surface-treated precipitated commercial grade calcium carbonate under trade name M 95T was supplied by *Reverté calcium carbonates* with an average particle size of 4 μm. The surface treatment is based on $MgCO_3$, Fe_2O_3, and amino group (Figure 3.2). Morphology of calcium carbonate particles can be observed in Figure 3.3.

Five different commercial talc grades differing in particle size, morphology, and specific surface area were kindly supplied by *Imerys*

Talc. The main features of them are summarized in Table 3.1 Morphology of talcs can be visually observed in Figure 3.3.

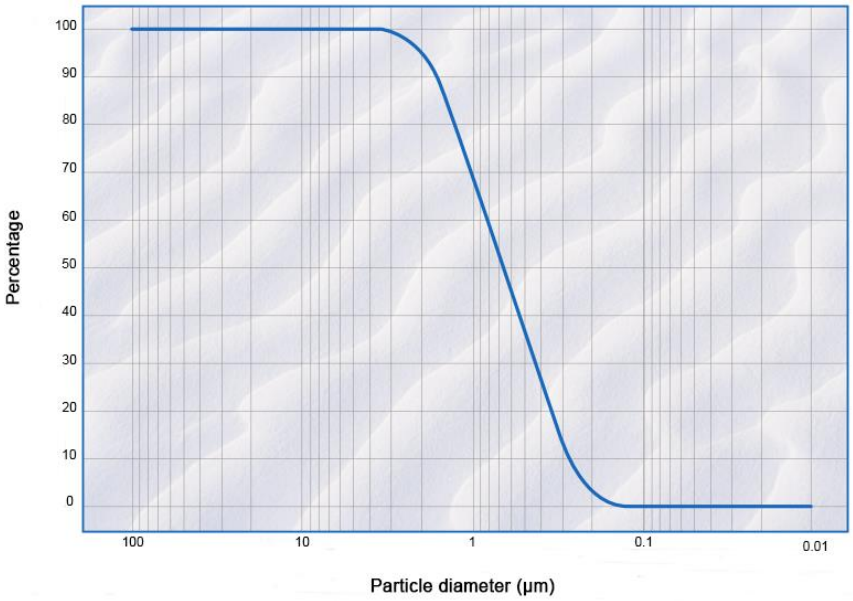

Figure 3.2 Average particle size distribution of M95 T calcium carbonate grade (data supplied by Reverté Calcium Carbonates).

Table 3.1 Key properties of employed talc grades.

Reference	Trade name	Morphology characteristics	Particle size d_{50} (µm)	BET ($m^2 \cdot g^{-1}$)
L 00S	Luzenac 00S	Lamellar	10.0	2.4
L 8218	Luzenac 8218	Lamellar fine-grind	3.9	5.4
M 90	Mistrocell M90	Micro-lamellar	3.3	13.0
M HAR	Mistron HAR	High aspect ratio	3.0	13.0
E 5936	E 5936	Micro-crystalline	1.1	21.3

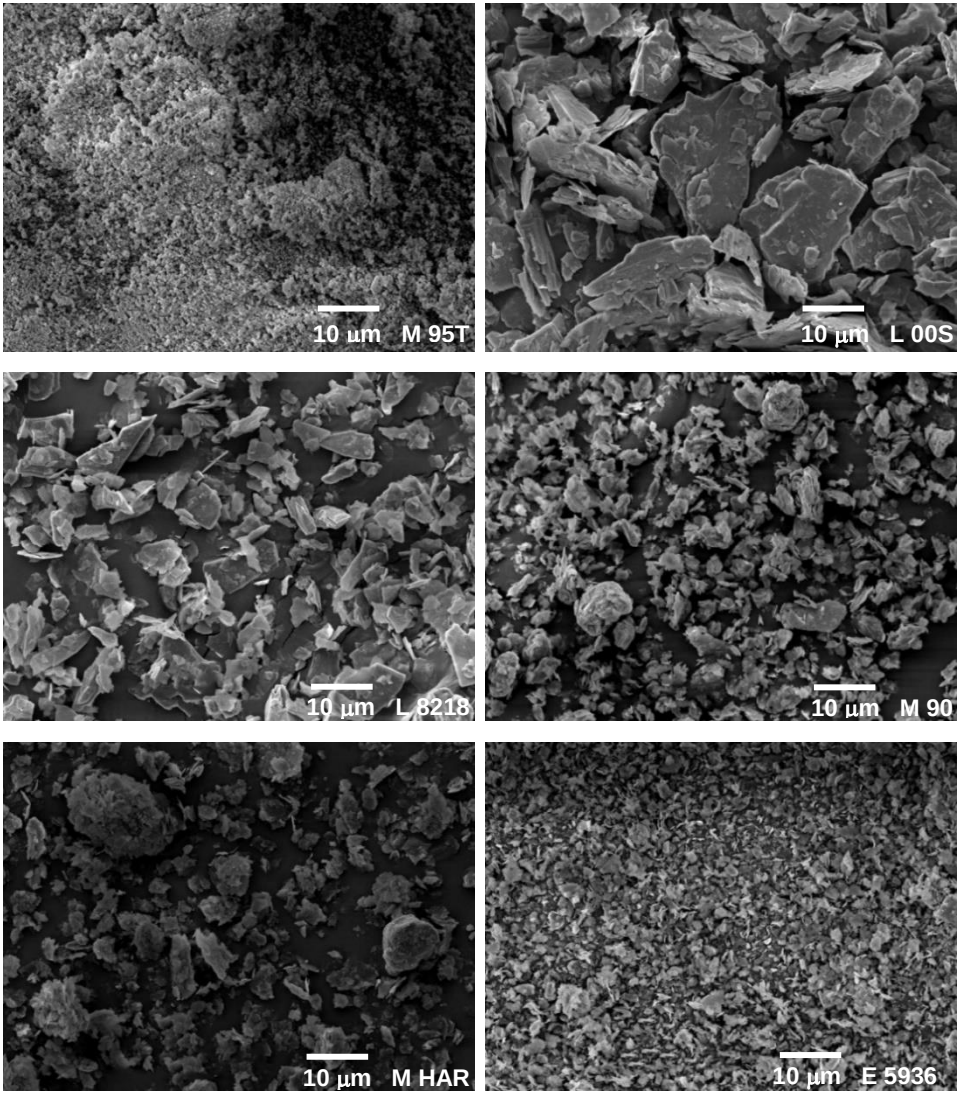

Figure 3.3 Morphological differences of the employed commercial grades of calcium carbonate and talc.

3.2 Compounding of polypropylene/calcium carbonate and PP/talc blends

A twin-screw extruder (*Collin GmbH-Kneter 25Z*) was used for the preparation of different polypropylene/filler blends. Filler contents of 1, 5, 10 wt.% were set. From now on, C1, C5 and C10 will refer to PP/$CaCO_3$ compounds with the previously mentioned weight percentages. The extrusion temperature from the hopper to die ranged from 180 to 240º C. A circular die (3 mm diameter) was adapted and the extrusion profile was cooled in a water bath and then pelletized (Figure 3.4).

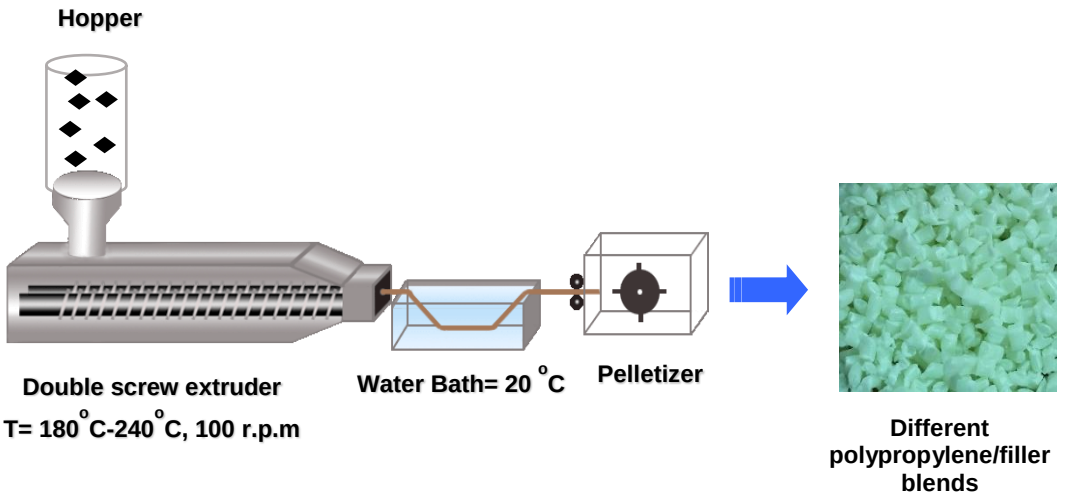

Figure 3.4 Process outline for the compounding of polypropylene/filler blends.

3.3 Membrane preparation

3.3.1 Production of precursor films

The first stage of MEAUS process is the production of a film with a row-lamellar structure. Usually, this film is called ‘’ precursor film’’, as it will be the precursor of the future membrane.

The production of precursor films was carried out using a twin-screw extruder for PP/ calcium carbonate and talc compounds. Extrusion temperature profile ranged from the hopper to die from 140 to 240º C. At the end of the extruder, a rectangular cross-section die was adapted, with nominal dimensions 122 mm x 1.9 mm.

Also, in order to study the influence of draw ratio on the orientation and permeability performance of some membranes, precursor films of some PP/calcium carbonate blends were produced by a single-screw extruder (*Eurotecno E-30/35D*). In this machine, a rectangular cross-section die was adapted, with 200 mm of nominal width. The gap die was varied between 1.6-2.6 mm to get different draw ratios.

For both cases (twin-screw extruder and single-screw extruder) a system of two air knives was mounted close to the die to provide air to the film surface right at the exit of the die and get a fast cooling. In all cases, the air pressure was kept in at 15 bar. After the air knife, a device of calender pulled the cooled film (Figure. 3.5). The nominal thickness of the films ranged between 25-35 μm. Draw ratio was 70

for twin-screw processing and ranged between 40-100 for the single-screw extruder.

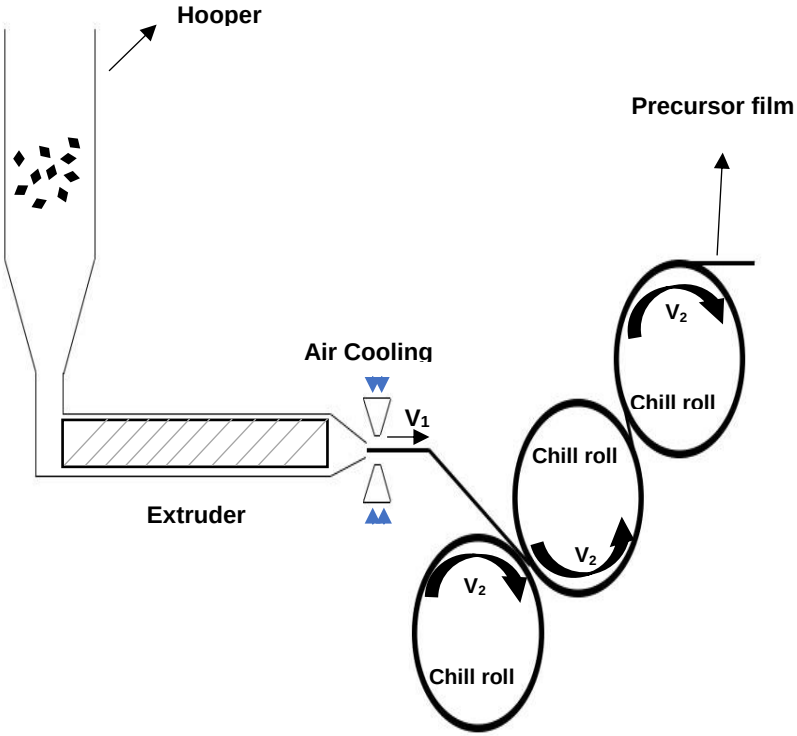

Figure 3.5 Process of the precursor films production and adjustment of air-knives for obtaining different precursor films.

3.3.2 Annealing of the precursor film

Annealing removes imperfections in the crystalline phase and increases lamellae thickness. Precursor films obtained by twin-screw extruder were annealed at 140 ºC for 15 min (polypropylene/calcium carbonate and polypropylene/talc compounds). A study of annealing influence was carried out for some polypropylene/calcium carbonate blends obtained by either twin and single-screw extruder. Three annealing temperature were tested: 90, 115, 140 ºC, and the annealing time was set at 15 min as suggested in other works [28, 35, 46].

3.3.3 Uniaxial strain of annealed precursor film

The annealed precursor films were then subjected to the uniaxially drawing stage. This stage is divided into two parts: a ‘’cold stretching’’ that aims to create pores, and a ‘’hot stretching’’ that aims to promote stable growth of pores. For both parts of the stretching stage, the key factors were stretching speed, the percentage of stretching and temperature of stretching. Uniaxial strain followed the extrusion direction of precursor films.

Rectangular samples with nominal dimensions of 75 mm x 60 mm were cut out from the annealing precursor films. A uniaxial strain was performed on a universal testing machine *Galdabini Sun 2500*, dotted with a load cell of 1 kN and a climatic chamber. Key parameters were: a) cold stage: 23 ºC, using a crosshead speed of 50 mm/min, reaching

an elongation of 35 %; b) hot stage: 140 ºC, using a crosshead speed of 10 mm/min reaching a total elongation of 200 %.

3.4 Characterization techniques

3.4.1 Rheological characterization

Rheological dynamic analysis (RDA) of neat polypropylene, polypropylene/calcium carbonate and polypropylene/talc compounds were done using a *Rheometric Scientific SR5000* stress-controlled rheometer with parallel plates (diameter 25 mm and a gap equal to 1.5 mm). The temperature was set at 190°C, and a nitrogen atmosphere was employed. A frequency sweep of 1 Hz was set. This technique did not only allow to determine the rheologic curve (viscosity vs. shearing speed, using the principle of Cox-Merz) but also aspects of the melt elastic behavior (shear storage modulus, G').

3.4.2 Polarized FT-IR

Polarized FT-IR was employed to evaluate the orientation of crystalline phase in non-annealed and annealed precursor films. For this purpose, a spectrophotometer *FT-IR Perkin Elmer Spectrum 1000* equipped with a light polarizer was employed. If a specific vibration is attributed to a specific phase, the orientation within that phase can be determined. If the films are oriented, the absorption of plane-polarized radiation by a vibration in two orthogonal directions,

specifically parallel and perpendicular to a reference axis (MD), should be different.

The absorbance determined with polarized light at 0º was parallel (A∥) to the extrusion flow of the precursor film. By other hands, the absorbance determined with polarized light at 90º was perpendicular (A⊥) to the extrusion flow. With these values, a dichroic relationship could be obtained (Eq.3.1) [56]:

$$D = \frac{A\parallel}{A\perp} \tag{3.1}$$

For polypropylene, the crystalline phase orientation (F_c) was obtained from the values of absorbance of the band at 998 cm^{-1} [43, 57], measured at 0º and 90 º, through the general Herman expression [43, 57].

$$F = \frac{D - 1}{D + 2} \tag{3.2}$$

The average orientation function (F_{av}) was obtained from Herman expression, from the absorbance signal at 972 cm^{-1} [56]. The orientation of the amorphous phase (F_{am}) can then be calculated according to:

$$F_{av} = X_m F_c + (1 - X_m)F_{am} \tag{3.3}$$

Where X_c is the degree of the crystallinity that was obtained through DSC as explained in section 3.4.3.

3.4.3 Differential Scanning Calorimetry (DSC)

DSC was employed for several aims. Firstly, to determine the nucleating activity of calcium carbonate and talc on polypropylene. Secondly, to analyze the evolution of the melting peak of non-annealed precursors films, annealed precursor films, and membranes, in order to get information about the structural changes in the different stages of MEAUS processing. A *TA DSC Q 1000* equipment was employed. Sample weight was approximately 5 - 7 mg.

Nucleating activity was studied by heating pellets of each sample at 200°C, keeping this temperature for three minutes (erasing thermal history) and then cooling to 30°C at a cooling rate of 20°C/min. The cooling peak temperature and the crystallization enthalpy (ΔH_c) was registered (Figure 3.6).

The evaluation of the crystalline phase was analyzed by the study of the melting endothermic signal of non-annealed precursor films, annealed precursor films, and membranes. Melting was carried out from 30-200°C at a heating rate of 20°C/min.

From these heating runs, the main melting peak and in some cases, a secondary melting peak appeared and/or a right shoulder to the main melting peak (Figure 3.6).

Melting enthalpies was obtained by integrating the area under the DSC curve around the melting temperature (T_m). Crystallinity values from cooling (X_c) and melting (X_m) were determined by dividing the corresponding enthalpy (ΔH_c and ΔH_m) into 207.1 J/g, The enthalpy of fusion of a 100 % crystalline polypropylene.

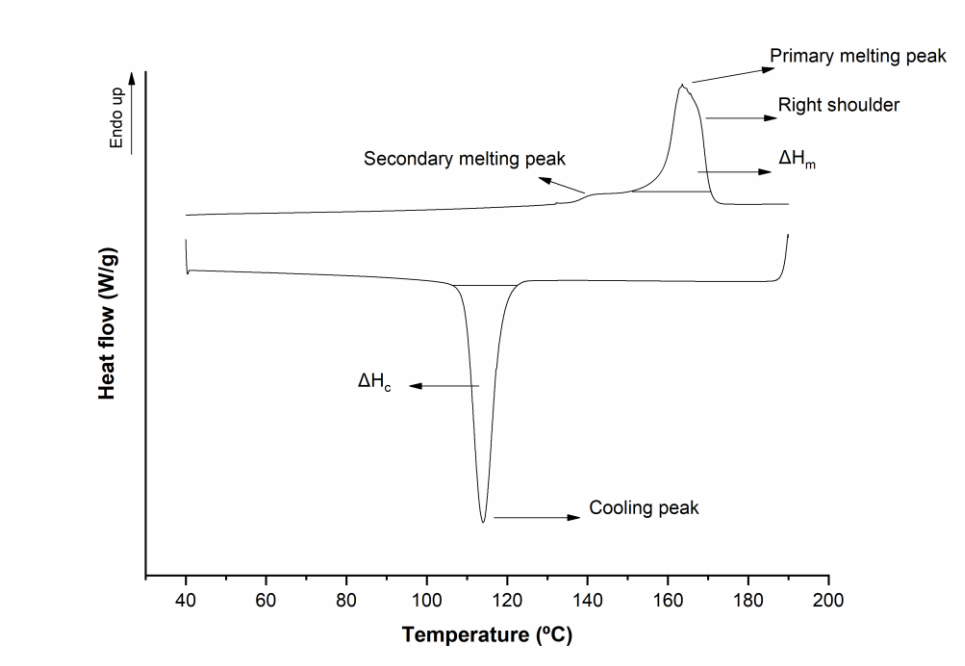

Figure 3.6 Typical experimental thermograms obtained in the thesis, showing the registered parameters.

3.4.4 Thermogravimetric Analysis (TGA)

This study was conducted to determine the mass loss due to decomposition of filled polypropylene membranes by using a *Mettler Toledo TGA 1 STARe System*. The samples of approximately 10 mg were heated from room temperature to 1000°C, at 10°C/min, in oxygen-rich air. With this technique aims to assess whether the addition of fillers and/or the morphological changes due to the pore morphology can affect the thermal stability of the membranes. $T_{0.1}$ is the temperature at which there was a loss of mass of 10 wt. %; $T_{0.5}$ is the temperature at which there was a loss of mass of 50 wt. %; T_{max} is the temperature of the maximum lost mass velocity.

3.4.5 Scanning Electron Microscopy (SEM)

The pore structure of the membranes surfaces was analyzed through scanning electron microscopy. A *JEOL JSM-5610* microscope was employed, applying a voltage of 15 kV. The membranes were previously gold-coated to ascertain electrical conductivity. The micrographs were analyzed using a software *Buehler Omnimet*. Values of pore density, pore size, and the porous area were obtained.

3.4.6 Porosity

Porosity is that portion of the membrane volume occupied by pore spaces. Among other techniques, it can be estimated through volumetric measurements. It was determined for non-annealed precursor films, annealed precursor films, and membrane samples.

In this study, the grain volume method was used to determine the porosity of our membranes. Hence, first we calculated the pore volume (V_p) by the given formula:

$$V_p = \frac{W_{sat} - W_{dry}}{\rho_{water}}. \quad (3.6)$$

Where saturated weight is (W_{sat}), dry weight of the sample is (W_{dry}) and density of certain fluid water in our case is ρ_{water}.

Therefore, we used the following equation to compute the grain volume (V_g) of our samples,

$$V_g = \frac{W_{dry}}{\rho_{sample}}. \quad (3.5)$$

Where ρ_{sample} is the density of our sample.

Then, the summation of V_p and V_g is the bulk volume (V_b).

$$V_b = V_p + V_g \quad (3.6)$$

Percentage of porosity was computed as:

$$\emptyset_{\%} = \frac{V_p}{V_b} \times 100 \quad (3.7)$$

3.4.7 Determination of membrane permeability

The permeation of membrane towards air was measured by a *Gurley equipment*. It is used to measure the air permeation of approximately 6.45 cm^2. A circular area of a membrane using a pressure differential of 1.22 kPa. The recommended range of the liquid column instrument was from 5 to 1800 seconds per 100 mL cylinder displacement.

Gurley permeability values were obtained as followed:

$$Z = \text{time}/(4.1461) \quad (3.8)$$

$$\text{Gurley permeability, } \mu m \cdot (Pa \cdot s)^{-1} = 135.5/z \quad (3.9)$$

Where time value is the number of seconds that is needed to permeate an amount of air.

3.4.8 Determination of mechanical properties (tensile configuration)

The precursor films were tested in the tensile configuration according to ASTM D-638 on a *Galdabini Sun 2500* universal testing

machine, equipped with an environmental chamber, and a load cell of 1 kN. The tensile tests were carried out in extrusion direction (MD) at room temperature. Three specimens were tested. A cross-head speed of 50 mm/min was employed. Young's modulus (E) and 1st yield point were obtained from the stress-strain curve.

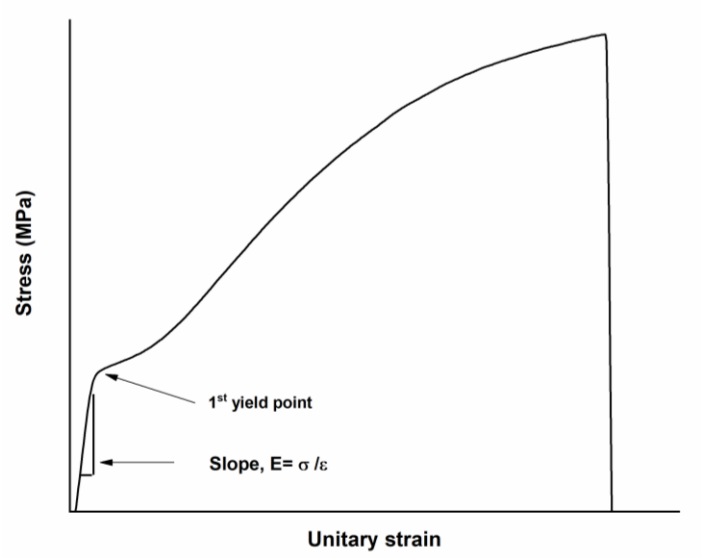

Figure 0.7 Registered parameters for stress-strain curves.

CHAPTER 4

RESULTS AND DISCUSSIONS

The sequence of the results will account for the rheology of the filled polypropylene compounds produced, the crystalline features (orientation and crystallinity) of precursor films (non-annealed and annealed) and membranes, the derived pore morphology of membranes and which consequences have them on the air permeability of the obtained membranes. Thermal stability of membranes and a mechanical characterization through tensile tests were conducted on precursor films.

4.1 Rheological behavior of polypropylene-based compounds

In the thermoplastic polymer, viscosity decreases as the strain rate increased behavior such as ‘shear thinning’ or ‘pseudo plastic’, as is our employed polymer. The term the ‘lower Newtonian region’ or ‘first Newtonian region’ is a constant value which the viscosity is nearly a constant at very low shear rates, and the viscosity value in this region is called the ‘zero shear viscosity’ λ_0. There is a decrease in the viscosity as the shear stress or shear rate is increased, and the viscosity once again saturates to a constant lower value at higher shear rates, referred to as the ‘higher Newtonian region’ or the ‘second Newtonian region’. The (lower) viscosity in this region is called η_∞.

The addition of the filler as a different chemical nature, size and content can affect the viscosity and shear rate and extrusion behavior during the production of the film precursor.

During production, where a good agreement of mixing and miscibility of components is expecting, temperature of extruding and the mechanism of extruder are important factors which by imposing stress and heating during the production time they might have an influence on the rheology behavior and change the viscosity and shear rate which may retard the motion of the chains along their backbone.

The main mechanism of production of components can influence on the fibrils or nuclei sites, as fibril mostly created from the long bridge chain and long bridge chains have a larger relaxation time, therefore, they may have not enough time during extrusion or might affect by the mechanism of mixing components by an extruder [58-61].

PP/Calcium carbonate compounds

As usual, in filled polymeric systems storage modulus increases as the amount of filler does. This is accomplished in the studied PP/calcium carbonate components as seen in Figure 4.1a. The storage modulus decreases proportionally in the limit of low frequency and attains a constant value at high frequency. C1 and C10 exhibit much higher storage modulus (G') at low strain amplitudes than does PP, which may indicate a higher degree of interaction between calcium carbonate and polypropylene macromolecules of internal

structure in C1 and C10. No reasonable explanation is deducted for the lower values showed by C5 compound

The loss modulus (G'') shows a direct proportion to angular frequency, therefore, decreases proportionally at low frequency and it also shows a reverse ratio to angular frequency moreover, increases proportionally at high frequency. The loss modulus (G'') for PP/calcium carbonate is shown as a function of frequency in Figure 4.1b. The loss modulus has a peak at high frequency, in the loss modulus spectrum. This may imply that there are two rheological relaxation mechanisms in the system and provides their time constants. This could be used to deduce the structure of these fluids.

The complex viscosity as functions of frequency for the neat PP and $CaCO_3$ compounds are shown in Figure 4.1c. The structure features of PP are influenced by the melt rheological characteristics. Neat PP and C1 exhibit a very similar rheological behavior. C10 shows a slightly larger complex viscosity and the zero-shear viscosity plateau is not reached at the lowest frequencies. The complex viscosity curve of C5 is similar to that of C10, but with much lower viscosity values. This goes to infinity at low frequency, indicating that the response is primarily viscous and at high frequency this goes to zero, indicating that the response is dominated by elasticity. This is indicative of a higher average filler percentage.

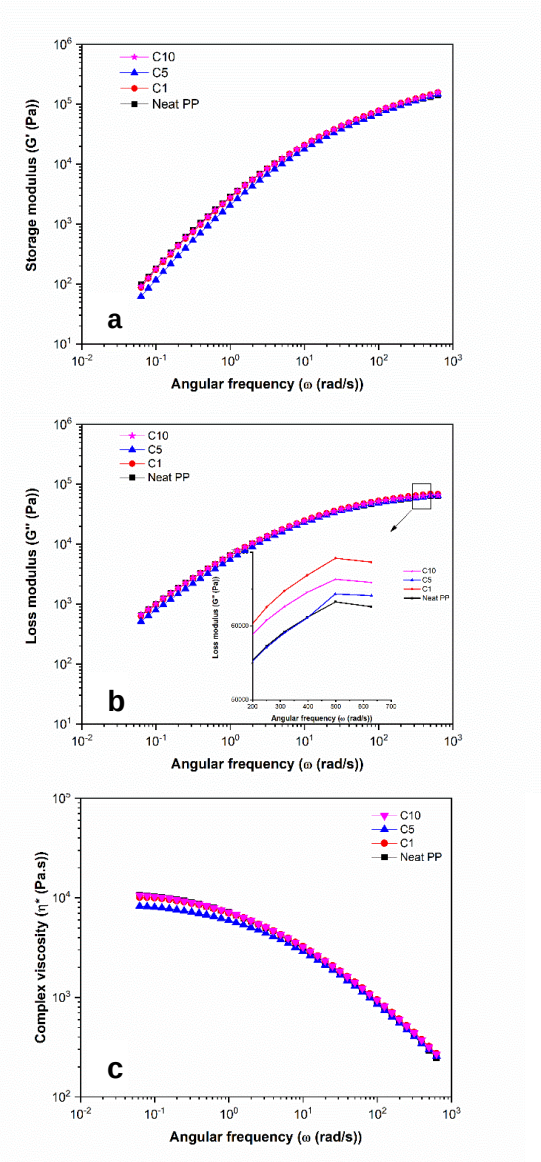

Figure 4.1 Evolution of storage modulus, loss modulus and complex viscosity of PP/calcium carbonate compound.

PP/talc compounds

As same as PP/calcium carbonate compounds, all talc compounds exhibited an increase in storage modulus as the filler content increased, (Figure 4.2a). Small particle size talc (E 5936) exhibits much higher storage modulus (G') at low strain amplitudes than does PP, (Figure 4.2b), which may indicate a higher degree of interaction between talc and polypropylene macromolecules of internal structure in the morphology of small particle size talc as we increase the amount of filler.

The same pattern with respect to filler content was obtained in the loss modulus (G''). More significant differences were found according to the talc type, as the bigger particle size talc gradually showed more value in the loss modulus as we increased the amount of filler (Figure 4.2c). This could be related to the filler morphology and internal interaction between the polymer matrix and filler. The loss modulus has a maximum at high frequency, this may imply that there are two rheological relaxation mechanisms in the system and provides their time constants.

The complex viscosity of talc components exhibited as the most remarkable effect that the small particle type of talc (E 5936) shows a slightly larger complex viscosity when the zero-shear viscosity plateau is not reached at the lowest frequencies Figure 4.2d. Other types of talc did not show significant differences. The structure features of PP

are influenced by the melt rheological characteristics. This might be indicating that the response is primarily viscous due to infinity at low frequency, and at high frequency this goes to zero, indicating that the response is dominated by elasticity which could be indicative of a higher average filler percentage.

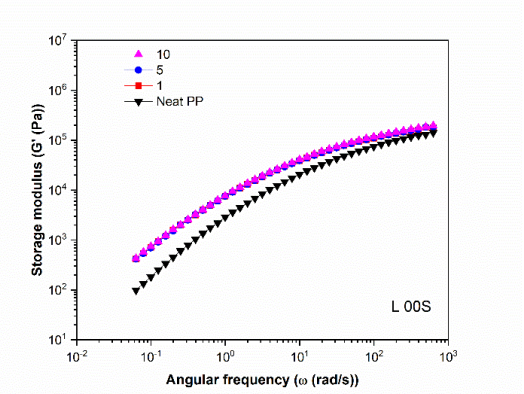

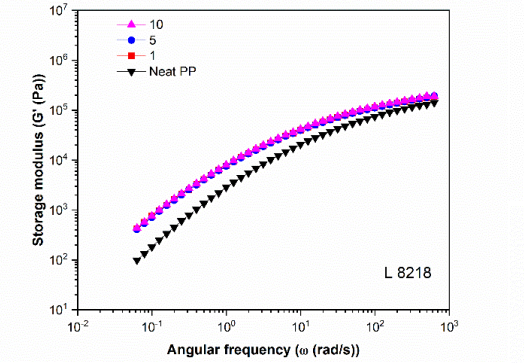

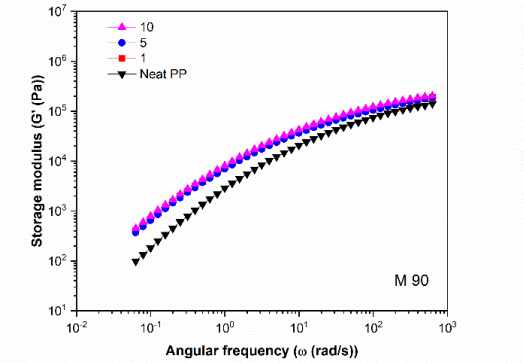

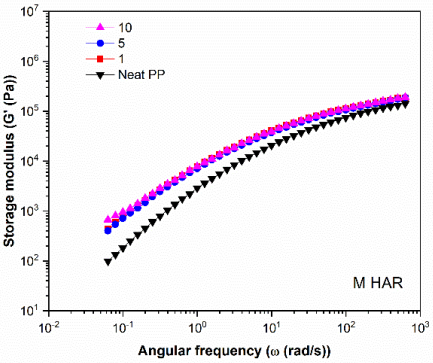

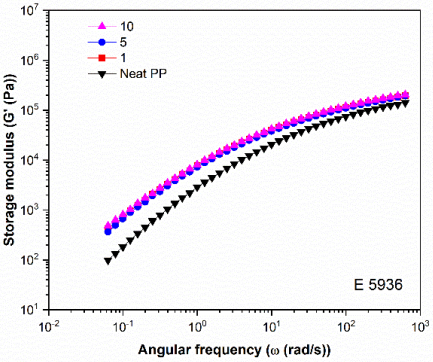

Figure 4.2a Evolution of storage modulus for PP/talc.

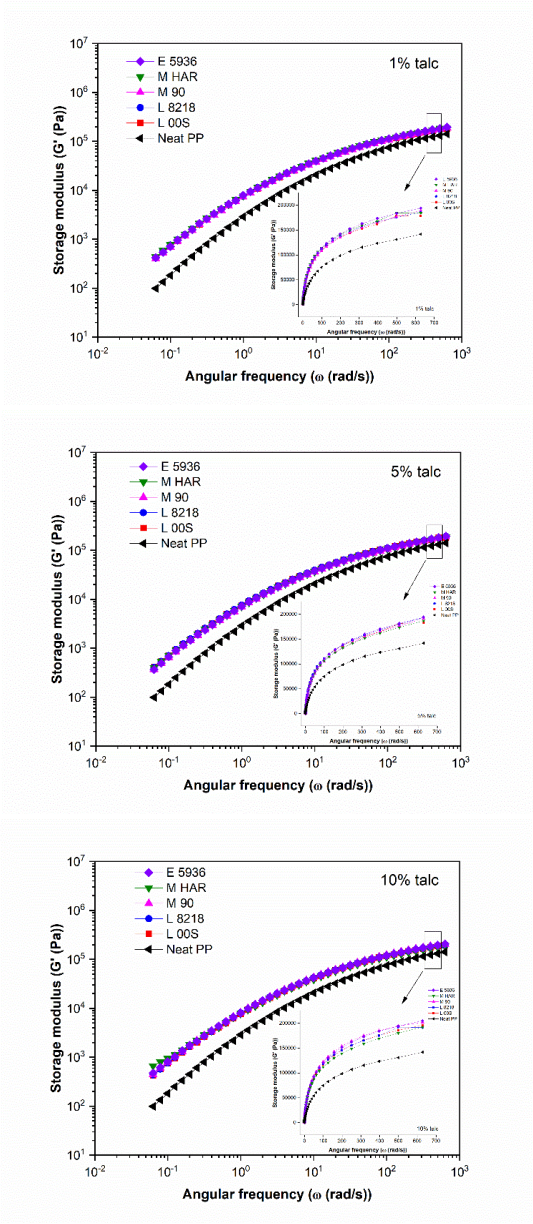

Figure 4.2b Influence of talc type on the evolution of storage modulus.

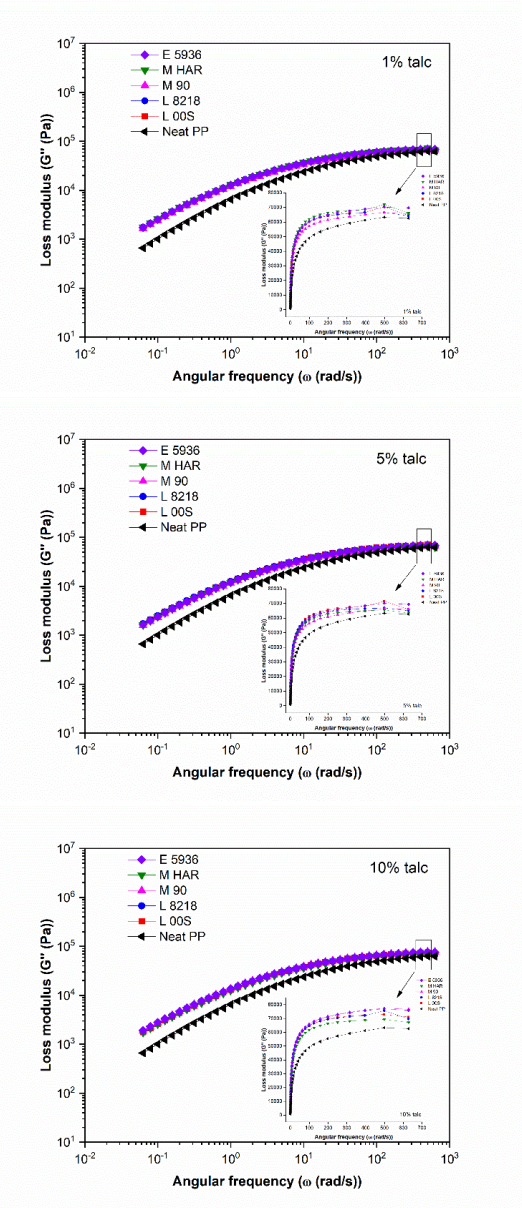

Figure 4.2c Influence of talc type on the evolution of loss modulus.

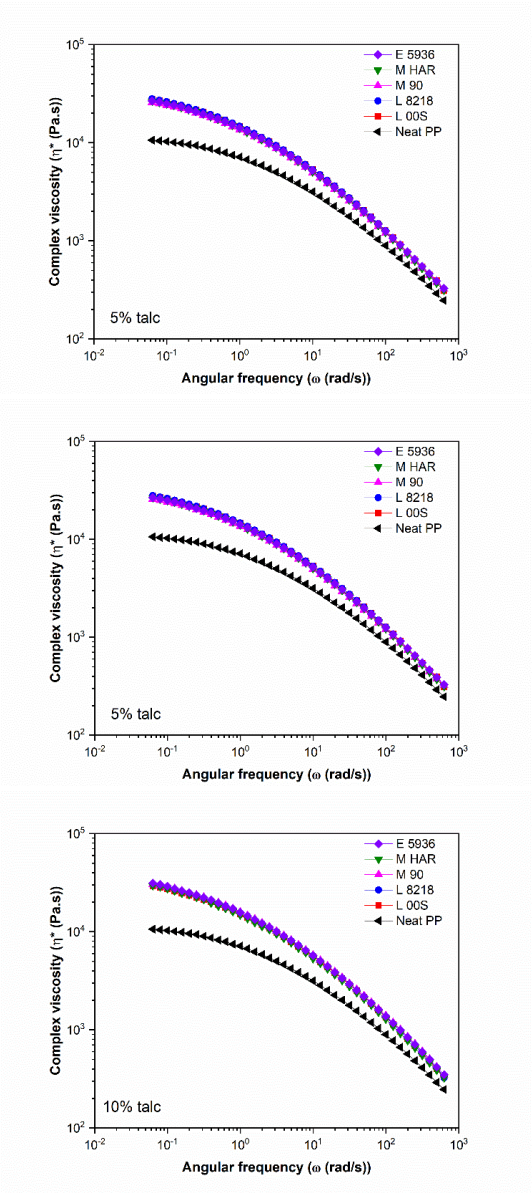

Figure 4.2d Influence of talc type on the evolution of complex viscosity.

4.2 Crystalline phase: orientation and crystallinity

The structure of the precursor film highly depends on the extrusion condition (temperature, shearing, stretching and calandering system) and the applied drawing ratio [62, 63]. Also, depends on the chemical nature of the compounds. It is generally agreed that some orientations, either in a plane or out of the plane, will be induced during the extrusion calandering can be processed through the MEAUS process to produce the flat sheet films.

Fourier transform infrared spectroscopy is one of the reliable techniques to measure the orientation of the amorphous and crystalline phases of the precursor and annealed precursor films. There are two important factors to control the lamellae separation process to control the lamellae separation process, one of them is the orientation and the other is the position of the crystal blocks in the precursor films, which results in pores formation.

There are factors that help in the selection of semi-crystalline polymers that capable of forming microporous membranes via crystal lamellae separation, and the factors are fast crystallization kinetics, a highly planar lamellar morphology for the extruded film, the high orientation of the crystalline phase, proper film thickness, and the presence of a α-relaxation.

Annealing has a significant effect on the orientation and also, it might as well effect on the thickness of the crystal lamellae. The

improvement of orientation and thickness could be the result of the crystallization of the trapped end chains between the lamellae and also, the melting of very thin lamellae and their recrystallization in the form of the thicker ones [64-66].

During annealing, crystalline defects and lamellae thickening take place (α-relaxation) if the annealing temperature to be sufficient to activate this relaxation. Although annealing usually takes place in a short time, its role is critical in membrane production. The crystalline locks will allow moving around at an annealing temperature above the α transition.

The importance of annealing for the formation of a microporous structure to possessing stacked lamellar structure prior to their drawing is necessary. By removing the defects in the crystalline phase annealing increases lamellae thickness and it could improve lamellae orientation and uniformity [67, 68].

4.2.1 Nucleating effect of fillers on polypropylene

Cooling runs carried out on sample pellets displayed that calcium carbonate slightly shifted the crystallization peak temperature to the higher values with respect of neat polypropylene (Table 4.1), by just adding 1 wt.%. of calcium carbonate; this effect is even more marked as the calcium carbonate content is increased (Figure 4.3a). Calcium carbonate seems to act as a potential nucleating site that helps to

arrange in a more oriented composition along the extrusion direction of the polymer macromolecules.

On the contrary, talc had a large impact on the crystallization behavior with respect to the neat PP (Table 4.2), which accounts for the high nucleation ability that talc has onto the crystallization process of polypropylene. This cooling run displayed that talc rose the crystallinity peak temperature up to 5 ºC with respect to the neat polypropylene, by just adding 1 wt.%. of talc (Figure 4.3b). This effect was even more marked as the talc content was increased (Figure. 4.3a and 4.3b). Size and morphology of the employed talc do not have a significant influence on its nucleation activity. Nevertheless, high contents of the smallest size (E 5936) or more oriented (M HAR) provided the high nucleation efficiency.

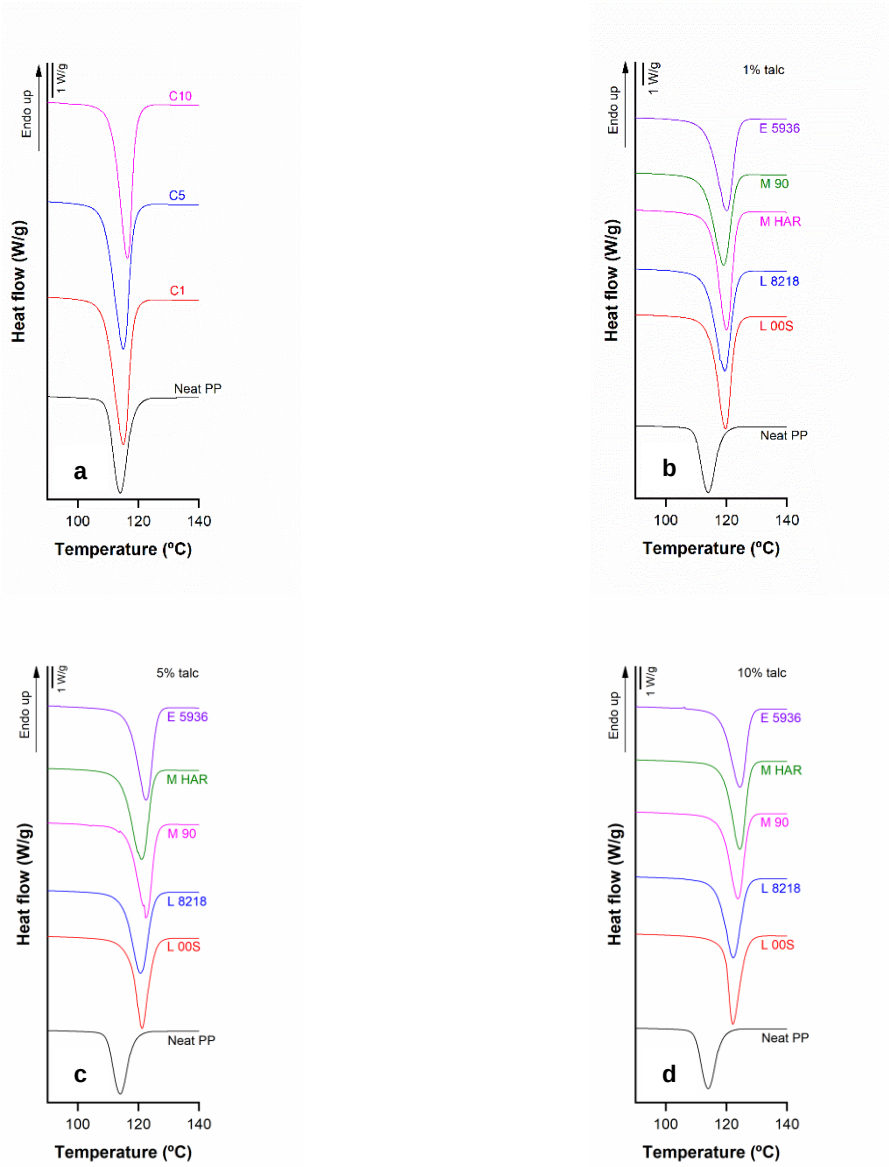

Figure 4.3 Nucleating effect of a) calcium carbonate and b, c, d) talc on crystallization peak of polypropylene.

Table 4.1 DSC thermal analysis for PP/calcium carbonate compounds obtained by a twin-screw extruder.

			Neat PP	C1	C5	C10
Cooling runs	P_c-Peak		114.0	113.5	115.0	116.4
Heating runs	1^{st} peak	Non-annealed precursor film	162.3	162.1	164.6	165.0
		Annealed Precursor film	161.7	162.1	163.9	163.1
		Membrane	163.7	160.1	162.1	161.8
	X_m (%)	Non-annealed precursor film	51.1	44.5	45.0	44.8
		Annealed Precursor film	46.7	47.2	49.3	48.5
		Membrane	48.3	53.1	55.0	54.6
	2_{nd} Peak (°C)	Membrane	172.7	171.2	172.0	169.1

Table 4.2 DSC thermal analysis for PP/talc compounds.

			Neat PP	L 00S		
				1 %	5 %	10 %
Cooling runs		P_c-Peak	114.0	119.7	121.6	122.9
Heating runs	1^{st} peak (°C)	Non-annealed Precursor	162.3	162.1	162.7	162.6
		Annealed precursor	161.7	163	163.6	163.7
		Membrane	163.7	165.7	166.3	165.5
	X_m (%)	Non-annealed Precursor	51.1	40.4	40.9	40.3
		Annealed precursor	46.7	48	47.5	47.2
		Membrane	48.3	51.0	51.9	42.9
	2^{nd} Peak (°C)	Membrane	172.7	176.0	179.2	174.2

			Neat PP	L 8218		
				1 %	5 %	10 %
Cooling runs		P_c-Peak	114.0	119.5	120.7	122.2
Heating runs	1st peak (°C)	Non-annealed Precursor	162.3	161.6	160.6	161.8
		Annealed precursor	161.7	161.2	162.1	161.6
		Membrane	163.7	164.9	165.5	165.6
	X_m (%)	Non-annealed Precursor	51.1	41.5	41.5	39.8
		Annealed precursor	46.7	47.3	46.3	45.3
		Membrane	48.3	53.5	51.4	36.5
	2nd Peak (°C)	Membrane	172.7	178.0	175.4	172.4

			Neat PP	M 90		
				1 %	5 %	10 %
Cooling runs		P_c-Peak	114.0	119.1	122.5	123.8
Heating runs	1^{st} peak (°C)	Non-annealed Precursor	162.3	161.9	161.5	161.5
		Annealed precursor	161.7	161.8	161.0	161.1
		Membrane	163.7	165.1	163.8	165.8
	X_m (%)	Non-annealed Precursor	51.1	40.6	40.8	41.9
		Annealed precursor	46.7	46.7	46.2	46.7
		Membrane	48.3	48.9	47.8	45.9
	2^{nd} Peak (°C)	Membrane	172.7	174.7	174.8	174.1

			Neat PP	M HAR		
				1 %	5 %	10 %
Cooling runs		P_c-Peak	114.0	120.1	121.1	124.5
Heating runs	1^{st} peak (°C)	Non-annealed Precursor	162.3	162.3	161.2	164.5
		Annealed precursor	161.7	162.2	161.1	162.1
		Membrane	163.7	164.9	164.7	165.6
	X_m (%)	Non-annealed Precursor	51.1	41.9	41.6	40.6
		Annealed precursor	46.7	45.9	46.9	45.5
		Membrane	48.3	51.1	45.6	40.3
	2^{nd} Peak (°C)	Membrane	172.7	176.7	176.4	174.4

			Neat PP	E 5936		
				1 %	5 %	10 %
Cooling runs		P_c-Peak	114.0	120.1	122.5	124.5
Heating runs	1^{st} peak (°C)	Non-annealed Precursor	162.3	163.2	163.2	165.7
		Annealed precursor	161.7	161.6	161.3	161.6
		Membrane	163.7	164.9	165.4	165.3
	X_m (%)	Non-annealed Precursor	51.1	41.8	42.6	41.1
		Annealed precursor	46.7	46.3	45.6	43.9
		Membrane	48.3	49.9	45.1	38.9
	2^{nd} Peak (°C)	Membrane	172.7	175.1	175.5	176.2

4.2.2 Orientation

Non-annealed precursor films

Calcium carbonate increased the orientation of crystalline phase compared to neat polypropylene (Table 4.3), leading to a higher macromolecular alignment. Just a small amount of calcium carbonate was necessary to achieve the maximum orientation degree. Further increase of calcium carbonate content did not lead to a greater orientation, but it was counteractive in terms of creating more macromolecular alignment. This higher crystalline phase orientation had the same consequence on the orientation of the amorphous phase and thus on the average orientation.

It can be seen (Table 4.3) that annealing improved the amorphous orientation along the machine direction compared to the neat polypropylene. Amorphous orientation significantly rose up when calcium carbonate was added to neat polypropylene. This is likely due to the participation of disrupted amorphous end chains in the crystallization and also the partial motion of the crystal blocks, which results in a slight stretching of the tie chains along the lamellae thickness.

An opposite trend in the orientation of the polypropylene matrix was observed when talc was employed as a mineral filler. Table 4.4 shows talc addition provoked a constraint of the orientation of the crystalline phase. This reduction is even more marked as the amount of talc

increased. This opposite trend can be directly related to the enhanced nucleating activity of talc on polypropylene that to some extent could increase the macromolecular alignment that leads to a final row lamellae structure. Another explanation could be based on an agglomeration of talc giving spherical like that could hinder orientation. But calcium carbonate has the quasi-spherical shape and did not show this behavior.

We hypothesized that the higher BET area that talc laminar particles with respect to calcium carbonate have some effect on this reduction of orientation, but further studies should be carried out to analyze more deeply this hypothesis. As we can see (Table 4.4) by adding talc, the orientation of the amorphous phase showed a higher value than the neat polypropylene. Although, as the amount of talc increased orientation amorphous phase decreased, which the lamellae could not well-aligned perpendicular to the flow direction.

Concerning to morphological features of talc employed, it is observed that high aspect ratio talc type (M HAR) is the grade that minimizes in more extent the reduction of orientation degree, combined with small particle size and high BET area. It is clearly seen the importance of using high aspect ratio grades, as the grade with the smallest particle size and the higher BET area, but not high aspect ratio (E 5936) leaded to very low orientation degrees.

Annealed precursor films

To determine the optimum annealing conditions that will lead to high orientation and crystallinity, annealing at 90°C, 115°C, 140°C was carried out on calcium carbonate compounds. The measured orientation values are written in Table 4.3. Annealing rose significantly up the orientation factor of crystalline phase as the temperature increased. this effect is more marked when 1 % of calcium carbonate was added. Higher amounts of calcium carbonate showed a not quite significant effect of annealing temperature.

Amorphous phase orientation and average orientation followed the same trend with respect of the one showed by crystalline orientation factor. As annealing is performed, it is suggested that during annealing, the lamellae orient perpendicular to the machine direction. Also, melting of small lamellae and their recrystallization with better orientation can occur. In row nucleated lamellar morphologies, lamellae can be twisted only if both α- and β-axes preferentially orient to MD. Therefore, the observed increase in the F_{am} values and the consequent increase in the F_c values after annealing demonstrates that annealing can increase the number of twisted lamellae in polypropylene/calcium carbonate cast film, in other words, annealing procedure is observed to promote parallel planar lamellae textures.

For PP/talc compounds, annealing carried out at 140 ºC, increased the crystalline orientation. (Table 4.4). Talc addition showed again a

reducing of crystalline orientation. Nevertheless, it seems that the morphology of talc grades with small particle size and high surface area, tend to minimize this effect (M 90, M HAR).

The amorphous phase orientation, F_{am}, for annealed precursor film of talc compound showed very small value compared to the polypropylene and its value considerably decreased. The F_{am} values for the annealed films are also in the same range, and it is seen that annealing treatment has not a major influence on the amorphous phase orientation of talc components. Talc addition might have provoked a constraint of the orientation of the amorphous phase orientation. Therefore, the observed decrease in the F_{am} values and the consequent decrease in the F_c values after annealing demonstrates that annealing can reduce the number of twisted lamellae in polypropylene/ talc compounds.

Table 4.3 Orientation analysis carried out through polarized FT-IR for PP/calcium carbonate compounds, obtained by a twin-screw extruder.

			Neat PP	C1	C5	C10
F_c	Non-annealed precursor		0.52	0.64	0.63	0.61
	Annealed precursor	90 (ºC)	0.60	0.47	0.66	0.65
		115 (ºC)	0.63	0.64	0.67	0.63
		140 (ºC)	0.61	0.75	0.69	0.65
F_{av}	Non-annealed precursor		0.36	0.46	0.47	0.45
	Annealed precursor	90 (ºC)	0.43	0.33	0.48	0.47
		115 (ºC)	0.46	0.42	0.49	0.45
		140 (ºC)	0.45	0.54	0.52	0.47
F_{am}	Non-annealed precursor		0.18	0.31	0.33	0.31
	Annealed precursor	90 (ºC)	0.30	0.22	0.35	0.34
		115 (ºC)	0.35	0.25	0.35	0.31
		140 (ºC)	0.28	0.36	0.35	0.33

Table 4.4 Orientation and an amorphous factor of precursors and annealing specimens of PP and talc.

	Talc wt.%	Particle size (μm)	F_c	F_{av}	F_{am}
Neat PP	0	*	0.61	0.59	0.57
L 00S	1	10.0	0.49	0.40	0.31
	5		0.26	0.24	0.22
	10		0.24	0.13	0.04
L 8218	1	3.9	0.52	0.44	0.34
	5		0.29	0.30	0.30
	10		0.26	0.18	0.13
M 90	1	3.3	0.56	0.47	0.38
	5		0.33	0.32	0.32
	10		0.29	0.27	0.24
M HAR	1	3.0	0.52	0.45	0.39
	5		0.35	0.35	0.36
	10		0.35	0.20	0.03
E 5936	1	1.1	0.45	0.38	0.31
	5		0.30	0.34	0.37
	10		0.26	0.23	0.21

4.2.3 Crystalline distribution and crystallinity

Non-annealed precursor films

The non-annealed precursor films of calcium carbonate-based compounds obtained by twin-screw extruder displayed melting endotherms (Figure 4.4a) with monomodal distributions. The melting peak shifted to higher temperatures in high calcium carbonate contents were added. This can be attributed, by one hand to thicker lamellae which could lead to the movement of the main melting peak to a higher temperature.

Talc-based compounds showed the same features in the shape of the endotherm curves (Figure 4.5a). In general, crystallinity degree decreased (Table 4.2). The melting peak temperature didn't show a notable effect with the talc addition, it may suggest a larger number of smaller crystals were nucleated at the talc particle surface, and they can be melted in lower temperature.

Annealed precursor films

Annealing carried out on precursor films at 140 ºC (both calcium carbonate and talc-filled compounds) provoked the apparition of a left shoulder (Figures 4.4b, 4.5b) attached to the main melting peak. Balas *et al* [69] stated that this annealing endotherm reveals the presence of a smectic metastable phase, and has been attributed to the melting of small monoclinic crystals formed during the original

quenching process suffered during the extrusion stage of MEAUS process. Nevertheless, Dudic *et al* [70]. believed that there was no direct relationship between the endotherm peak and smectic phase; they attributed the existence to the crystallization of polymer portions which were somewhere between amorphous and smectic phases.

Annealing stage has the aim in MEAUS process to increase the lamellar thickness indicating some crystallization behavior. Similar to the conclusions given by Dudic *et al* [70], Caihong *et al* [71] assumed that the appearance of the low-temperature plateau in DSC curves came from some tie chain crystallization around initial lamellae. Sang-Young Lee [63] also proposed that at higher annealing temperatures, the loose tie chain segments probably evolved into crystallites. Sadeghi *et al* [43], also established that new stable recrystallized structure, coming from some tie chain crystallization around initial lamellae which converts to connecting bridges between lamellae [42, 43, 72, 73].

From the analysis of the influence of annealing temperature carried out on calcium carbonate-based compounds obtained by a twin-screw extruder (Figure 4.4b), it is extracted that an increase in the annealing temperature shifted this secondary annealing peak to higher temperatures. This indicates, that the new stable crystalline structure evolved from annealing has a more lamellar thickness when annealing was performed at 140 ºC.

This secondary peak that comes from annealing shifts at higher temperatures in filled compounds with respect to the neat polypropylene annealed precursor films. This effect is more marked in talc filled compounds (Figure 4.5b), as well as the intensity of this secondary peak. So, as in the case of nucleation activity, again, calcium carbonate and talc behaved in a different manner. No significant differences about the intensity and temperature shifting of this annealing peak have been observed related with the filler content, nor with the type of talc employed.

Effect of annealing on the change of morphological structure one may conclude that two competitive processes occur. On the one hand, whole crystallites or parts of them may melt and new crystallites develop from the molten phase. On the other hand, the thickening process occurring continuously and involving parts of the original crystals. Which mechanism predominates depends on molecular weight distribution, crystallization temperature, heating rate and annealing temperature [74-76].

In fact, the difference in the crystallinity of non-annealed and annealed precursor films suggests that the less stable microcrystallites progressively melt, while almost simultaneously, new crystallites, which are increasingly thicker and/or stable are formed, thus compensating the endothermic melting process by a re-ordering process.

Both calcium carbonate and talc-filled annealed precursor films developed higher crystallinity values than their respective non/annealed ones. Crystallinity was not significantly affected by the filler content on the annealed precursor films, nor the type of talc employed.

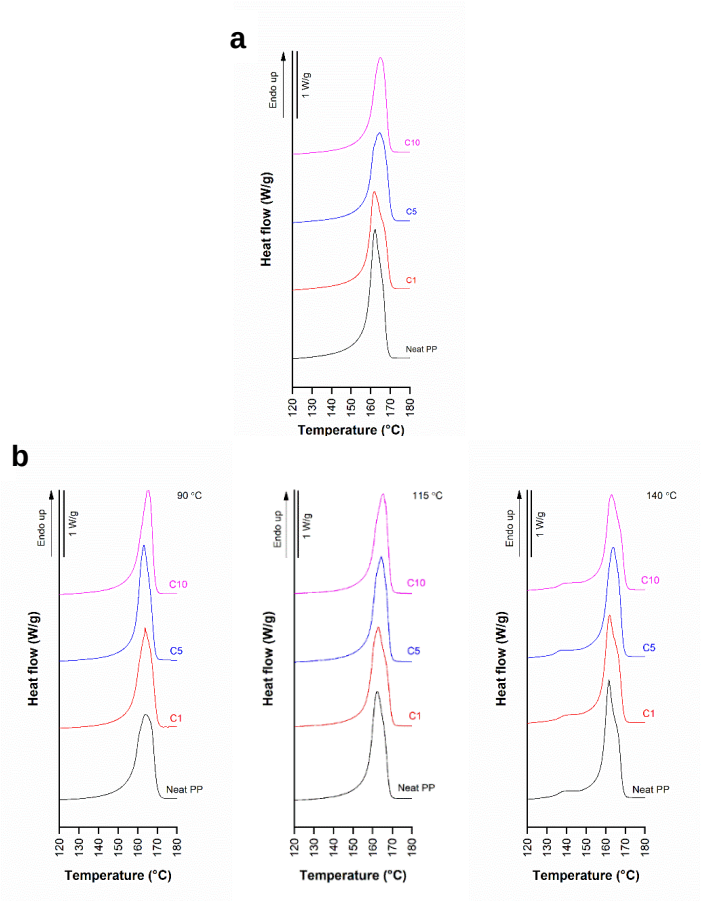

Figure 4.4 Melting endotherms of neat PP and PP/calcium carbonate compounds a) precursor films b) annealed precursor films at 90°C, 115°C, 140°C, obtained by a single-screw extruder.

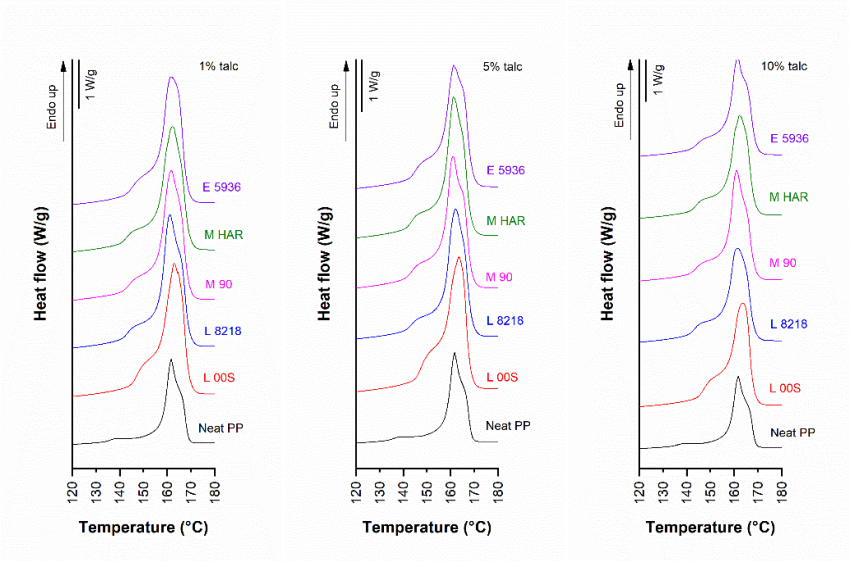

Figure 4.5a Precursor films melting endotherms for neat PP and PP/talc compounds.

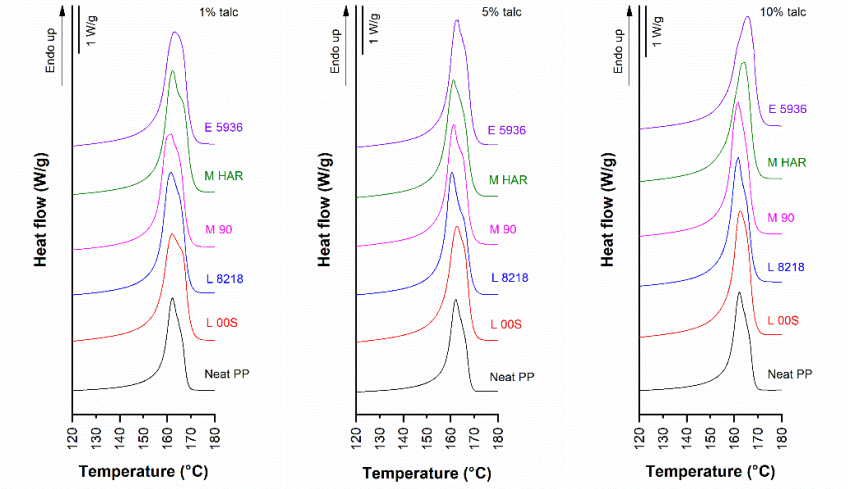

Figure 4.5b Annealed precursor films melting endotherms for neat PP and PP/talc compounds.

Membranes

Melting of membranes is analyzed in Figures 4.6 and 4.7 As a consequence of the uniaxial strain stage of MEAUS process, two main effects are observed. Firstly, it can be seen that the secondary shoulder due to annealing has completely disappeared, suggesting that the grown crystals around initial lamellae during annealing were unstable and could be converted into more stable crystals during stretching [77-79].

Secondly, the melting peak shows a bimodal distribution, with a marked second melting peak (right shoulder) appearing at higher temperatures than the primary melting peak that was observed in non-annealed and annealed precursor films. The main peak belongs to lamellae crystals whereas the right shoulder comes crystals with interconnected bridges between the lamellae [80, 81]. One possible reason could be that some pores are closed due to the break of weak connecting bridges resulting in the appearance of thicker lamellae, and crystals of the interconnected bridges between the lamellae can be leading to the appearance of this shoulder.

This second melting peak appeared in some annealed precursor films, but in a less intense way. The strong bridges under annealing may lead to the appearance of the shoulder, but its content is lower than that of main lamellae crystals, therefore, the only small shoulder can be observed. As will be commented in further morphological

section, during the cold and hot stretching step, pores are created and enlarged resulting in the stretching of short and long tie chains. This resulted in a local crystallization, which explains the appearance of interconnected bridges between lamellae, and provokes more intensity in this second melting peak observed in membranes [82, 83].

Primary melting peak shifts to a slightly higher temperature in membranes compared to non-annealed and annealed precursor films. When polypropylene is filled, two different behaviors are observed in membranes: whereas calcium carbonate shifts the main melting peak values to lower ones, talc increased the values. As for the calcium carbonate [63], it has explained the shifting of the main melting peak to lower temperatures based on the pulling out of some macromolecules from the initial lamellae. As for the talc effect, this may be due to the melting of very thin lamellae and their recrystallization in the form of thicker ones [63]. No significant changes in this main melting peak have been observed for the amount of filler, nor the talc grade employed.

The secondary melting peak, related to the connecting bridges between lamellae, showed a different behavior depending on the filler employed. Calcium carbonate, showed similar values of neat polypropylene, whereas talc shifted the melting values to higher temperatures. This is related with the strength of this connecting bridges, being stronger in talc filled membranes. Non-significant

differences were found concerning with the amount of filler and the type of talc employed.

The appearance of the secondary melting peak in membranes has as an outcome of increasing the crystallinity values obtained from melting signals when comparing membrane signals to pellet signals Table 4.3. The trends of crystallinity values depend on the filler employed. Calcium carbonate leads to higher crystallinity values when compared to annealed precursor films, and it is observed that an increase in calcium carbonate content tends to increase crystallinity. On the contrary, an increase in talc content decreases the membrane crystallinity. 1 and 5 wt. % talc membranes showed higher crystallinity values than the annealed precursor films, but 10 wt. % talc membranes inverted this trend.

Small differences between the different types of talc were observed, with regard to the main peak melting temperature of membranes. However, differences were found concerning the width of the shoulder after the main peak melting temperature, being broader when using microcrystalline talc.

Effect of the type of extruder on orientation and crystallization

Tables 4.5, 4.6 summarizes the previous studies carried out on polypropylene/calcium carbonate compounds produced initially by a single screw-screw extruder. Similar trends are observed and it is not clear to see any remarkable influence of the types of the extruder.

Despite the different shearing heating that these two extruders apply to the polypropylene compounds, this has not revealed a clear influence on the orientation and crystallization factors.

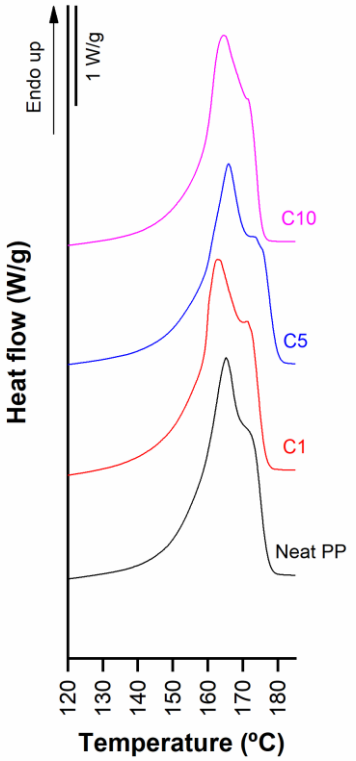

Figure 4.6 Melting endotherms for membranes of neat PP and PP/calcium carbonate.

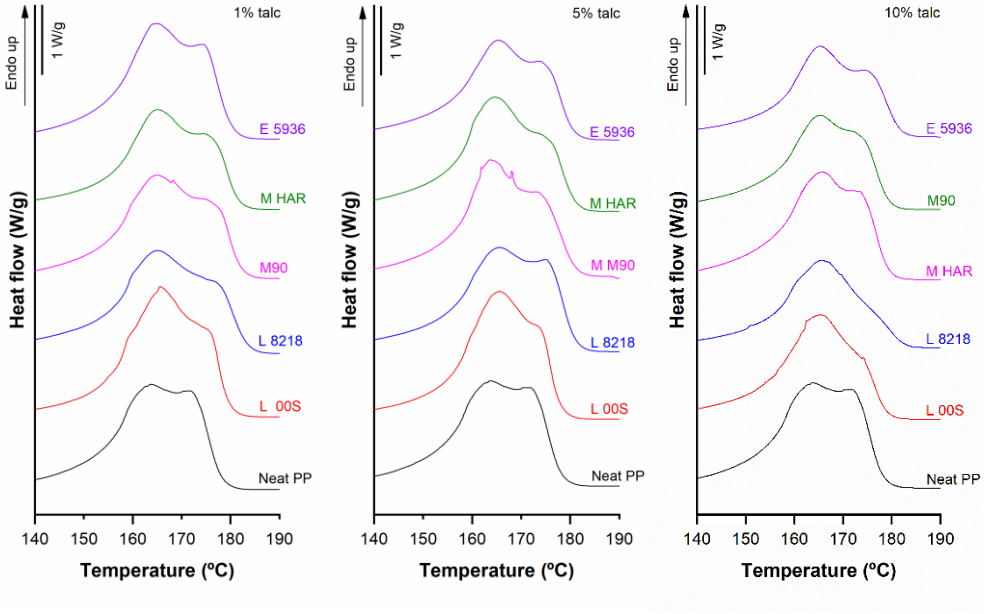

Figure 4.7 Melting endotherms for membranes of neat PP and PP/talc compounds.

Table 4.5 Orientation analysis carried out through polarized FT-IR for PP/calcium carbonate compounds, obtained by a single-screw extruder.

			Neat PP	C5	C10
F_c	Non-annealed precursor		0.56	0.57	0.6
	Annealed precursor	90 (ºC)	0.66	0.64	0.74
		115 (ºC)	0.67	0.69	0.69
		140 (ºC)	0.69	0.73	0.64
F_{av}	Non-annealed precursor		0.4	0.54	0.42
	Annealed precursor	90 (ºC)	0.48	0.48	0.59
		115 (ºC)	0.49	0.52	0.52
		140 (ºC)	0.59	0.54	0.51
F_{am}	Non-annealed precursor		0.26	0.52	0.25
	Annealed precursor	90 (ºC)	0.32	0.34	0.47
		115 (ºC)	0.35	0.35	0.38
		140 (ºC)	0.5	0.36	0.35

Table 4.6 DSC thermal analysis for PP/calcium carbonate compounds obtained by a single-screw extruder.

			Neat PP	C5	C10
Cooling runs		P_c-Peak	114.0	115.0	116.4
Heating runs	1^{st} peak (°C)	Non-annealed precursor	163.2	162.7	163.3
		Annealed precursor	163.6	162.5	163.5
		Membrane	162.8	163.1	165.2
	X_m (%)	Non-annealed precursor	45.9	46.4	42.3
		Annealed Precursor	47.1	46.6	50.4
		Membrane	48	52.3	51.1
	2_{nd} Peak (°C)	Membrane	170.9	173.2	169

4.3 Membrane pore morphology and permeability

During cold stretching, these chains part convert to initial connecting bridges. Then during hot stretching, some chains are pulled out from the initial lamellae and these stretched chains convert to connecting bridges. This is similar to the melt of crystalline lamellae under tension followed by the re-crystallization into oriented fibrillar structure [84, 85]. The connecting bridges enlargement process during stretching is proposed by Nilsson *et al* [86]. Based on the fact that some tie chains did not result from the chain entanglements, but the number of such species was small. The tie chains were concentrated mostly around the vicinity of the entanglement. During annealing, some chains around the initial lamellae are involved in the crystallization process. A typical folded chain lamellar assembly is shown where the frozen entanglement points are confined in the interlamellar amorphous region.

Caihong *et al* [71] established that, with an increase in annealing temperature, uniform connecting bridges and pore structure are obtained in the stretched microporous membrane. Results of Caihong [71] proved that, during annealing, the lamellar structure is improved due to the occurrence of melting and recrystallization behavior. During cold and hot stretching, the disappearing secondary crystals convert to initial connecting bridges and the improved lamellar structure supports the scaffold of pore structure. Both cold and hot stretching lead to the best connecting bridge arrangement for the microporous

membrane annealed. Annealing induces a difference of lamellar structure. The initial stable lamellae are improved; at the same time, some weak secondary crystals are induced.

With respect to the hot strain stage, Zuo *et al* [50], reports that at high temperatures, the enhanced chain mobility can significantly weaken the amorphous entanglement network. As a result, the tensile deformation would lead to chain disentanglement, reducing the constraints for tie chains. These loosened tie chains convert to bridges when stretched. These connecting bridges result in the formation of the pore structure and they also contribute to the stabilization of pore structure compared with that only through stretching under room temperature.

A porous morphology was obtained for the different calcium carbonate and talc-based compounds as a consequence of the final MEAUS stage, giving as result porous-based membranes. This final stage consists of a uniaxial stretching divided into two stages: cold strain (room temperature, 50 mm/min and 35 % strain) and hot strain (140ºC, 10 mm/min, 200 % strain). In this stage, it is expected that the lamellae of the row-lamellar structure are forced to get separated, and the length of the connecting bridges between lamellae is increased, leading to an increase of the pore size.

Calcium carbonate-based membranes

It is observed that the addition of 1 wt. % of calcium carbonate resulted in a dramatic increase in the pore-density (Table 4.7). Calcium carbonate could have had an effect on the conversion of stretched chains to connecting bridges during stretching followed by affecting on the row-lamellae structure, where the microsecond crystals at the lamellae ends could be stronger under a stress field converting to bridges connecting lamellae [87-89]. As a result, the calcium carbonate affected the tensile deformation, which led to having a better chain entanglement and increasing the constraints for tie chains. These connecting bridges result in the better formation of pore structure, and they also contributed to the higher pore density compared to the only polypropylene. The increasing trend within the range 1-10 wt. % calcium carbonate is maintained.

The addition of calcium carbonate caused a gradual increase in pore size, and porous area might as well show an increase. One of the possible explanations could be because of the presence of calcium carbonate and its debonding with polypropylene, where the lowest amount of pore size belongs to the lowest porous area percentage. Gurley permeability values drastically increased by adding 1 wt. % calcium carbonate, and further filler addition leading to a decrease of Gurley permeability value. One possible effect may be based on the effect of calcium carbonate dispersion, which at higher filler loading, dispersion of the fillers resulting in compacted

properties. Also, the presence of calcium carbonate which is intrinsically impermeable occupied the polypropylene networks and reduced the effective spaces for permeation could be other possible explanation.

The synergistic effect of the MEAUS process in filled samples was noticeable due to the combination of the generation of pores, because of the separation of lamellar blocks, along with the debonding mechanisms of calcium carbonate from the polymeric matrix (Figure 4.8). Both factors led to an increase of permeability with respect to the neat polypropylene, where a maximum of permeability belongs to the membrane with less percentage of calcium carbonate, and as the percentage of calcium carbonate increased the fewer membrane values obtained.

An aspect that has not been possible to be measured is the interconnection state between the pores along the thickness is the important issue, which controls the permeability factor, which in fact interconnected pores determine the membrane performances. This factor may also affect the decrease of permeability at high filler contents, despite the high pore density and high porous area.

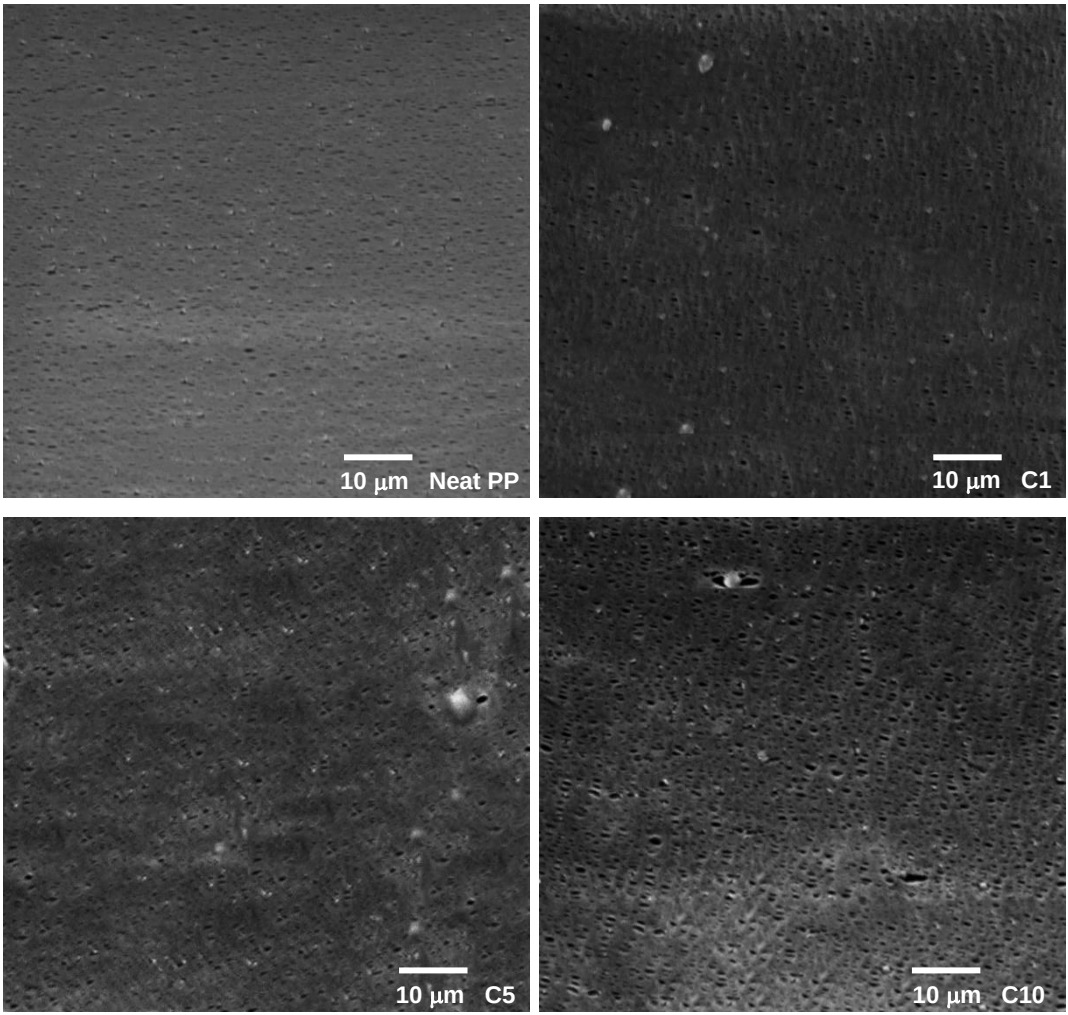

Figure 0.8 SEM micrographs of neat PP and PP/calcium carbonate membrane.

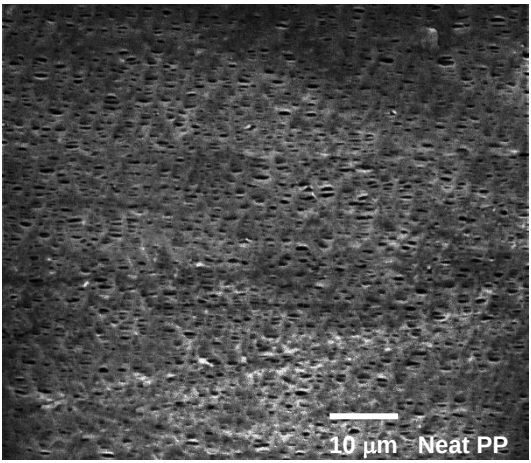

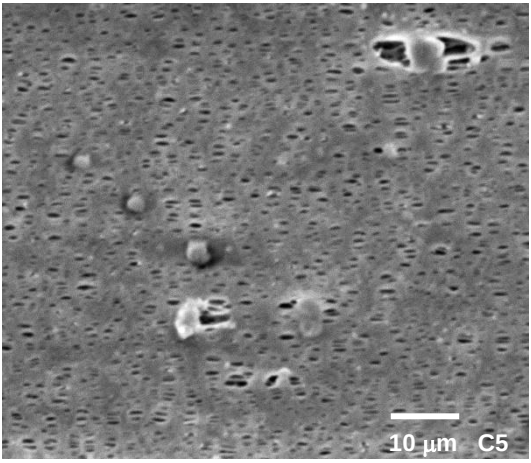

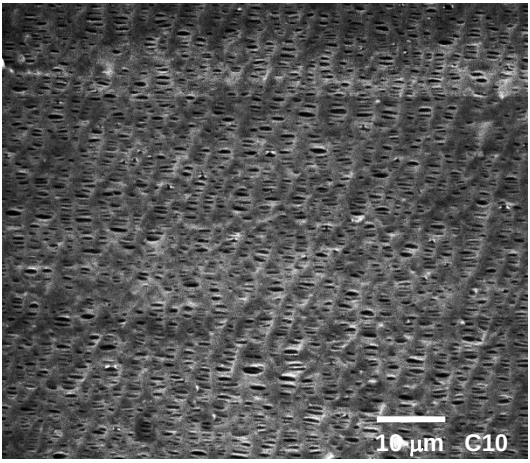

Figure 4.9 SEM micrographs of neat PP and PP/calcium carbonate membrane obtained by a single-screw extruder.

Table 4.7 Morphological analysis and permeability values of PP/calcium carbonate membranes obtained from a twin-screw extruder.

Reference	F_c	Pore density (pores/μm^2)	Porous area (%)	Average pore size $10^3(\mu m)$	Porosity %	Gurley permeability $10^3\mu m$ $(Pa{\cdot}s)^{-1}$
Neat PP	0.61	9	6.1	51	1.5	104
C1	0.75	67	7.1	85	1.7	276
C5	0.69	101	10.7	89	1.8	242
C10	0.65	109	15.0	97	1.9	212

Calcium carbonate-based membranes from a single-screw extruder

Some previous approaches to the production of these membranes were prepared by using a single-screw extruder, and pore morphology results of polypropylene/calcium carbonate membrane from single-screw extruder are presented in Table 4.8 and morphology showed in Figure 4.9. As it can be seen, in the most terms membrane from single-screw extruder and twin-screw have shown the same trend, in pore-density, the two of them showed an increasing trend when more calcium carbonate added, but the values that obtained from twin are much higher than the ones from single. Porous area values also showed an increasing trend compare to the neat polypropylene but in case of a single-screw extruder, it is seen that when calcium carbonate percentage rose up the porous area decreased.

It is observed that the average pore size showed an increase compared to the neat polypropylene, and by adding more calcium carbonate increased except for the single extruder that showed by increasing in the calcium carbonate loads the average pore size decreased. However, there is an increasing in the porous area and average pore size, Gurley permeability decreased in both membranes from single and twin-screw extruder when more calcium carbonate added, but Gurley values obtained from single-screw are significantly higher than those from a twin-screw extruder.

In this sense, a higher shearing effect due to the use of single-screw extruder could affect a micromolecular alignment during the extrusion process, having consequences of row lamellae structure generated during this stage. Also, in a twin-screw extruder the orientation factor obtained as quite higher than a single-screw extruder. Too high orientation can cause that during stretching stage the ability of separation of lamella blocks is restricted that resulted in lower pore sizes. It is quite controversial than single-screw extruder average pore size and the porous area in calcium carbonate 10 wt. % gives different so high values. It must be also considered that some pore construction thickness can take place.

Table 4.8 Morphological analysis and permeability values of PP/calcium carbonate membranes obtained from a single-screw extruder.

Reference	F_c	Pore density (pores/μm^2)	Porous area (%)	Average pore size 10^3(μm)	Porosity %	Gurley Permeability 10^3· μm·(Pa·s)$^{-1}$
PP	0.56	9	6.30	50	1.0	308
C5	0.49	14	15.3	100	1.8	643
C10	0.54	16	14.2	96	1.7	491

Talc-based membranes

The effect of talc on pore morphology and permeability is summarized by all numerical results in Table 4.9. membrane surface morphology was analyzed in Figure 4.10. The pore density of talc-filled samples showed an obvious increase with respect to the neat polypropylene as 1 wt.% of talc was added. Further talc content did not yield a significant trend in pore-density. As it is observed, small particle size (range of 1-4 μm) provided high pore-density, whereas bigger particle size notably reduced the pore-density value.

The addition of talc might have affected the conversion of stretched chains to connecting bridges during stretching and affected the row-lamellae structure. As can be seen an increase in the pore-density compared to the neat polypropylene. Except for the lamellar type talc (L00S), which showed low value in pore-density, the rest of the talc types showed an increase in the pore-density. One possible

explanation could be the lamellar talc type might have not affected the tensile deformation to have a better chain entanglement in increasing the constraints for tie-chains. The aftermath of this constrains may cause these connecting bridges couldn't result in the better formation of pore structure and they also may have not contributed to the higher pore density compared to the neat polypropylene [90-92].

It has been observed that talc addition provoked a remarkable decrease in the crystalline orientation of polypropylene. So, this should affect the creation of pores, due to the lamellae block separation. Nevertheless, in most of the deployed talc types, the pore-density is much higher than the neat polypropylene. The reason that could explain that is the debonding of talc with polypropylene matrix during the stretching stage.

Porous area followed a similar pattern than that of pore-density. In this sense for the studied system, it seems that a particle size range of 3-4 μm provides the best balance of all the studied talc types. Average pore size showed no significant differences.

Pore-density and porous area have a significant effect on permeability. At 1 wt. % talc content, membranes that used talc providing highest values of pore-density and porous area, permeability is the highest. The second factor is talc content. All membranes showed a decreasing trend when talc was high. The reduction of permeability at high talc contents might be related directly

to the reduction of permeable area, as these rigid fillers are not permeable to the pass of air.

One of the possible explanations for this reduction in the permeability at high percentages of talc loading could be because of talc's particle properties restrict liquid and gas diffusion increasing the diffusion path and impermeability, the highest amount of permeability belongs to the micro-lamellar talc type (M 90) which might be coming from the improvement of stiffness at the lower density when this talc type added to polypropylene. However, the occupation of the polypropylene networks by the presence of talc which might have reduced the effective spaces for permeation could be another possible explanation for the reduction in permeability at the higher talc loadings.

Correlationship between analysis of orientation factor and permeability

Figure 4.11 and 4.12 evidenced the high dependency that permeability had on the crystalline orientation. Thus, high orientation was promoted in the production of precursor films and filled annealed. The higher the crystalline orientation reach, the higher the permeability obtained. In both filler, there is a similarity in terms that higher filled content reduced orientation and the permeability.

Table 4.9 Morphological analysis and permeability values of PP/talc membranes.

	Morphology	Particle size (μm)	BET ($m^2 \cdot g^{-1}$)	Talc wt. %	F_c	Pore density (pores/μm^2)	Porous area (%)
Neat PP					0.61	8.98	6.1
L 00S	Lamellar	10.0	2.4	1	0.49	8.98	5.0
				5	0.26	7.52	5.2
				10	0.24	8.32	4.8
L 8218	Lamellar – fine grind	3.9	5.4	1	0.52	40.1	14.5
				5	0.29	25.71	12.1
				10	0.26	36.73	12.8
M 90	Micro-lamellar	3.3	13.0	1	0.56	31.24	13.6
				5	0.33	37.30	15.9
				10	0.29	31.24	12.5
M HAR	High aspect ratio	3.0	13.0	1	0.52	40.04	16.2
				5	0.35	54.82	16.2
				10	0.35	32.04	15.0
E 5936	Microcrystalline	1.1	21.3	1	0.45	36.24	15.6
				5	0.30	27.74	8.6
				10	0.26	21.28	7.3

	Morphology	Particle size (μm)	BET ($m^2 \cdot g^{-1}$)	Talc wt. %	Average pore size $10^3 \cdot (\mu m)$	Porosity	Gurley permeability $10^3 \mu m \cdot (Pa \cdot s)^{-1}$
Neat PP					0.05	1.5	104
L 00S	Lamellar	10.0	2.4	1	0.07	1.4	120
				5	0.07	1.9	101
				10	0.07	1.5	100
L 8218	Lamellar – fine grind	3.9	5.4	1	0.06	1.8	109
				5	0.07	1.8	100
				10	0.06	1.3	71
M 90	Micro-lamellar	3.3	13.0	1	0.07	1.9	138
				5	0.07	1.5	124
				10	0.06	1.3	100
M HAR	High aspect ratio	3.0	13.0	1	0.06	1.9	132
				5	0.05	1.7	117
				10	0.07	1.0	103
E 5936	Microcrystalline	1.1	21.3	1	0.07	1.3	116
				5	0.06	1.9	110
				10	0.06	1.6	104

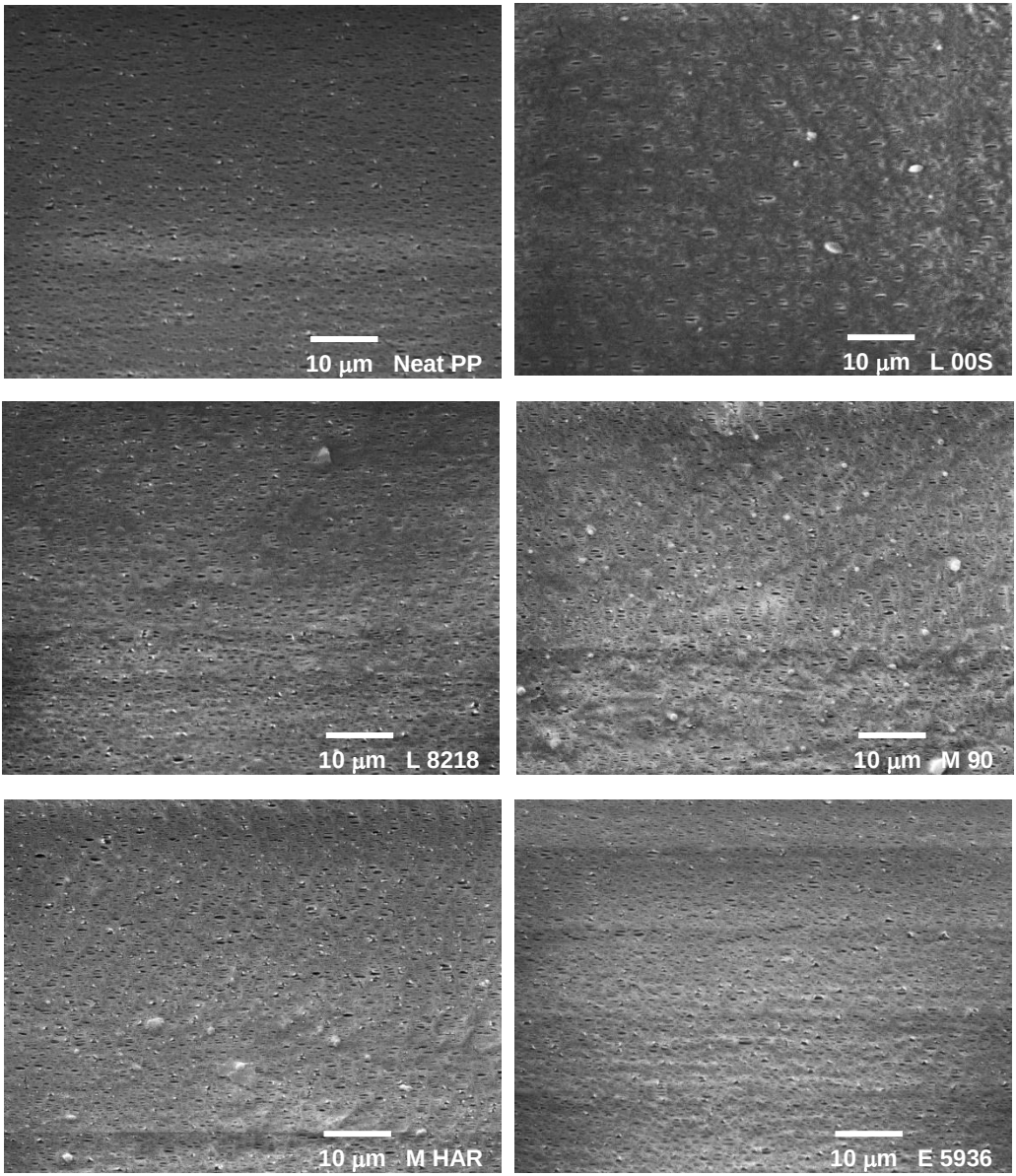

Figure 4.10a SEM micrographs of neat PP and PP/talc 1 wt.% membranes.

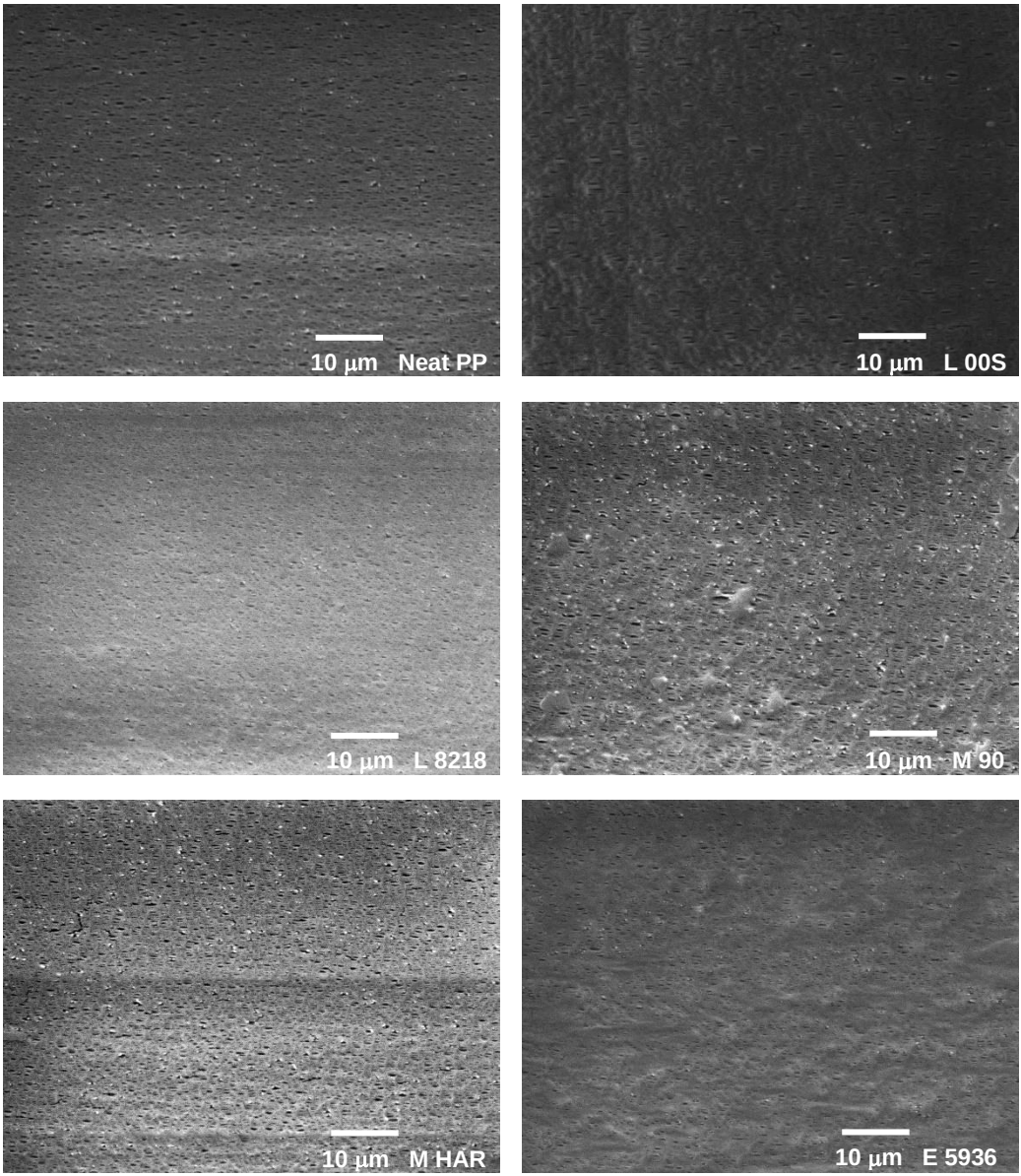

Figure 4.10b SEM micrographs of neat PP and PP/talc 5 wt.% membranes.

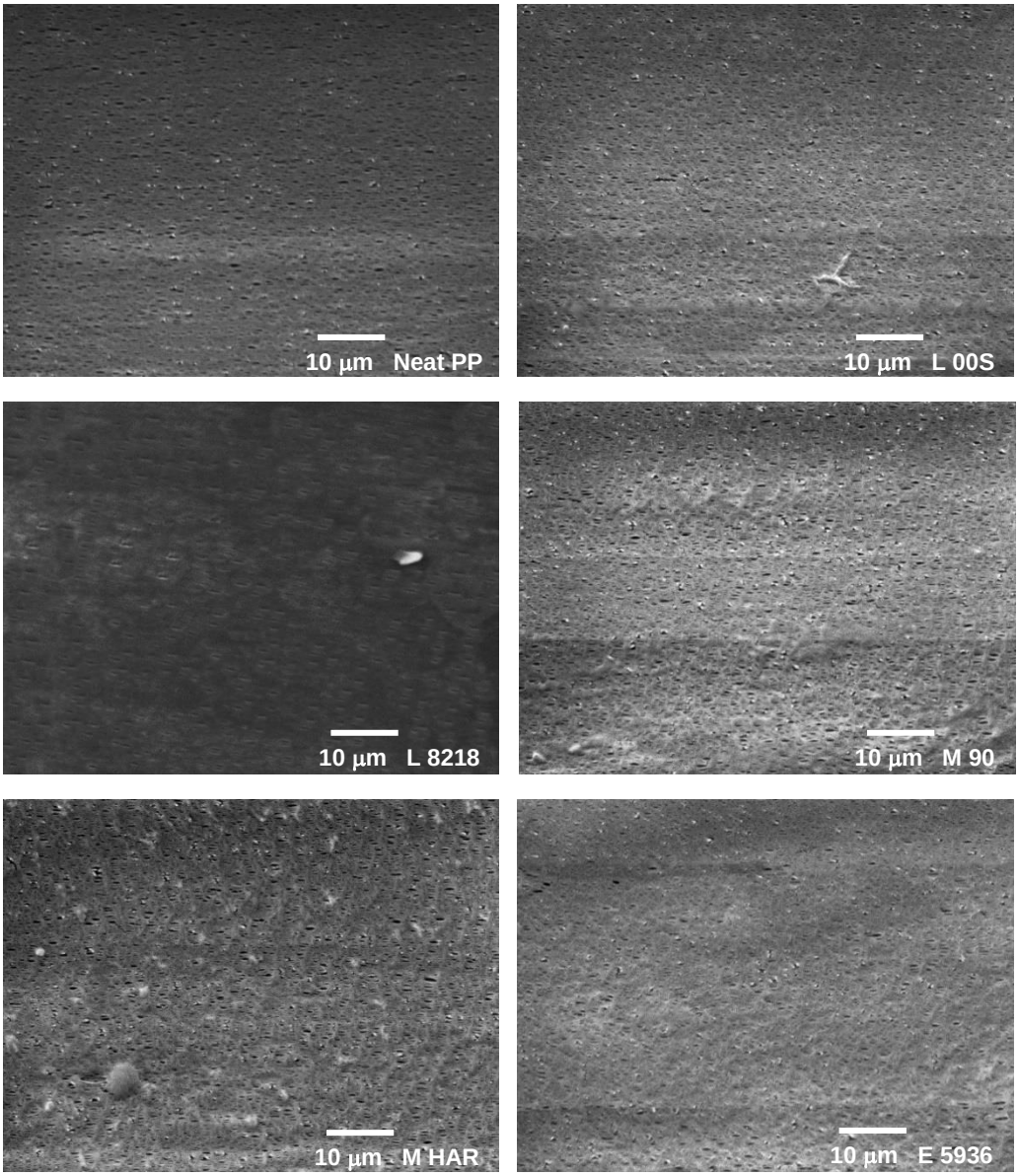

Figure 4.10c SEM micrographs of neat PP and PP/talc 10 wt.% membranes.

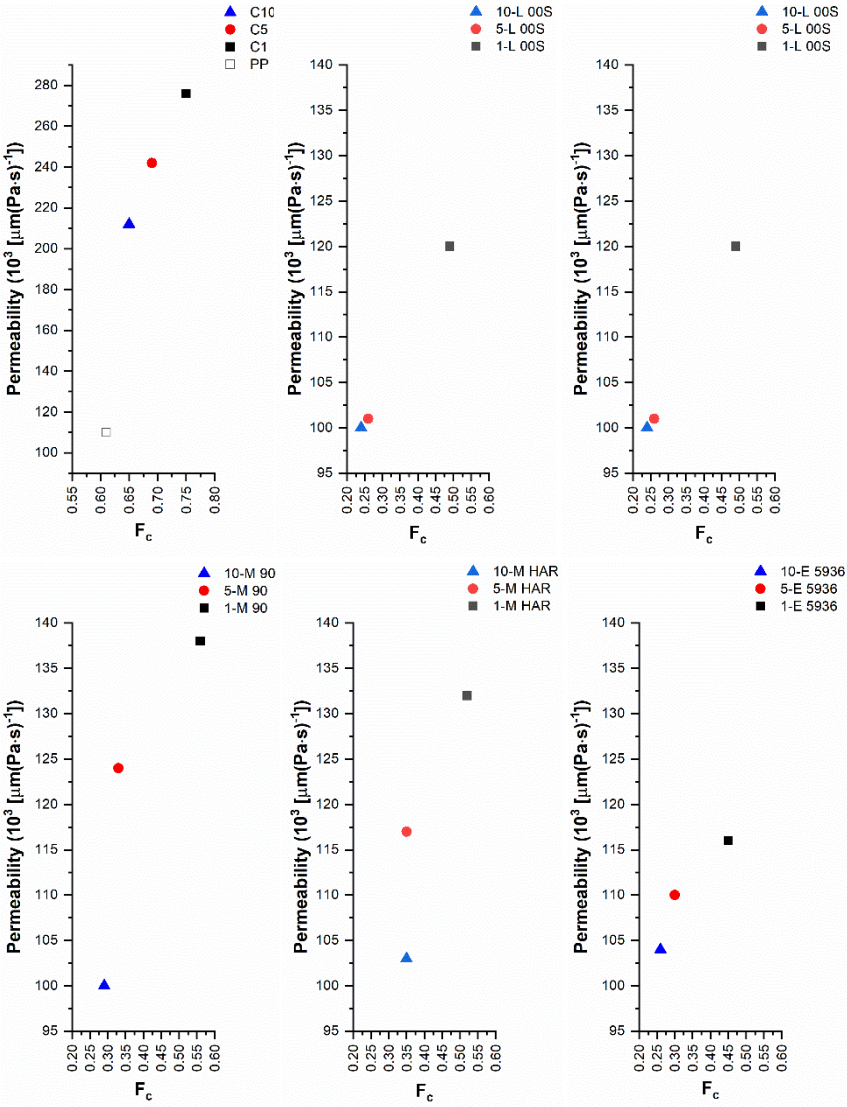

Figure 4.11 Correlationship between permeability and crystalline orientation factor.

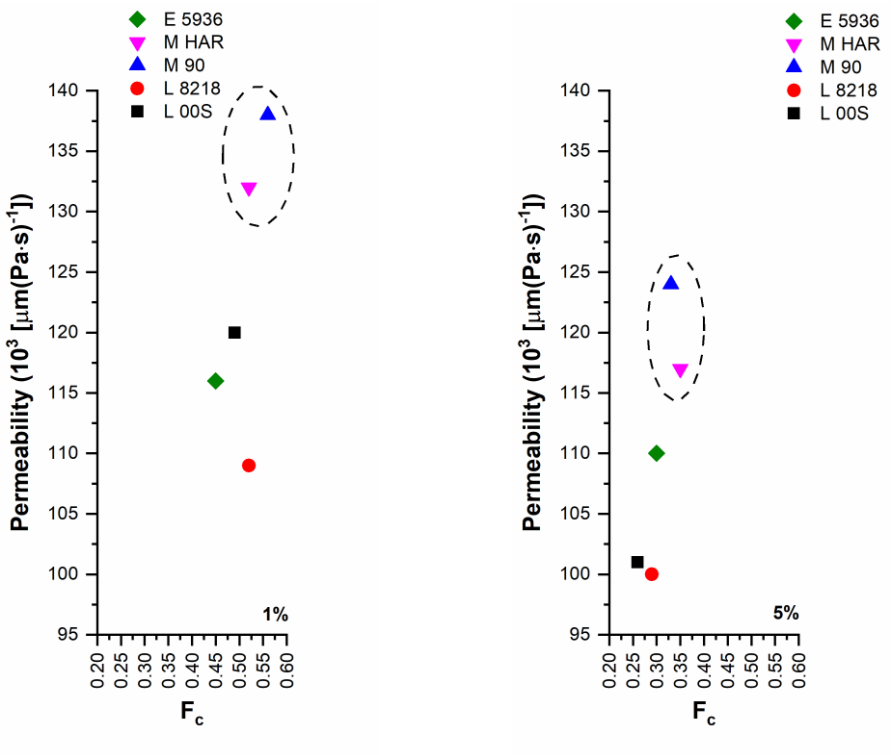

Figure 4.12 Effect of talc type on the correlation ship between permeability and crystalline orientation factor.

4.4 Thermogravimetric analysis

Loss weight mass and their respective first derivative (DTG) for all the calcium carbonate and talc membranes processed by twin screw extruder are shown in Figure 4.13 and Figure 4.14. From these plots, values were collected for the temperatures at which there was a loss of mass of 10 wt. % ($T_{0.1}$) and 50 wt. % ($T_{0.5}$), the relative lost mass at 400 and 600°C, and the temperature of maximum lost mass velocity (T_{max}) (Table 4.10 and Table 4.11).

For both types of filled membranes, the experimental plots correspond to one-single step process that can be described through an apparent first order mechanism, where the only variable is the mass conversion into volatiles [93-96]. This feature can also be seen in the DTG curves, where one single peak is detected.

A general trend can be extracted for the values of temperatures at 50 % decomposition. Talc filled membranes have shifted to higher temperatures with respect to the membrane of neat polypropylene. Also, increasing filler content increases the thermal stability of membranes. With respect to calcium carbonate membranes, only when a high amount of filler (10 wt. %) is added, (Figure 4.10) enhanced thermal stability is achieved.

Both fillers have higher volumetric heat capacities and thermal conductivities than polypropylene [97], thus the filled membranes would absorb more heat as compared to the pure polypropylene

membrane. Because of the colligative thermodynamic effect, the temperature of the filled membrane would increase and the polypropylene would start to degrade at higher temperatures [98-103].

The influence of air traces adsorbed in the amorphous phase of the initial degradation states of pyrolysis has been reported [103-108]. The results of crystallinity obtained by DSC (Table 4.1) for calcium carbonate membranes suggests that in this kind of membranes, a reduced amorphous phase can be a factor to help to increase the thermal stability of the membranes. Nevertheless, this hypothesis is not suitable for talc membranes, as we have observed that increasing talc content reduced overall crystallinity, and thus increased the amorphous character of the membrane.

Table 4.10 Thermal stability analysis of PP/calcium carbonate membranes.

Membrane	$T_{0.1}$ (ºC)	$T_{0.5}$ (ºC)	Lost mass 400ºC (%)	Lost mass 600ºC (%)	T_{max} (ºC)
Neat PP	311.9	378.8	72.2	100.0	400.2
C1	304.8	365.4	83.8	99.4	394.9
C5	303.1	371.7	77.2	95.2	394.9
C10	302.9	388.0	62.5	91.3	405.0

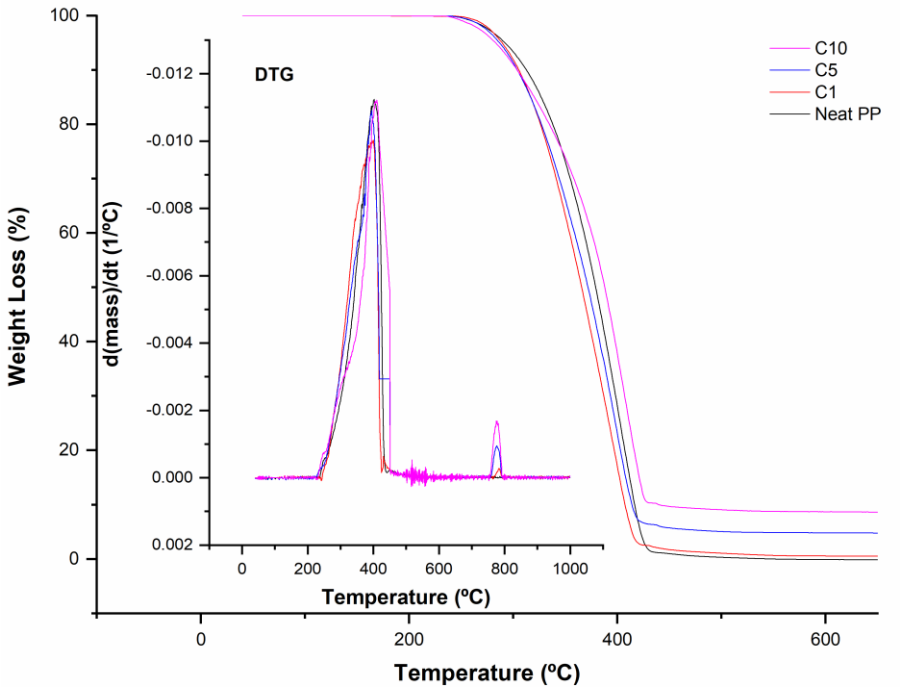

Figure 4.13 Plots of thermogravimetric analysis (TGA) of PP/calcium carbonate membranes.

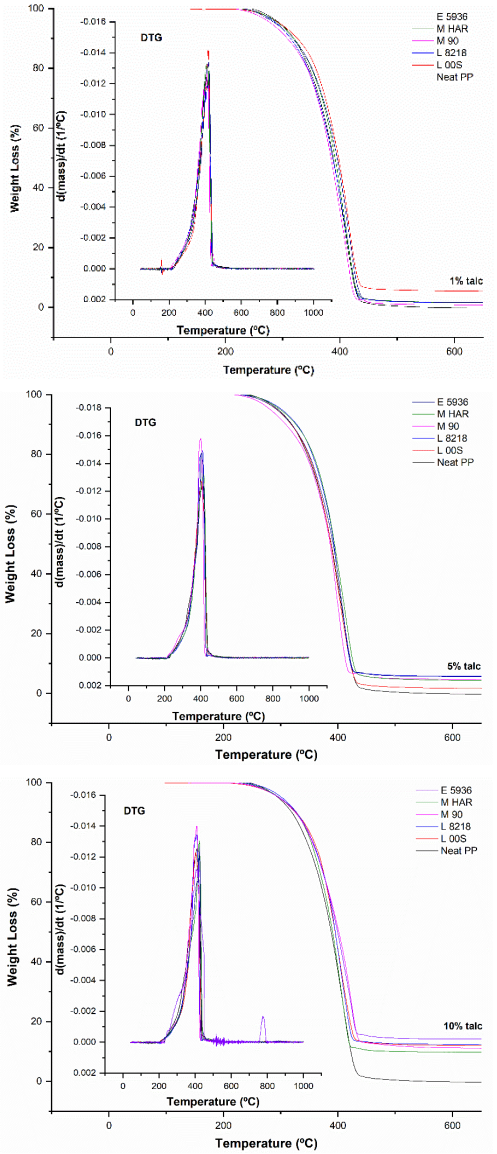

Figure 4.14 Plots of thermogravimetric analysis (TGA) of PP/talc membranes.

Table 4.11 Thermal stability analysis of PP/talc membranes.

Membrane		$T_{0.1}$ (ºC)	$T_{0.5}$ (º)	Lost mass 400ºC (%)	Lost mass 600ºC (%)	T_{max} (ºC)
Neat PP	**Wt.%**	311.9	378.8	72.2	100.0	400.2
L00S	1	317.4	387.3	66.0	98.2	402.0
	5	325.4	398.0	53.0	94.5	417.0
	10	327.0	395.4	56.1	88.0	404.0
L 8218	1	314.1	387.6	62.2	98.3	410.0
	5	327.1	392.2	61.0	94.1	409.4
	10	327.5	395.0	56.7	87.6	408.3
M 90	1	308.0	483.5	67.6	99.1	414.0
	5	308.0	386.3	71.0	95.3	400.1
	10	325.0	390.0	62.7	90.1	409.0
M HAR	1	319.6	390.9	59.6	98.3	408.9
	5	326.4	393.2	57.8	95.6	415.5
	10	325.0	401.0	49.4	88.7	423.2
E 5936	1	316.2	395.0	56.4	98.2	417.1
	5	319.0	396.0	60.3	94.3	406.0
	10	326.3	399.0	51.5	85.8	426.0

4.5 Mechanical behavior

For all the samples, during the stretching of the film, a stress-withering phenomenon was observed [109], but no necking was observed, which is a typical behavior of a row nucleated structure [110] Two significant points were noticed (Figure 4.15), known as “first yield point” and “second yield point” [111]. At first yield point, fine chain slip is combined with a transformation a rearrangement within the lamellae being oriented in the stretching direction without breaking. Second yield point might be related to the deformation of the secondary crystalline lamellae. After yielding, the tensile curves presented an increase in the nominal stress with the beginning of the strain hardening.

The stress applied involved a pre-orientation of the amorphous tie chains prior to crystal chain unfolding, which can be related to the first yield point [112]. On the other hand, the strain hardening of second yield point has been related to the deformation of the secondary crystalline lamellae (formed during the annealing process). Translating these terms into pore morphology, according to Samuels [113], the first and second yield points correspond to the beginning of macropore formation in the amorphous region and disruption of the lamellar structure, respectively, and the lamellae are stretched apart along the tensile direction between these two yield points [114]. It has also been reported the importance of the slope between the first yield point and second yield point. An increasing of this slope has been

related [80] to more lamellar separation instead of interlamellar slippage during the stretching process.

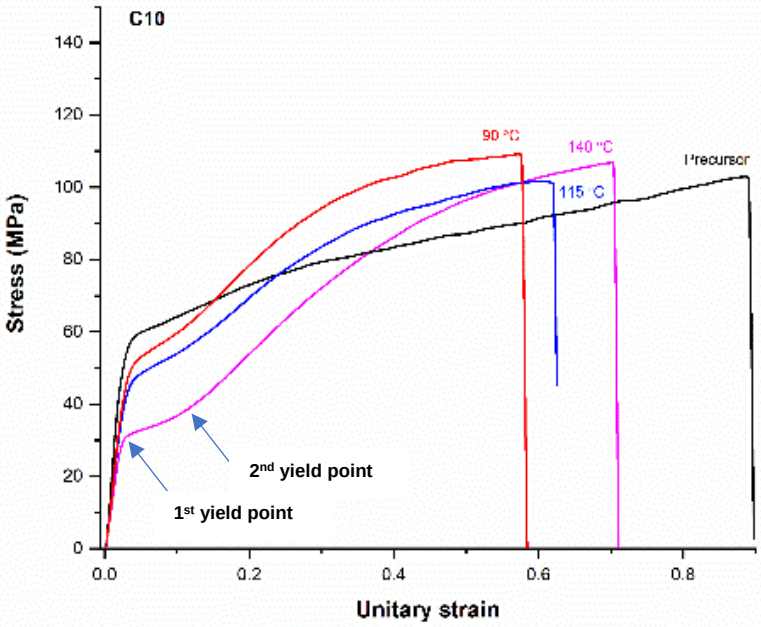

Figure 4.15 Representative stress-strain curve showing 1st yield and 2nd yield point.

Effect of annealing temperature

As stated in previous sections, a study on the effect of annealing temperature was conducted for calcium carbonate/polypropylene compounds (Figure 4.16). It is seen that an increase in annealing temperature led, as a general trend, to a decrease in the values of the first yield point (Table 4.12). This trend is completely reverse to that observed for neat polypropylene for Saffar [111], but the trend is similar as observed by Caihong [51], also for neat polypropylene. Also, increasing annealing temperature leaded to a major unitary strain.

Based on the relationship between the mechanical properties and the fraction of the tie chains in the amorphous region proposed by Nitta and Takayanagi [115] the decrease of yielding point after annealing is related to the fact that some tie chains disappear during annealing. These tie chains during annealing crystallize [116]. The crystallization of these tie chains indicates the occurrence of secondary crystallization during annealing, similar to the conclusion drawn by others. With increasing annealing temperature from 90°C to 140°C, the decrease of the yielding point may indicate that more secondary crystals are formed.

It can be seen, above all in 10 wt. % $CaCO_3$ samples that annealed polypropylene/calcium carbonate samples at different temperatures showed a higher slope between first and second yield point that the

corresponding precursor film. It is also noticeable how the annealing temperature affects notably to the stiffness of the films (Table 4.12), as the show a remarkable decrease as the annealing temperature is increased in almost all cases. As annealing increases the size and amount of lamellae, precursor films have a large elongation at break than annealed films.

Effect of filler addition

Figures 4.17 (a-d) show the comparison of annealed precursor films of neat polypropylene with the different filler/polypropylene compounds studied. Results of elastic modulus and first yield point are collected in Table 4.13. Here a combination of two effects is observed. Although first yield point of polypropylene has one of the lowest values of all the studied materials (which would help to have a first micropores creation), in all cases, the total elongation at break of neat polypropylene annealed precursor films is more restricted than in filled annealed precursor films. It suggests that the stage of stable pore growth is more enhanced when the filler is added to the polypropylene matrix, as stated by the values of pore density and porous area recorded for filled systems. No significant differences are found in the slope between the first and second yield point between filled and non-filled polypropylene.

A logical pattern of increasing elastic modulus as filler content does is found in calcium carbonate compounds, but controversially, a decreasing trend is observed for most of the talc employed.

Effect of talc type

Concerning to the type of talc (Figure 4.18) low particle size talcs (as M 90, M HAR, and E) seems to have lowest values of the first yield strength (Table 4.13), which would favor the origin of micropores [117-119], if compared with other types of talc. For instance, the highest first yield point values of L 00S could explain the low pore density observed in morphological studies. Increasing of talc content diminishes the first yield point values, but this has not a positive effect on increasing in general terms porous area, and so permeability values. In this sense, as commented in morphological section, the higher amount of talc restricts the permeable area and hinders the effect of pore creation.

Tensile strength increased as the amount of calcium carbonate filler increased, in polypropylene/talc compound as the amount of the talc increased the tensile strength decreased.

As it can be seen Table 4.12, the first yield point in polypropylene/calcium carbonate compounds showed an increase as the amount of the calcium carbonate filler increased, but in case of polypropylene/talc Table 4.13 compounds a decline in the value of fist yield point observed.

Table 4.12 Elastic modulus and 1st yield point of the non-annealed and annealed precursor of PP/calcium carbonate. Standard deviation in brackets.

	$CaCO_3$ wt. %	E (MPa)				1st Yield point (MPa)			
		Non-annealed precursor film	Annealing temperature °C			Non-annealed precursor film	Annealing temperature °C		
			90	115	140		90	115	140
Neat PP		1478 (189)			820 (122)	43 (5)			22 (2)
PP/$CaCO_3$	1	1802 (433)	1645 (199)	1413 (186)	859 (332)	57 (8)	53 (5)	41 (3)	22 (9)
	5	1701 (111)	1588 (207)	1498 (39)	1076 (550)	51 (6)	45 (7)	46 (2)	41 (20)
	10	1733 (331)	1717 (793)	1224 (109)	1146 (221)	47 (9)	44 (4)	50 (3)	42 (2)

Table 4.13 Mechanical properties, Elastic modulus and 1st yield point of the non-annealed and annealed precursor of PP/talc compound. Standard deviation in brackets

	Talc wt. %	E (MPa)		1st Yield point (MPa)	
		Non-annealed-precursor film	Annealed precursor film	Non-annealed-precursor film	Annealed precursor film
PP		1478 (189)	820 (122)	43 (5)	22 (2)
L 00S	1	1359 (251)	1078 (191)	53 (7)	37 (8)
	5	1634 (241)	1032 (158)	48 (6)	26 (3)
	10	1642 (103)	859 (267)	44 (3)	22 (7)
L 8218	1	1456 (689)	1319 (57)	65 (3)	34 (3)
	5	1915 (135)	1284 (101)	57 (8)	32 (3)
	10	1968 (71)	1014 (188)	47 (2)	26 (3)
M 90	1	1739 (104)	959 (161)	64 (2)	24 (4)
	5	1877 (446)	907 (421)	62 (4)	23 (11)
	10	1976 (114)	529 (115)	48 (9)	13 (3)
M HAR	1	1883 (117)	863 (385)	57 (4)	28 (10)
	5	1895 (476)	1141 (88)	54 (14)	22 (2)
	10	1946 (218)	758 (314)	52 (6)	20 (7)
E 5936	1	1851 (637)	696 (88)	63 (11)	28 (2)
	5	1871 (283)	1093 (77)	57 (9)	17 (3)
	10	1892 (287)	670 (309)	54 (12)	16 (8)

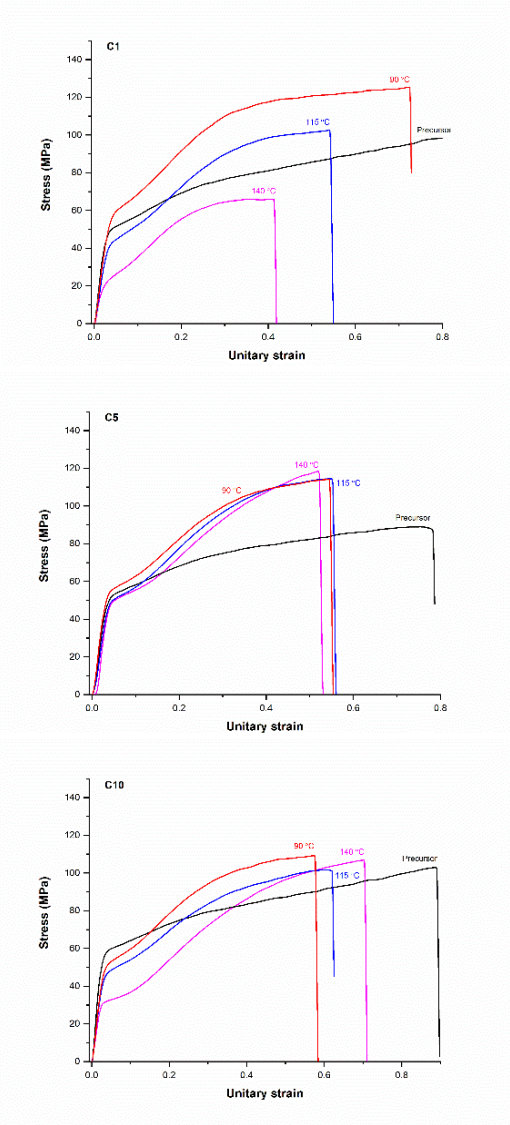

Figure 4.16 Effect of annealing on stress-strain curves for PP/calcium carbonate precursor films.

(a)

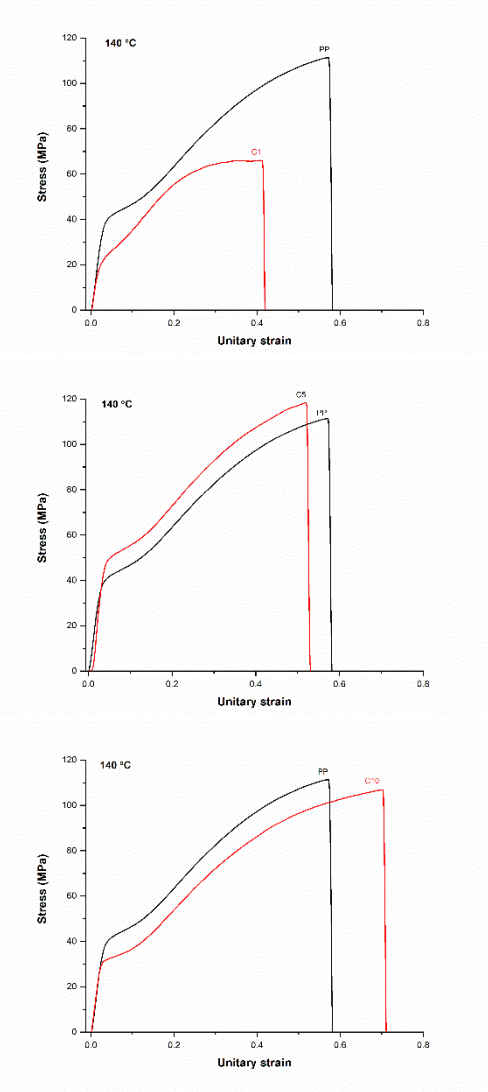

Figure 4.17 Effect of filler content on stress-strain curves for filled PP annealed precursors with (a) calcium carbonate, (b) 1 % wt. talc, (c) 5 % wt. talc and (d) 10 % wt. talc.

(b)

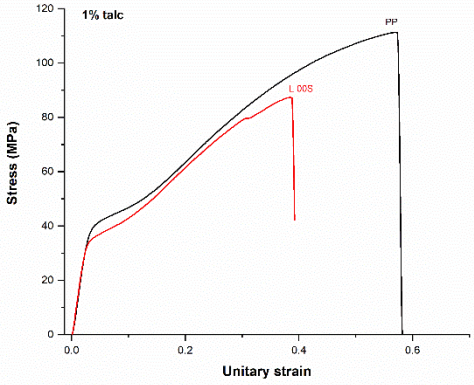
1% talc
PP
L 00S
Stress (MPa)
Unitary strain

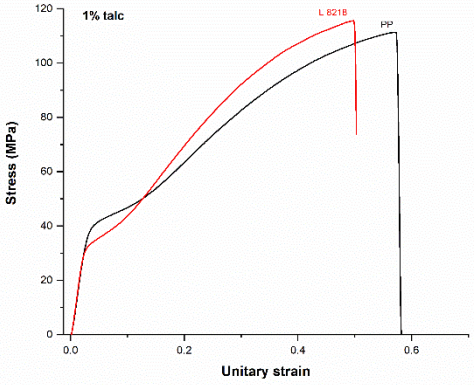
1% talc
L 821B
PP
Stress (MPa)
Unitary strain

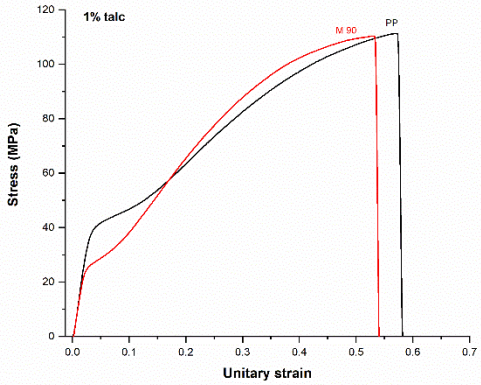
1% talc
M 90
PP
Stress (MPa)
Unitary strain

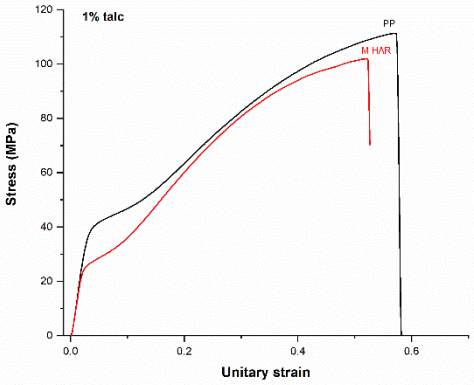
1% talc
PP
M HAR
Stress (MPa)
Unitary strain

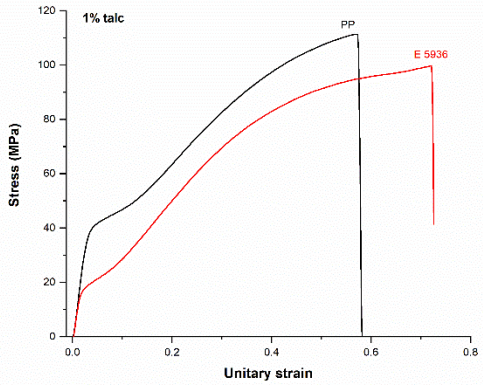
1% talc
PP
E 5936
Stress (MPa)
Unitary strain

(c)

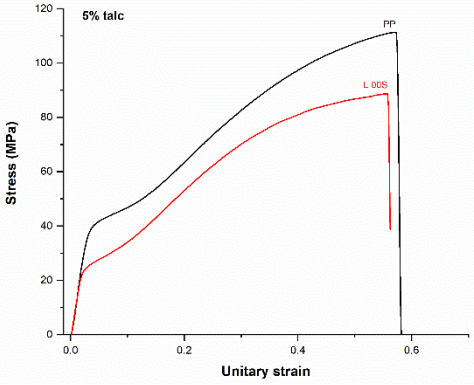
5% talc
PP
L 0DS
Stress (MPa)
Unitary strain

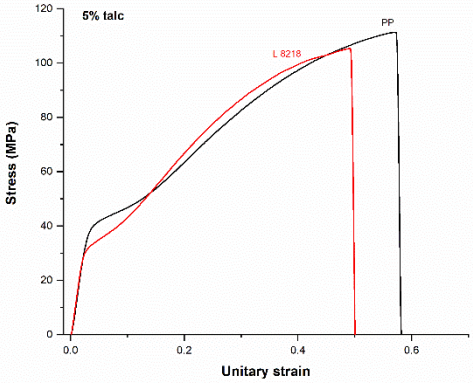
5% talc
PP
L 8218
Stress (MPa)
Unitary strain

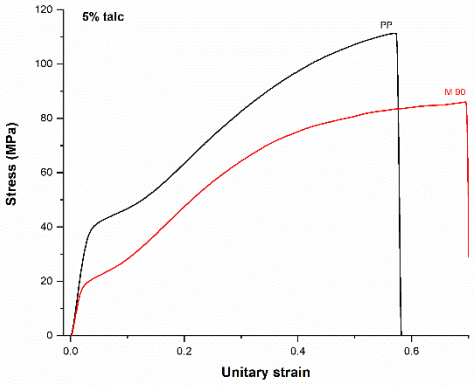
5% talc
PP
M 90
Stress (MPa)
Unitary strain

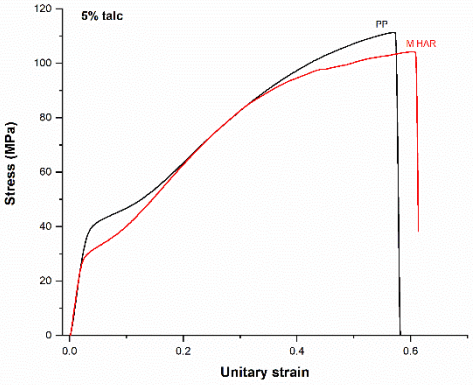
5% talc
PP
M HAR
Stress (MPa)
Unitary strain

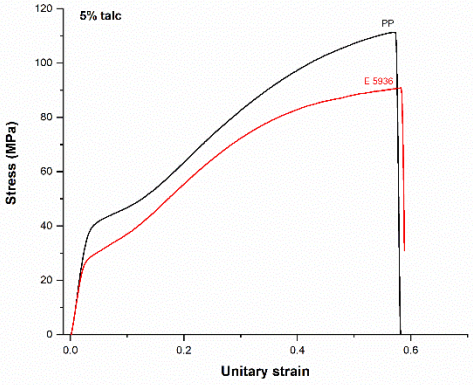
5% talc
PP
E 5936
Stress (MPa)
Unitary strain

(d)

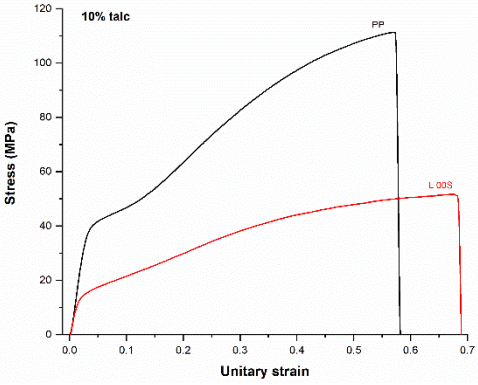
10% talc
PP
L 008
Stress (MPa)
Unitary strain

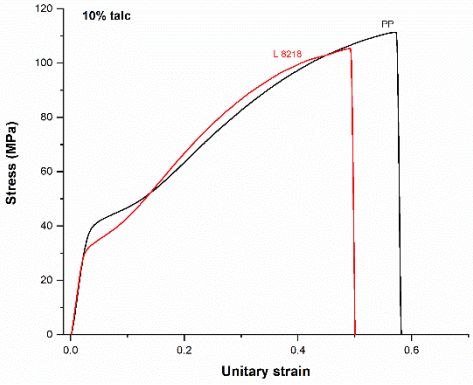
10% talc
PP
L 8218
Stress (MPa)
Unitary strain

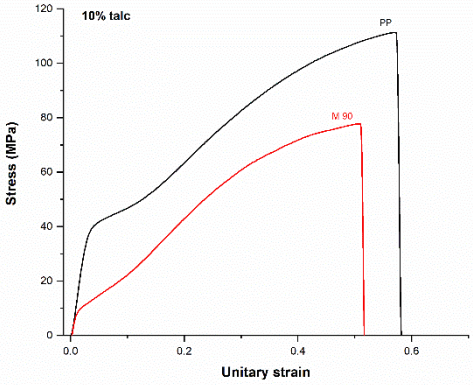
10% talc
PP
M 90
Stress (MPa)
Unitary strain

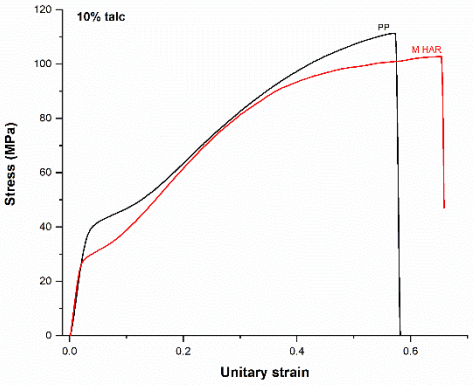
10% talc
PP
M HAR
Stress (MPa)
Unitary strain

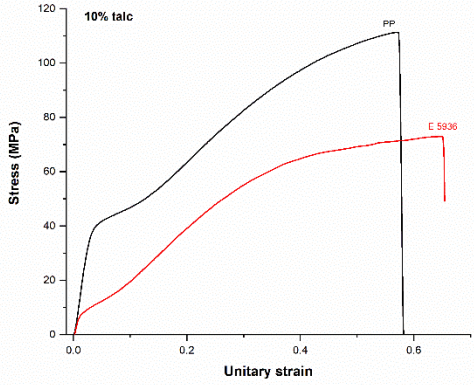
10% talc
PP
E 5936
Stress (MPa)
Unitary strain

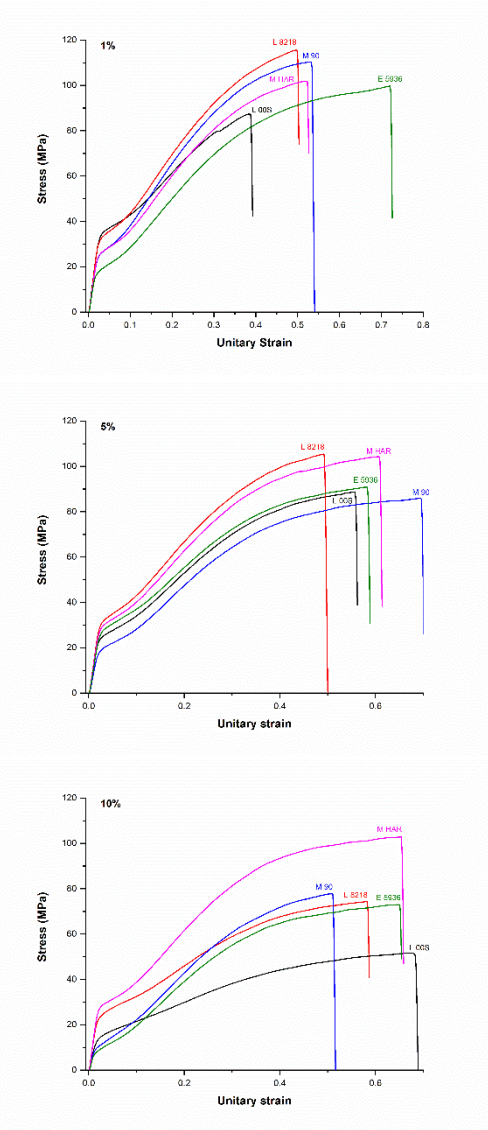

Figure 4.18 Effect of talc type on stress-strain curves.

CHAPTER 5

GENERAL CONCLUSIONS AND FUTURE PERSPECTIVES

5.1 General conclusions

A series of studies carried out, some main conclusions can be extracted:

MEAUS process has been proved to be a suitable process technology for the production of porous membranes of polypropylene filled with calcium carbonate or talc. A proper adjustment of the extrusion conditions, air pressure and draw ratio led to the production of stable precursor films of nominal thickness 25 μm. For comparison purposes, all the membranes were produced under the same extrusion temperature profile and draw ratio.

No significant differences in the rheological behavior of the polypropylene compounds have been observed, within the filler content range employed, and/or the types of filler employed. Although other studies have shown the influence of rheological behavior on the first stage of MEAUS process, in our study, this has not been a relevant factor to be considered.

For calcium carbonate compounds, two kinds of the extruder were employed, a single and twin-screw extruder. The membranes obtained from single extruders provided higher crystalline orientation values, probably promoted in some way for the high shearing capability of single screw extruders. After stretching stages, higher pore density, higher porous area and porosity and thus, higher Gurley permeability

values were obtained, when compared with those of calcium carbonate membranes obtained from a twin-screw extruder.

it has been shown that annealing rose significantly up the orientation factor of crystalline phase as the temperature increased. This effect is more marked when 1 wt. % of calcium carbonate was added. Higher amounts of calcium carbonate showed a not quite significant effect of annealing temperature. It has seen that in annealed talc compounds annealing made the orientation factor of crystalline phase decreased. This decrease is even more noticeable when 1 wt.% of talc was added. It seems that talc with higher particle sizes alongside with smaller particle sizes had not a significant effect of annealing temperature on the orientation factor of crystalline phase when higher amounts of talc deployed.

As a matter of fact, annealing improved the amorphous orientation along the machine direction compared to the neat polypropylene. In non-annealed precursor films, amorphous orientation significantly rose up when calcium carbonate was added to neat polypropylene. This is likely due to the participation of disrupted amorphous end chains in the crystallization and also the partial motion of the crystal blocks, which results in a slight stretching of the tie chains along the lamellae thickness. It has observed that by adding talc, the orientation of the amorphous phase showed a higher value than the neat polypropylene. Although, as the amount of talc increased orientation

amorphous phase decreased, which the lamellae could not well-aligned perpendicular to the flow direction.

The orientation of the crystalline phase, evaluated through polarized FT-IR has been proved to be very dependent on the type of filler employed. Whereas calcium carbonate increased the crystalline phase orientation, talc grades had a reverse effect. Both trends were even maximized when the filler content was increased. No significant differences in the crystalline orientation factor were observed for the different types of talc employed.

It has observed that amorphous phase orientation and average orientation in polypropylene/calcium carbonate compound followed the same trend with respect of the one showed by crystalline orientation factor. The amorphous phase orientation, F_{am}, for annealed precursor film of talc compound showed very small value compared to the polypropylene and its value considerably decreased. The F_{am} values for the annealed films are also in the same range, and it is seen that annealing treatment has not a major influence on the amorphous phase orientation of talc components. Talc addition might have provoked a constraint of the orientation of the amorphous phase orientation.

The nucleating activity of these fillers was different, talc was the one that showed a higher nucleating ability than calcium carbonate. Calcium carbonate seemed to act as a potential nucleating site that

helped to arrange in a more oriented composition along the extrusion direction of the polymer macromolecules. In case of talc filler, size and morphology of the employed talc didn't have a significant influence on its nucleation activity. Nevertheless, high contents of the smallest size (E 5936) or more oriented (M HAR) provided the high nucleation efficiency.

Annealing stage in MEAUS process is necessary to increase the lamellar thickness indicating some crystallization behavior. The appearance of the low-temperature plateau (left shoulder) in DSC curves came from some tie chain crystallization around initial lamellae. new stable recrystallized structure, coming from some tie chain crystallization around initial lamellae which converts to connecting bridges between lamellae. Both calcium carbonate and talc-filled annealed precursor films developed higher crystallinity values than their respective non/annealed ones. Crystallinity was not significantly affected by the filler content on the annealed precursor films, nor the type of talc employed.

Annealing temperature was studied for calcium carbonate compounds. Higher annealing temperatures promoted an increase in the secondary annealing peak and shifted this secondary annealing peak to higher temperatures. This secondary peak that comes from annealing shifted at higher temperatures in filled compounds with respect to the neat polypropylene annealed precursor films. This effect is more marked in talc filled compounds, as well as the intensity

of this secondary peak. No significant differences about the intensity and temperature shifting of this annealing peak have been observed related with the filler content, nor with the type of talc employed.

All membranes showed a melting peak from DSC with a bimodal distribution, with the apparition of a right shoulder to the main peak. The main melting peak belongs to lamellae crystals. Primary melting peak shifted to a slightly higher temperature in membranes compared to non-annealed and annealed precursor films. When polypropylene is filled, two different behaviors are observed in membranes: whereas calcium carbonate shifted the main melting peak values to lower ones, talc increased the values. Although, small differences between the different types of talc were observed, with regard to the main peak melting temperature of membranes. However, differences were found concerning the width of the shoulder after the main peak melting temperature, being broader when using microcrystalline talc.

The secondary melting peak, related to the connecting bridges between lamellae, showed a different behavior depending on the filler employed. Calcium carbonate, showed similar values of neat polypropylene, whereas talc shifted the melting values to higher temperatures. This is related with the strength of this connecting bridges, being stronger in talc filled membranes. Non-significant differences were found concerning with the amount of filler and the type of talc employed.

Porous-based membranes given as a porous morphology was obtained for the different calcium carbonate and talc-based compounds as a consequence of the final MEAUS stage. This final stage consists of a uniaxial strain (carried out in two stages, room temperature, and 140 ºC) created porous morphologies for all the samples studied. During cold stretching, the pores are formed progressively and the initial few pores are from the deterioration crystalline structure, not amorphous regions. Also, for a constant hot stretching level, polypropylene/calcium carbonate compounds showed higher Gurley value and better air permeability than the polypropylene/talc compounds which is related to the constant hot stretching.

The addition of 1 wt. % of calcium carbonate resulted in a dramatic increase in the pore-density. Calcium carbonate also, caused a gradual increase in pore size, and porous area might show an increase which the lowest amount of pore size belongs to the lowest porous area percentage.

In the most terms of uniaxial strain, membrane from single-screw extruder and twin-screw have shown the same trend, in pore-density, the two of them showed an increasing trend when more calcium carbonate added, but the values that obtained from twin are much higher than the ones from single. Porous area values also showed an increasing trend compare to the neat polypropylene but in case of a

single-screw extruder, it is showed that when calcium carbonate percentage rose up the porous area decreased.

The average pore size showed an increase compared to the neat polypropylene, and by adding more calcium carbonate increased except for the single extruder that showed by increasing in the calcium carbonate loads the average pore size decreased. However, there is an increasing in the porous area and average pore size, Gurley permeability decreased in both membranes from single and twin-screw extruder when more calcium carbonate added, but Gurley values obtained from single-screw are significantly higher than those from a twin-screw extruder.

Talc-filled samples showed an increase in the pore density with respect to the neat polypropylene as 1 wt.% of talc was added. Further talc content did not yield a significant trend in pore-density. Small particle size (range of 1-4 μm) provided high pore-density, whereas bigger particle size notably reduced the pore-density value. Porous area demonstrated a similar pattern than pore-density. It seems that a particle size range of 3-4 μm provides the best balance of all the studied talc types. Average pore size showed no significant differences in all types of talc.

Pore-density and porous area have a promising effect on permeability. At 1 wt. % talc content, membranes that used talc providing highest values of pore-density and porous area,

permeability is the highest. All membranes showed a decreasing trend when talc was high. The reduction of permeability at high talc contents might be related directly to the reduction of permeable area, as these rigid fillers are not permeable to the pass of air. the highest amount of permeability belongs to the micro-lamellar talc type (M 90) which might be coming from the improvement of stiffness at the lower density when this talc type added to polypropylene.

In terms of a correlation between orientation factor and permeability it is showed that the higher the crystalline orientation reach, the higher the permeability obtained. In both filler, there is a similarity in terms that higher filled content reduced orientation and the permeability.

For both types of filled membranes, Los weight mass and their respective first derivative (DTG) carried out, and a general trend extracted for the values of temperatures at 50 % decomposition. Talc filled membranes have shifted to higher temperatures with respect to the membrane of neat polypropylene. Also, increasing filler content increased the thermal stability of membranes. With respect to calcium carbonate membranes, only when a high amount of filler (10 wt. %) is added, enhanced thermal stability is achieved.

During the stretching of the precursor film, two significant points were noticed “first yield point” and “second yield point”. First and second yield points correspond to the beginning of macropore formation in the amorphous region and disruption of the lamellar structure, respectively, and the lamellae are stretched apart along the

tensile direction between these two yield points. An increasing of this slope has been related to more lamellar separation instead of interlamellar slippage during the stretching process. The decrease of a yielding point after annealing is related to the fact that some tie chains disappear during annealing. It has been observed that in 10 wt. % calcium carbonate samples that annealed at different temperatures showed a higher slope between first and second yield point that the corresponding precursor film. It has also found that how the annealing temperature affected notably to the stiffness of the films. No significant differences are found in the slope between the first and second yield point between filled and non-filled polypropylene. It is found that there is a logical pattern of increasing elastic modulus as filler content does in calcium carbonate compounds, but controversially, a decreasing trend is observed for most of the talc employed.

5.2 Future perspectives

The most prominent association that many people have when thinking of a membrane resembles that of a filter, that is, a device capable of separating various components from a mixture according to their size.

This dissertation has focused on systematic characterization of the porous membrane obtained through MEAUS process. Two types of the filled porous membrane (PP/calcium carbonate and PP/talc) in a

different wt. % for both produced. Due to each type of membrane specifics and the experimental results reported in this dissertation, suggesting industrial applications are divided as follows:

Deploying these types of the membrane in water waste treatment in order to save disposal costs. During the treatment of natural gas in refinery sites several waste streams are generated. Waste contaminated by so many chemical components that are harmful to an environment (Mercury, Glycol, Coalescence etc.) have to be handled very carefully and treated or disposed of hazardous waste. Producing potable water from the sea, to clean industrial effluents and recover valuable constituents.

Dehydration (Sweetening) of natural gas is one the promising process in Oil and gas industry, natural gas contains H_2O in either liquid and/or gaseous form. Among methods that exist to sweetening the natural gas by removing acid gases CO_2, H_2S and sulfur species, membrane separation is on the top of the separation process.

In one the newest technology in the refinery industry which is called Ultra-low-sulfur diesel production and vacuum gas an oil deep hydrotreatment, this technique is very effective in sulfur removal from fuel oil, where the molecules that contain sulfur lose that atom by hydrogenation reactions. The sulfur-containing components are converted to H_2S and Hydrocarbons in presence of Hydrogen on solid catalyst. Hydrodesulfurization process is mostly carried out in trickle

bed reactors where membranes emulsifier uses in catalyst vendors surface which is one of the factors that influences to minimize the rate of sulfur in natural gas separation in the reactor.

They are also key components in energy conversion and storage systems such as batteries and fuel cells. Within a fuel cell that are highly efficient devices that convert the chemical energy stored in a fuel directly into electricity, the polymer electrolyte membrane (PEM) serves as the conducting interface between the anode and cathode, transporting the ions, the PEM is a central, and often performance-limiting, component of the fuel cell. Nafion, the most widely used PEM material due to its remarkable proton conductivity and mechanical strength, combines a hydrophobic Teflon-like backbone with hydrophilic ionic side groups. Upon hydration, these components self-assemble into a bicontinuous nanostructure comprised of a hydrophobic matrix containing ionic nanochannels. The free movement of protons through these ionic nanochannels is the source of Nafion's impressive conductivity.

REFERENCES

[1] R.W. Baker, Membrane technology and applications, in, Wiley Chichester, 2004, pp. 3–17, ISBN 0-470-85445-6.

[2] N. N. Li, A. G. Fane, W. S. W. Ho, and T. Matsuura, Advanced Membrane Technology and Applications, Hoboken, NJ, USA: John Wiley & Sons, Inc., 2008.

[3] M. Mulder, Basic principles of membrane technology, Journal of Membrane Science, vol. 72, no. 3, p. 564, 1996.

[4] Ma, Y. H. (n.d.), Hydrogen Separation Membranes, Advanced Membrane Technology and Applications, 671–684, 2008.

[5] H. B. Park, Y. M. Lee (n.d.), Polymeric Membrane Materials and Potential Use in Gas Separation, Advanced Membrane Technology and Applications, 633–669, 2008.

[6] A. Peterlin, J. Williams, H Olf, Process for the preparation of opencelled microporous films. US Patent (1974) 3839516 A.

[7] P. Luis, T. Van Gerven, B. Van der Bruggen, Recent developments in membrane-based technologies for CO2 capture. Progress in Energy and Combustion Science, 38(3), 419–448, (2012).

[8] S. N. Dhoot, Sorption and transport of gases and organic vapors in poly (ethylene terephthalate), 2004.

[9] E. Kimball, A. Al-Azki, A. Gomez, E. Goetheer, N. Booth, D. Adams, D. Ferre, Hollow Fiber Membrane Contactors for CO_2 Capture: Modeling and Up-Scaling to CO_2 Capture for an 800 MWe Coal Power Station. Oil & Gas Science and Technology – Revue d'IFP Energies Nouvelles, 69(6), 1047–1058, (2013).

[10] M. Rezakazemi, I. Heydari, Z. Zhang, Hybrid systems: Combining membrane and absorption technologies leads to more efficient acid

gases (CO_2 and H_2S) removal from natural gas. Journal of CO_2 Utilization, 18, 362–369, (2017).

[11] L. Caihong, X. Ruijie, Melt-Stretching Polyolefin Microporous Membrane, Submicron Porous Materials, 81-105, (2017).

[12] SS. Zhang, A review on the separators of liquid electrolyte Li-ion batteries. J Power Sources 164(1):351–364, (2007).

[13] P. Bernardo, E. Drioli, G. Golemme, Membrane gas separation: a review/state of the art. Ind Eng Chem Res 2009; 48:4638e63.

[14] P. Arora, Zh (John) Zhang, Battery separators. Chem. Rev. 2004, 104, 4419–4462.

[15] T. Hasegawa, T. Kondo, Short circuit-resistant polyethylene microporous film. US. patent 6054498, (2000).

[16] F. Macedonio, E. Drioli, a. a. Gusev, a. Bardow, R. Semiat, M. Kurihara, Efficient technologies for worldwide clean water supply, Chemical Engineering and Processing: Process Intensification, vol. 51, pp. 2–17, 2012.

[17] M. Xu, S. Hu, J. Guan, X. Sun, W. Wu, W. Zhu, Polypropylene microporous film. US patent 5134174, (1992).

[18] A. Hashimoto, K. Yagi, H. Mantoku, Porous film of high molecular weight polyolefin and process for producing same. US. patent 6048607, (2000).

[19] L.M. Robeson, Correlation of Separation Factor versus Permeability for Polymeric Membranes, J. Membr. Sci. 62, 165 (1991).

[20] S.A. Stern, Polymers for Gas Separation: The Next Decade, J. Membr. Sci. 94, 1 (1994).

[21] R.W. Baker and J.G. Wijmans, Membrane Separation of Organic Vapors from Gas Streams, in Polymeric Gas Separation Membranes, D.R. Paul and Y.P. Yampol'skii (eds), CRC Press, Boca Raton, FL, pp. 353–398 (1994).

[22] C. Arnold, Stability of high-temperature polymers. Journal of Polymer Science: Macromolecular Reviews, 14(1), 265–378, (1979).

[23] M. Rezakazemi, M. Sadrzadeh, T. Mohammadi, Separation via Pervaporation Techniques Through Polymeric Membranes. Transport Properties of Polymeric Membranes, 243–263, (2018).

[24] T. C. Merkel, M. Zhou, R. W. Baker, Carbon dioxide capture with membranes at an IGCC power plant. Journal of Membrane Science, 389, 441–450, (2012).

[25] S. D. Vora, J. D. Figueroa, S. Zhou, Hybrid Membrane/Absorption Process for Post-combustion CO2 Capture, National energy technology laboratory, Existing Plants, Emissions & Capture, 2011.

[26] P. Meares, The manufacture of microporous membranes and their structure and properties. Journal of Chemical Technology & Biotechnology, 37(3), 189–194, (2007).

[27] F. Sadeghi, development of microporous polypropylene by stretching (PhD thesis), Ecole Polytechnique de Montreal, Canada, 2006.

[28] F. Sadeghi, A. Ajji, P.J. Carreau, Analysis of microporous membranes obtained from polypropylene films by stretching, Journal of Membrane Science, 292 (2007) 62-71.

[29] K. Habibi, P. Castejón, A. B. Martínez, D. Arencón, Effect of filler content, size, aspect ratio and morphology on thermal, morphological and permeability properties of porous talc filled-Polypropylene obtained through MEAUS process. Adv Polym Technol, 1–10. (2018).

[30] P. Castejón, K. Habibi, A. Saffar, A. Ajji, A.B. Martínez, D. Arencón, Polypropylene-Based Porous Membranes: Influence of Polymer Composition, Extrusion Draw Ratio and Uniaxial Strain. Polymers, 10(1), 33, (2017).

[31] S. Nakamura, S. Kaneko, Y. Mizutani, Microporous polypropylene sheets containing CaCO3 filler, Journal of applied polymer science, 49 (1993) 143-150.

[32] S. Nagō, Y. Mizutani, Microporous polypropylene sheets containing CaCO3 filler: Effects of stretching ratio and removing CaCO3 filler, Journal of applied polymer science, 68 (1998) 1543-1553.

[33] L. Caihong, Q. Cai, R. Xu, X.Chen, J. Xie, Influence of magnesium sulfate whiskers on the structure and properties of melt-stretching polypropylene microporous membranes, Journal of Applied Polymer Science, 133 (2016) 43884.

[34] Q. Cai, R. Xu, X. Chen, C. Chen, H. Mo, C. Lei, Structure and properties of melt-stretching polypropylene/silicon dioxide compound microporous membrane, Polymer composites, 37 (2016) 2684–2691.

[35] S.H. Tabatabaei, P.J. Carreau, A. Ajji, Microporous membranes obtained from polypropylene blend films by stretching, Journal of Membrane Science, 325 (2008) 772-782.

[36] A. Saffar, P.J. Carreau, A. Ajji, M.R. Kamal, Development of polypropylene microporous hydrophilic membranes by blending with PP-g-MA and PP-g-AA, Journal of Membrane Science, 462 (2014) 50-61.

[37] M. G. Buonomenna, S.-H. Choi, F. Galiano, E. Drioli, Membranes Prepared via Phase Inversion, Membranes for Membrane Reactors, (2011), 475–490.

[38] B.V.H. Strathmann, Introduction to Membrane Science and Technology, Angewandte Chemie, 124(38), (2012), 9623–9623.

[39] Cheryan, M. Ultrafiltration and Microfiltration Handbook, 2nd ed.; CRC: Boca Raton, FL.

[40] D. PAUL, Reformulation of the solution-diffusion theory of reverse osmosis. Journal of Membrane Science, 241(2), (2004), 371–386.

[41] F. Sadeghi, A. Ajji, P.J. Carreau, Microporous membranes obtained from polypropylene blends with superior permeability properties, Journal of Polymer Science Part B: Polymer Physics, 46 (2008) 148-157.

[42] S.H. Tabatabaei, Development of microporous membranes from PP/HDPE films through cast extrusion and stretching (PhD thesis), Ecole Polytechnique de Montreal, Canada, 2009.

[43] F. Sadeghi, A. Ajji, P.J. Carreau, Analysis of row nucleated lamellar morphology of polypropylene obtained from the cast film process: effect of melt rheology and process conditions, Polymer Engineering & Science, 47 (2007) 1170-1178.

[44] M.B. Johnson, G.L. Wilkes, Microporous membranes of polyoxymethylene from a melt-extrusion process: (II) Effects of thermal annealing and stretching on porosity, J. Appl. Polym. Sci., 2002, 84: 1762.

[45] M. B. Johnson, Investigation of the processing-structure-property relationship of selected semi-crystalline polymers (PhD thesis), Virginia Polytechnic Institute and State University, United states, 2000.

[46] L. Caihong, H. Weiliang, X. Ruijie, X. Yunqi, the correlation between the lower temperature melting plateau endotherm and the stretching-induced pore formation in annealed polypropylene films, Journal of Plastic Film & Sheeting, 28 (2012) 151-164.

[47] J. Zhang, J. Fang, J.L. Wu, J. Wu, H. Mo, Z.M. Ma, N.L. Zhou, J. Shen, Study on the viscosity of polypropylene composites filled with different size and size distribution $CaCO_3$, Polymer Composites, 32 (2011) 1026-1033.

[48] S. Kitade, N. Ochiai, Y. Takahashi, I. Noda, Y. Matsushita, A. Karim, C. C. Han, Lamellar Orientation of Diblock Copolymer Solutions under Steady Shear Flow. Macromolecules, 31(23), (1998), 8083–8090.

[49] A. Nogales, BS. Hsiao, RH. Somani, Shear-induced crystallization of isotactic polypropylene with different molecular weight distribution: in situ small- and wide-angle X-ray scattering studies. Polymer 2001; 42(12): 5247–5256.

[50] F. Zuo, JK. Keum, X. Chen, BS. Hsiao, H. Chen, SY. Lai, R. Wevers, J. Li, The role of interlamellar chain entanglement in deformation-induced structure changes during uniaxial stretching of isotactic polypropylene. Polymer 48:6867–6880, (2007).

[51] L. Caihong, W. Shuqiu; C. Qi, X. Ruijie, H. Bing, S. Wenqiang, Influence of heat-setting temperature on the properties of a stretched polypropylene microporous membrane. Polym. Int. 2014, 63, 584–588.

[52] B. Rotenberg, A. J. Patel, D. Chandler, Molecular Explanation for Why Talc Surfaces Can Be Both Hydrophilic and Hydrophobic Journal of the American Chemical Society 2011 133(50), 20521-20527.

[53] B. S. Sprague, J. L. Riley, H. D. Noether, Factors Influencing the Crystal Structure of Cellulose Triacetate. Textile Research Journal, 28(4), (1958), 275–287.

[54] CB. Chen, CH. Lei, Q. Cai, HB. Mo, RJ. Xu, Influence of annealing time on the structure and properties of HDPE microporous membrane, J Plast Film Sheeting 31(1):78–95, (2015).

[55] T. Wu, M. Xiang, Y. Cao, F. Yang, Influence of annealing on stress–strain behaviors and performances of β nucleated polypropylene stretched membranes, J Polym Res 21:1–13, (2014).

[56] I.M. Ward, P.D. Coates, M.M. Dumoulin, Solid Phase Processing of Polymers, Hanser, 2000.

[57] S.H. Tabatabaei, P.J. Carreau, A. Ajji, Effect of processing on the crystalline orientation, morphology, and mechanical properties of polypropylene cast films and microporous membrane formation, Polymer, 50 (2009) 4228-4240.

[58] G. Perego, G. Domenico cella, C. Bastioli, Effect of Molecular Weight and Crystallinity on Poly (lactic acid) Mechanical Properties, Journal of Applied Polymer Science, Vol. 59,37-43 (1996).

[59] H. Bai, H. Deng, Q. Zhang, K. Wang, Q. Fu, Z. Zhang, Y. Men, Effect of annealing on the microstructure and mechanical properties of polypropylene with oriented shish-kebab structure, Polym Int 61:252–258, (2012).

[60] SC. Tjong, Structural and mechanical properties of polymer nanocomposites, Materials Science and Engineering R. 2006; (53): 73-197.

[61] A. Lazzeri, SM. Zebarjad, M. Pracella, K. Cavalier, R. Rosa, Filler toughening of plastics. Part 1—The effect of surface interactions on physico-mechanical properties and rheological behaviour of ultrafine $CaCO_3$/HDPE nanocomposites. Polymer. 2005; 46(3): 827-844.

[62] K. Ishikiriyama, B. Wunderlich, Crystallization and melting of poly (oxyethylene) analyzed by temperature-modulated calorimetry, Journal of Polymer Science Part B: Polymer Physics, 35 (1997) 1877-1886.

[63] M. Kamal, C.S. Sharma; P, Upadhyaya, V, Verma, K.N, Pandey, V, Kumar, D.D, Agrawal, Calcium carbonate (CaCO3) nanoparticle

filled polypropylene: Effect of particle Surface treatment on mechanical, thermal, and morphological performance of composites. J. Appl. Polym. Sci. 2012, 124, 2649–2656.

[64] L. J. Michot, F. Villieras, M. Francois, J. Yvon, R. Le Dred, and J. M. Cases, The Structural Microscopic Hydrophilicity of Talc, Langmuir 1994 10 (10), 3765-3773.

[65] E. Ferrage, F. Martin, S. Petit, S. Pejo-Soucaille, P. Micoud, G. Fourty, J. Ferret, S. Salvi, P. De Parseval, J. Fortune, Evaluation of talc morphology using FTIR and H/D substitution 5 October 2000, in, 2003.

[66] H. Holland, M. Murtagh, An XRD morphology index for talcs: the effect of particle size and morphology on the specific surface area, Adv. X-ray Anal, 42 (2000) 421-428.

[67] A. Makhlouf, H. Satha, D. Frihi, S. Gherib, R. Seguela, Optimization of the crystallinity of polypropylene/submicronic-talc composites: The role of filler ratio and cooling rate, Express Polymer Letters, 10 (2016) 237.

[68] R. Seguela, E. Staniek, B. Escaig, Plastic deformation of polypropylene in relation to crystalline structure. J Appl Polym Sci 1999; 71(11): 1873–1885.

[69] D. Ferrer-Balas, M. L. Maspoch, A. B. Martinez, O. O. Santana, Influence of annealing on the microstructural, tensile and fracture properties of polypropylene films. Polymer, 42(4), (2001), 1697–1705.

[70] D. Dudic, D. Kostoski, V. Djokovic. Formation and behaviour of low-temperature melting peak of quenched and annealed isotactic polypropylene. Polym Int 2002; 51(2): 111–116.

[71] L. Caihong, W. Shuqiu, X. Ruijie, X. Yunqi, P. Xinlong, A study of plastic plateau disappearance in stress– strain curve of annealed

polypropylene films during stretching, In: The 2012 World Congress on ACEM'12, Seoul Korea, p 241, (2012).

[72] W. Shuqiu, L. Caihong, C. Qi, X. Ruijie, H. Bing, S. Wenqiang, P. Xinlong, Study of structure and properties of polypropylene microporous membrane by hot stretching, Polym. Bull. (2014) 71: 2205.

[73] M. D, Guiver, Y.M Lee, Polymer Rigidity Improves Microporous Membranes, Science, 339, (2013), 284.

[74] Z. Ding, R. Bao, B. Zhao, J. Yan, Z. Liu, M. Yang, Effects of annealing on structure and deformation mechanism of isotactic polypropylene film with row-nucleated lamellar structure. J. Appl. Polym. Sci. 2013, 563 130, 1659–1666.

[75] A. Qaiss, H. Saidi, O. Fassi-Fehri, M. Bousmina, Porosity formation by biaxial stretching in polyolefin films filled with calcium carbonate particles, Journal of Applied Polymer Science, 123 (2012) 3425-3436.

[76] R. Hiss, S. Hobeika, C. Lynn, G. Strobl, Network stretching, slip processes, and fragmentation of crystallites during uniaxial drawing of polyethylene and related copolymers. A comparative study. Macromolecules 32:4390–4403, (1999).

[77] S. Lee, S. Park, H. Song. Lamellar crystalline structure of hard elastic HDPE films and its influence on microporous membrane formation. Polymer 2006; 47(10): 3540–3547.

[78] C. Xiande; X. Ruijie, X. Jiayi, L. Yuanfei, L. Caihong, L. Liangbin, the study of room-temperature stretching of annealed polypropylene cast film with row-nucleated crystalline structure. Polymer 2016, 94, 566 31–42.

[79] Guo Shaoyun, Fabrication of microporous membranes from melt extruded polypropylene precursor films via stretching: Effect of annealing, Polymer Science: English version, 1028-1037, (2015).

[80] CH. Lei, SQ. Wu, RJ. Xu, Q. Cai, B. Hu, XL. Peng, WQ. Shi, Formation of stable crystalline connecting bridges during hot stretching of polypropylene hard elastomer film, Polym Bull 70(4):1353–1366, (2013).

[81] C. Qi, X. Ruijie, W. Shuqiu, Ch. Changbin, M. Haibin, L. Caihong, L. Liangbin, Z. Lic, Influence of annealing temperature on the lamellae and connecting bridge structure of stretched polypropylene microporous membrane, Polym Int 64 (3):446–452, (2015).

[82] XD. Chen, RJ. Xu, JY. Xie, CH. Lei, the study of room-temperature stretching of annealed polypropylene cast film with row-nucleated crystalline structure, Polymer 94:31–42, (2016).

[83] SQ. Wu, CH. Lei, Q. Cai, RJ. Xu, B. Hu, WQ. Shi, XL. Peng, Study of structure and properties of polypropylene microporous membrane only by hot stretching, Polym Bull 71 (9):2205–2217, (2014).

[84] M. Xanthos, C. Chandavasu, K. Sirkar, C. Gogos, Melt processed microporous films from compatibilized immiscible blends with potential as membranes, Polymer Engineering & Science, 42 (2002) 810-825.

[85] M. Alonso, J. Velasco, Constrained crystallization and activity of filler in surface modified talc polypropylene composites, European Polymer Journal, 33 (1997) 255-262.

[86] F. Nilsson, X. Lan, T. Gkourmpis, M. S. Hedenqvist, U. W. Gedde, Modelling tie chains and trapped entanglements in polyethylene. Polymer, 53(16), (2012), 3594–3601.

[87] JA. Degroot, AT. Doughty, KB. Stewart, Effects of cast film fabrication variables on structure development and key stretch film properties. J Appl Polym Sci 52(3):365–376, (1994).

[88] RJ. Xu, XD. Chen, JY. Xie, Q. Cai, CH. Lei, Influence of melt-draw ratio on the crystalline structure and properties of polypropylene cast film and stretched microporous membrane, Ind Eng Chem Res 54(11):2991–2999, (2015).

[89] A. Saffar, PJ. Carreau, MR. Kamal, A. Ajji, Hydrophilic modification of polypropylene microporous membranes by grafting TiO_2 nanoparticles with acrylic acid groups on the surface, Polymer 55(23):6069–6075, (2014).

[90] F. Qiu, M. Wang, Y. Hao, S. Guo, The effect of talc orientation and transcrystallization on mechanical properties and thermal stability of the polypropylene/talc composites, Composites Part A: Applied Science and Manufacturing, 58 (2014) 7-15.

[91] J. Velasco, J. De Saja, A. Martinez, Crystallization behavior of polypropylene filled with surface-modified talc, Journal of applied polymer science, 61 (1996) 125-132.

[92] T. Hirata, H. Nagayasu, T. Yonekawa, M. Inui, T. Kamijo, Y. Kubota, T. Tsujiuchi, D. Shimada, T. Wall, J. Thomas, Current Status of MHI CO2 Capture Plant technology, 500 TPD CCS Demonstration of Test Results and Reliable Technologies Applied to Coal Fired Flue Gas, ScienceDirect, Energy Procedia 63 (2014) 6120 – 6128.

[93] J. Guo, H. Huang, Microstructure and Rheologic Development of Polypropylene/Nano-CaCO3 Composites Along Twin-Screw Extruder, J. Appl. Polym. Sci, 2009, 1687–1693.

[94] C. Chan, J. Wu, J. Li, Y. Cheung, Polypropylene/calcium carbonate Nanocomposites, Polymer, 43 (2002), 2981-2992.

[95] A. Galeski, Strength and toughness of crystalline polymer systems, Progress in Polymer Science, 2003; 28(12): 1643–1699.

[96] J. Diez, C. Alvarino, J. Lopez, C. Ramirez, MJ. Abad, J. Canol, Influence of the stretching in the crystallinity of biaxially oriented polypropylene (BOPP) films, J Therm Anal Calorim 2005; 81: 21–25.

[97] Guo Shaoyun, Fabrication of microporous membranes from melt extruded polypropylene precursor films via stretching: Effect of annealing, Polymer Science: English version, 1028-1037, (2015).

[98] T. Wu, M. Xiang, Y. Cao, J. Kang, F. Yang, Influence of lamellar structure on double yield behavior and pore size distribution in β nucleated polypropylene stretched membranes, RSC Adv 4:43012–43023, (2014).

[99] J. Grebowicz, SF. Lau, B. Wunderlich, The thermal properties of polypropylene, J Polym Sci Polym Symp 71:19–37, (1984).

[100] F. Chu, Y. Kimura, Structure and gas permeability of microporous film prepared by biaxial drawing of the beta-form polypropylene, Polymer 37 (1996) 573.

[101] AS. Argon, RE. Cohen, Toughen ability of polymers, Polymer. 2003; 44(19): 6013–6032.

[102] WCJ. Zuiderduim, C. Westzaan, J. Huétink, RJ. Gaymans, Toughening of polypropylene with calcium carbonate particles, Polymer. 2003; 44(1): 261-275.

[103] RN. Rothon, M. Hancock. In Particulate-Filled Polymer Composites, Rothon RN. (Ed.). England: Longman Scientific &Technical; 1995. p. 1-42.

[104] Y. Lin, H. Chen, CM. Chan, J. Wu, High Impact Toughness Polypropylene/$CaCO_3$ Nanocomposites and the Toughening Mechanism. Macromolecules. 2008; 41(23): 9204-9213.

[105] K. Renner, MS. Yang, J. Móczó, HJ. Choi, B. Pukanszky, Analysis of the debonding process in polypropylene model composites, European Polymer Journal. 2005; 41(11): 2520-2529.

[106] K. Renner, J. Móczó, B. Pukánszky, Debonding in particulate filled polymers: effect of specific surface area and adhesion, Polymeric Materials P2008, 24 - 26, 2008.

[107] M. Dupire, J. Michel, Polypropylene with high melt strength and drawability, US Patent 6,723,795 (2004).

[108] Z. Bashir, J.A. Odell, A. Keller, Stiff and strong polyethylene with shish kebab morphology by continuous melt extrusion, J. Mater. Sci. 21 (1986) 3993.

[109] K. D. Pae, H.-C. Chu, J. K. Lee, J.-H. Kim, Healing of stress-whitening in polyethylene and polypropylene at or below room temperature. Polymer Engineering & Science, 40(8), (2000), 1783–1795.

[110] R.H. Rane, K. Jayaraman, K.L. Nichols, T.R. Bieler, M.H. Mazor, Evolution of crystalline orientation and texture during solid phase die-drawing of PP-Talc composites, Journal of Polymer Science Part B: Polymer Physics, 52 (2014) 1528-1538.

[111] A. Saffar, A. Ajji, P. J. Carreau, M. R. Kamal, The impact of new crystalline lamellae formation during annealing on the properties of polypropylene based films and membranes. Polymer, 55(14), (2014), 3156–3167.

[112] E. A. Franco-Urquiza, J. Gámez-pérez, J. C. Velázquez-Infante, O. Santana, A. M. Benasat, M. L. Maspoch, Effect of the Strain Rate and Drawing Temperature on the Mechanical Behavior of EVOH and EVOH Composites. Advances in Polymer Technology, 32(S1), (2012), E287–E296.

[113] R. J. Samuels, High strength elastic polypropylene. Journal of Polymer Science: Polymer Physics Edition, 17(4), (1979), 535–568.

[114] S. Wang, A. Saffar, A. Ajjib, H. Wu and S. Guo, Fabrication of Microporous Membranes from Melt Extruded Polypropylene Precursor Films via Stretching: Effect of Annealing, Chinese Journal of Polymer Science Vol. 33, No. 7, (2015), 1028-1037.

[115] K.H. Nitta, M. Takayanagi, Tensile yield of isotactic polypropylene in terms of a lamellar-cluster model. Journal of Polymer Science Part B: Polymer Physics, 38(8), (2000), 1037–1044.

[116] DM. Liu, J. Kang, M. Xiang, Y. Cao, Effect of annealing on phase structure and mechanical behaviours of polypropylene hard elastic films, J Polym Res 20(5):1–7, (2013).

[117] E. Ferrage, F. Martin, A. Boudet, S. Petit, G. Fourty, F. Jouffret, P. Micoud, P. De Parseval, S. Salvi, C. Bourgerette, J. Ferret, Y. Saint-Gerard, S. Buratto, J. P. Fortune, Talc as nucleating agent of polypropylene: morphology induced by lamellar particles addition and interface mineral-matrix modelization, JOURNAL OF MATERIALS SCIENCE 37 (2002) 1561 – 1573.

[118] K. Ushui, Y. Kondo, K.Hatada, S. Gima, Effect of tie molecules on the craze strength of polypropylene, polymer 37(24): 5375-5379, 1996.

[119] W. Wan, D. Yu, Y. Xie, X. Guo, W. Zhou, J. Cao, Effects of Nanoparticle Treatment and Mechanical properties of Polypropylene/Calcium Carbonate Nanocomposites, Journal of Applied Polymer Science. 2006; (102): 3480-3488.

PUBLICATIONS AND COMMUNICATIONS

K. Habibi, P. Castejón, A.B .Martínez, D. Arencón, *Effect of filler content, size, aspect ratio and morphology on thermal, morphological and permeability properties of porous talc filled—Polypropylene obtained through MEAUS process*, Adv Polym Technol, 2018; https://doi.org/10.1002/adv.22116.

P. Castejón, K. Habibi, A. Saffar, A. Ajji, A.B. Martínez, D. Arencón. *Polypropylene-Based Porous Membranes: Influence of Polymer Composition, Extrusion Draw Ratio and Uniaxial Strain*, Polymers 2018, 10(1), 33; https://doi.org/10.3390/polym10010033.

Kian Habibi, Antonio B. Martínez and David Arencón, *Development and improvement of the polymeric membrane by MEAUS process for gas separation*, ‘’3rd World Congress on Materials Science, Engineering, Oil, Gas and Petrochemistry’’, Aug 26, 2017, Barcelona, Spain.

Kian Habibi, Antonio B. Martínez and David Arencón, *Development and improvement of the polymeric membrane by MEAUS process*, ‘’3rd World Congress on Materials Science, Engineering, Oil, Gas and Petrochemistry’’, Aug 24, 2017, Barcelona, Spain.

Pilar Castejón, Kian Habibi, Antonio B. Martínez and David Arencón *Influencia en la etapa de estiramiento en la morfología porosa de membranas de polipropileno obtenidas mediante extrusión*, XIV Reunión del Grupo Especializado de Polímeros (GEP) de la RSEQ y RSEF Burgos, 5-8 septiembre 2016.

Society of Petroleum Engineers (SPE), Since 2012, Training courses, lecturer and conferences.

American Association of Petroleum Geologists (AAPG), Since 2014, lecturer, Developing software and conferences.